Master thesis : Analysis of shape distortion resulting from the manufacturing process for thermoset composites

Auteur : Pereira Sanchez, Clara Andrea
Promoteur(s) : Noels, Ludovic
Faculté : Faculté des Sciences appliquées
Diplôme : Master en ingénieur civil en aérospatiale, à finalité spécialisée en "turbomachinery aeromechanics (THRUST)"
Année académique : 2016-2017
URI/URL : http://hdl.handle.net/2268.2/2645

Faculty of Applied Sciences
Final year project
Academic promoter: Ludovic Noels

Analysis of Shape Distortion Resulting from the Manufacturing Process of Thermoset Composites

Clara Andrea Pereira Sánchez

Joint master programme in Turbomachinery Aeromechanical University Training (THRUST)

Academic year 2016-2017

June 2017

Abstract

Composite materials are gaining importance day a day due to their light weight, exceptional mechanical properties and long durability when compared to metallic materials. Integral composite parts are being manufactured for different applications and fields, such as the aerospace or the automotive among others. The importance of studying the manufacturing process of such materials becomes vital since the thermal effect and the method itself will influence the final shape and the distribution of residual stresses within the material. Due to the relevance of such materials, their characterization and manufacturing need to be investigated so that the cost and time are minimized whilst keeping an adequate geometric accuracy.

This thesis assists to the understanding of the different manufacturing techniques that can be applied, and the possible sources of process induced deformations of composite materials. The main objective is to comprehend the phenomenon and to identify the main parameters of the curing procedure that affects the final shape of the structure. For this reason, the first part of this thesis consists on the study of the properties of a resin during cure and how to obtain them experimentally. In particular, Differential Scanning Calorimetry (DSC) measurements of a certain resin material are used to obtain the experimental curing degree, among other parameters. With this in mind, an analytical model is applied in order to appropriately simulate the evolution of the curing degree with time. This is a computational model that uses a non-linear least-square method to fit a formula to the experimental curve, giving as a result a set of fitting (optimized) parameters.

As a next step, a finite element software is employed to carry out a chained thermo-mechanical analysis of an L-shaped beam, whose material is a composite made of fibres and the resin previously studied. The thermal analysis based on the fitting parameters identified previously using the analytical model, together with some other thermal characteristics of the material. A simple thermal cycle was specified to simulate the DSC cycle. As a result, the temperature distribution in the structure was obtained at all times, together with the development of the curing degree.

The data resulting from the thermal simulation is entered as input of the mechanical. By just specifying the material's elastic properties and simple boundary conditions, the finite element code is able to predict the shape distortion of the L-shape beam. This deformation consists of a change in angle, from the initial value of 90 degrees to a smaller one. Finally, and with the aim of further understanding the phenomenon, certain sensitivity analyses are performed to discover which parameters are more important to correctly identify, and what the consequences of a wrong identification would be.

I. List of figures

II. List of Tables

Table of contents

1. Introduction

1.1. Motivation and goal

Many different engineering fields are nowadays relying in the use of advanced composite materials. Ranging from the aircraft industry to sport equipment or ballistic protection, composite materials have gained importance due to their light-weight, long durability and exceptional mechanical properties when compared to conventional metallic materials. Seeing the increase in use of composite materials, their characterization and manufacturing processes need to be studied with the goal of finding a robust method that minimizes cost and time whilst keeping an adequate geometric accuracy of the manufactured part.

Composite materials for advanced industrial applications are made of a thermosetting matrix resin, such as epoxy. Reinforcing fibres are embedded in the resin before curing. The thermosetting resin generally cures upon the application of heat, transforming from liquid to solid. During this process, the material's molecules undergo cross-linkage and form longer molecular chains.

When big integral structures are to be built out of fibre reinforced composites, there are still troubles when designing a manufacturing process that results in high quality parts, since process induced deformations may arise. In general, an empirical optimization approach is used in order to achieve a manufacturing process which meets the appropriate quality and tolerances [1]. A considerable amount of time and money are invested in order to perform the characterization of each material, or its application to a new geometry. Manufacturing and curing of thermoset-based composites are complex processes to study [2]. Some difficulties may arise during the production as a result of the heterogeneity of these materials, such as matrix fracture or shape distortion [3]. Furthermore, the final shape of the part and the amount (and distribution) of residual stresses on the structure heavily depend on manufacturing. They may be, hence, a source of significant expenses if the part needs to be re-designed or re-built. Using trial and error on physical prototypes to optimize the manufacturing process is very demanding in terms of time and cost.

As a result, one can imagine how important the process simulation is, so that time and cost are minimised. The manufacturing process of thermoset composite materials can be simulated with a chained thermal-chemical-mechanical finite element analysis [1]. At each stage of the analysis, specific models are used. For the mechanical part, the evolution of the mechanical properties of the resin during the curing must be modelled. For the thermal-chemical analysis, specific cure kinetic models are needed and are injected in the heat transfer balance equation. Different models exist in the literature and are nowadays available in commercial software. These models include

some parameters, whose values must be determined based on specific experimental results. The accuracy of the shape distortion obtained by simulation strongly depend on how the parameters were identified, wrong or bad inputs leading to inaccurate results. It is therefore essential to develop a robust procedure for the parameters identification.

This project is conceived in the interest and using the facilities of GDTech, a Belgian engineering company, to study and model the manufacturing process of thermosetting matrix fibre composites and accurately predict the shape distortion. The main objective will be the development of a procedure for the identification of the parameters appearing in the cure kinetic models available in the Samcef finite element code. These values will be obtained based on the interpretation of specific experimental isothermal and dynamic DSC curves. For that purpose, a review of the characterization techniques is first completed. In a latter step, the effect of the variability of some parameters on the resulting shape distortion will be studied.

A general overview of the thesis, in a schematic way, is available in Figure 1. The three main blocks into which the contents can be divided are:

- Experimental part (red block in Figure 1): starting from experimental isothermal DSC curves, the degree of cure versus time is obtained by applying its definition (arrow **A**). At the same time, the total enthalpy of the curing reaction will be obtained by integrating the dynamic DSC experimental results (arrow **C**).

- Identification procedure (green block in Figure 1): with this in mind, this thesis will apply a certain curing kinetic model to find an analytical formulation for the degree of cure that resembles the experimental curves. It will be shown how the identification procedure of the cure kinetic parameters can be extracted from experimental DSC curves (arrow **B**) by utilizing a non-linear optimization (Levenberg-Marquadt algoritm).

- Computer aided model (purple block in Figure 1): the curing kinetic parameters, together with other material parameters and a temperature cycle, will be inserted in a thermal simulation (arrow **D**) of an L shape composite beam. The results of this thermal simulation will be the evolution of the predicted degree of curing, the temperature history and the glass transition temperature. The degree of cure resulting from the numerical software Samcef resembles perfectly the curing kinetics predicted with the analytical model. Later on, by performing a mechanical simulation, it will be seen how the curing process will cause the beam to deform into a slightly smaller (less than 0.3 degrees) angle due to the thermal conditions that are applied (and transferred from the thermal simulation, arrow **E**). The numerical results agree very well with the analytical expression for change in angle of that kind of geometry under a curing process. Furthermore, the sensitivity

analysis will show that some parameters from the cure kinetics identification ought to be accurately estimated, as well as the importance of the gelation point in the whole procedure.

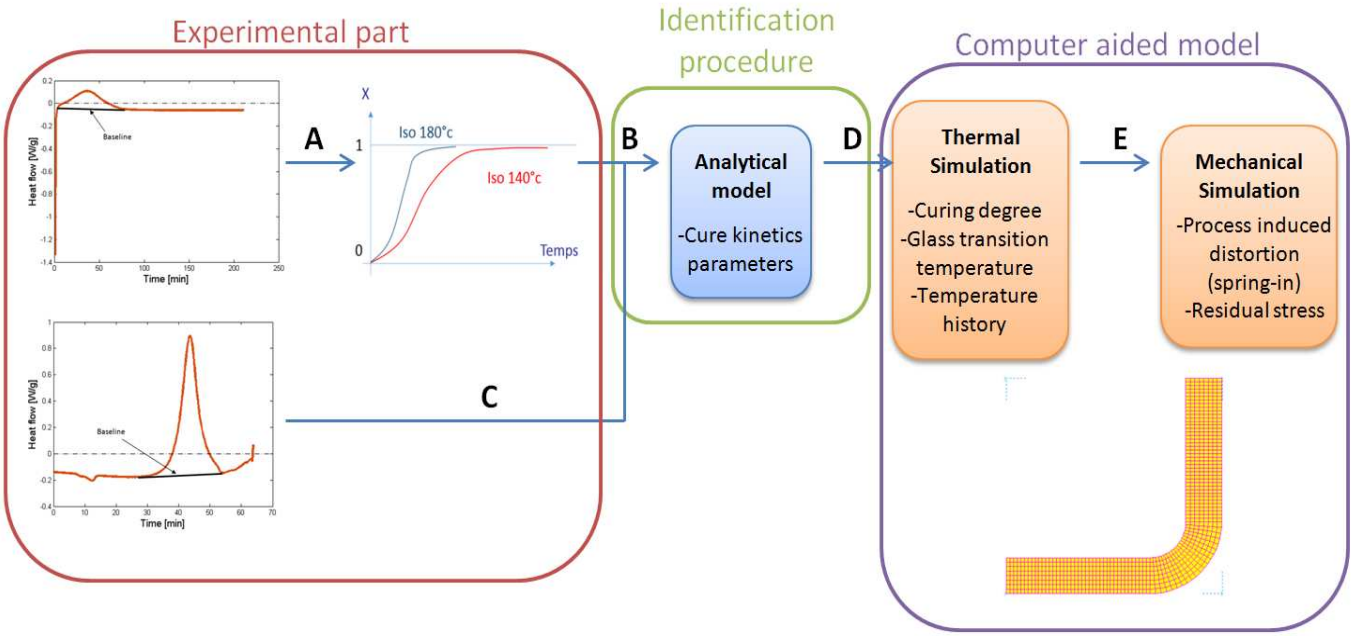

Figure 1: Schematic overview of the thesis and the steps followed to achieve a prediction of process induced deformations in an L-shape composite beam

1.2. Structure of the thesis

This thesis is organized in three main sections as follows:

Section 1: chapters 2 and 3, offering an introduction of the topic of curing of composite materials. Chapter 2 starts with basic concepts on what a composite material is and common manufacturing and curing techniques. Chapter 3 deals with theory of how to model the thermal part of the curing process of a thermosetting resin, followed by the common sources of manufacturing induced distortions. The most common material models to simulate the composite are briefly introduced. Lastly, a list of characterization techniques that may be used to identify the necessary model parameters is provided.

Section 2: containing chapters 4 and 5. Chapter 4 explains the methodology used in this project for the identification of parameters to apply in curing kinetic models. This chapter uses real experimental data from Dynamic Scanning Calorimetry provided by C. Brauner. A Matlab program was developed in the thesis to identify the kinetic model parameters. The results obtained from this identification were compared to the ones reported in his thesis [1]. Chapter 5, on the other hand, explains the implementation and validation of the thermo-mechanical simulations and the methodology followed to

predict the manufacturing induced distortions. The results will be presented for a reference study, and for a series of sensitivity analyses.

Section 3: formed by chapter 6. It consists of a summary of the results and findings, some conclusions and potential future work for the topic.

2. Composite materials: definition and generalities

This chapter contains an introduction on the topic of composite materials, from basic definitions to the manufacturing processes of composites, and the main methods of curing used in the industry.

2.1. What is a composite material

A composite material is defined as one which is formed by two or more different materials with different properties that combine in order to produce a material with unique properties. Going from natural (e.g. wood, bones) to the so called "advanced composites" (e.g. glass or carbon fibre reinforced composites), these materials are becoming more and more common in our everyday lives. Contrary to alloys, for example, the components of these materials do not blend or solve into each other, but they can be differentiated in the micro scale.

Compared to traditional materials, such as metals, composites show in general a higher specific strength and stiffness, which are very attractive properties in certain industries such as the aerospace or the automotive. Good fatigue resistance is another of their main advantages, although it is difficult to accurately predict.

This thesis is dealing with advanced composites, also known as advanced polymer matrix composites. Generally they are layered composites involving a fibrous material embedded in a resin matrix orthotropic (reference to [4], [5] for further information about orthotropy), as sketched in Figure 2. Fibres function as the carrying elements within the composite and therefore, their alignment and orientation determine the direction/s in which predominant mechanical properties are found, i.e. a unidirectional fibre composite has better mechanical properties only in the direction parallel to its fibres. Therefore, layers are normally stack-up with alternating fibre orientations to provide high strength and stiffness in more than one direction, as sketched in Figure 3. The stack-up sequence plays a major role in the material's final mechanical properties.

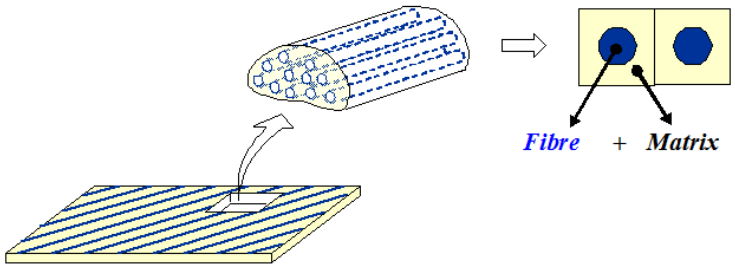

Figure 2: Sketch of an orthotropic ply formed by unidirectional fibres embedded in a matrix [6]

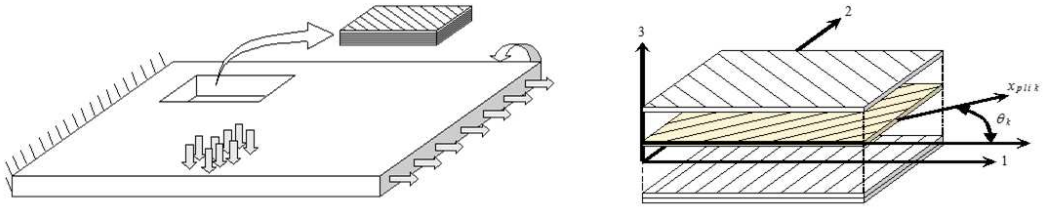

Figure 3: Sketch of a composite material made of several plies of unidirectional fibres. On the right, the angle θ_R defines the orientation of a ply with respect to the reference direction (direction 1) [6]

The most common types of fibres include glass, aramid, carbon and ceramic fibres. The former one can function as electrical insulator, and it exhibits good chemical resistance. Aramid fibres are used in applications where impact resistance is needed, although they are weak in compression. On the other hand, despite their higher cost, carbon fibres are very stiff and strong fibres that appropriately resist corrosion. Ceramic fibres are mainly used for applications where high temperatures are involved [7].

As far as the matrix is concerned, its basic functions include bonding the fibres and keeping their position and orientation within the material as well as increasing the fibres' resistance to shear forces [8]. It also transfers the load to the fibres. The matrix specifies the range of temperatures in which the material can be used. Polymer matrices can be thermosetting resins such as polyester, epoxy, or phenolic resins or, on the other hand, thermoplastic resins such as polyether ether ketone (PEEK) or polypropylene (PP). Composites using either type of matrix are manufactured very differently. Thermoplastic resins require an increase of temperature in order to be deformed and a decrease of it to be hardened. On the contrary, thermosetting resins have a more complex curing mechanism that will be discussed in section 3.1.

Specially in the aerospace industry, due to the high requirements that are needed, epoxy resins are preferred because of their thermal stability. For this reason, from this point on, this report will only focus on thermosetting resin matrix composites.

There are several aspects that are important to take into consideration when designing a polymer matrix composite and that will greatly influence its final properties. These are:

- The particular materials used as fibres and matrix of the composite. Each matrix (or fibre) material has its own properties (Young's modulus, Poisson ratio, coefficient of thermal expansion, etc.) that will influence those of the final composite.
- Within the same layer, the orientation of the fibres within the matrix, as well as their length are important. Within the composite, the stack-up sequence of

layers will also affect the final properties, and hence will strongly affect the deformation and the distribution of stresses within the material when subjected to certain loads.

- The quality of the curing process, because an appropriate adhesion between the fibres and the matrix needs to be fulfilled, minimizing impurities or pores.
- The fibre volume fraction will make an effect on the final properties. Normally, the law of mixtures (discussed in 3.3.3) is applied in order to obtain the homogenized properties of the orthotropic ply.
- The manufacturing process used in order to produce the composite may improve the void content, the adhesion and curing process, or limit the fibre volume content.

2.2. Manufacturing processes

Depending on the type of resin, the size of the component or the application, composites can be manufactured in different ways. The manufacturing process of thermosetting resin composites requires the deposition of resin and a fibrous reinforcement in/on a mould before curing is performed. This chapter will explain the principal methods used in the industry [9], [10] for building the desired lay-up. Furthermore, the main curing techniques will be assessed afterwards.

2.2.1. Methods to build the desired lay-up

- Hand lay-up: simple geometries can be manufactured using a hand lay-up method. A wet matrix is used to impregnate the fibres, which have been previously cut to the appropriate size. The mixture is put on a mould surface, typically covered with some release agent and gel coating to prevent sticking. Next, it is hand rolled in order to guarantee that there are no air bubbles and that the resin is evenly distributed (see Figure 4). This process is continuously repeated until the adequate thickness is achieved. Another way of hand lay-up involves pre-impregnated layers of an already made mixture of resin and fibre reinforcement. Curing is performed after the desired lay-up is built.

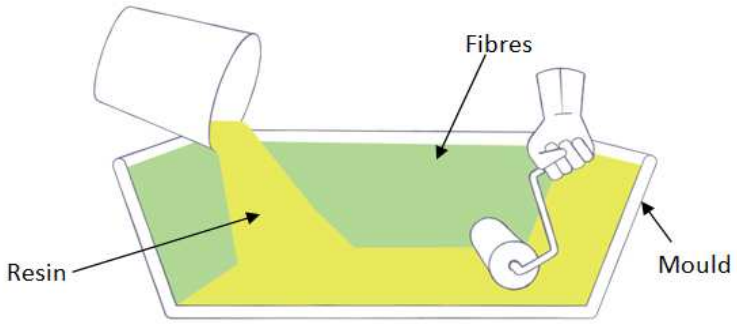

Figure 4: Sketch of composite manufacturing process performed by hand lay-up (adapted from [9])

- Spray lay-up: a mixture of resin and cut continuous fibres are sprayed onto a mould surface (open mould), as sketched in Figure 5. After spraying the

mixture, hand rolling is normally performed to avoid air bubbles. The material is then cured.

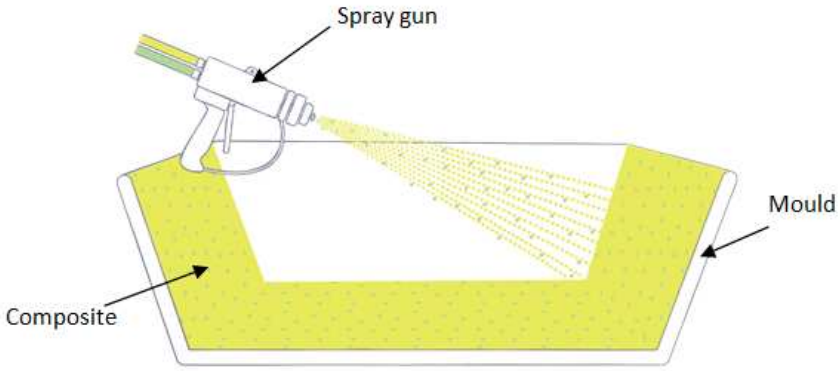

Figure 5:Sketch of composite manufacturing process performed by spray lay-up (adapted from [9])

- Vacuum bag moulding: it is used to achieve a uniform combination of resin and fibres, resulting in materials with better quality. The procedure consists in placing the uncured composite material on a mould and covering the set-up with a bag. The void content is reduced by decreasing the pressure inside the bag where the mixture of fibres and resin is placed, as shown in Figure 6. Furthermore some excess resin will be removed. The mould is then placed in an autoclave (see sketch in Figure 7) or heated up itself for curing.

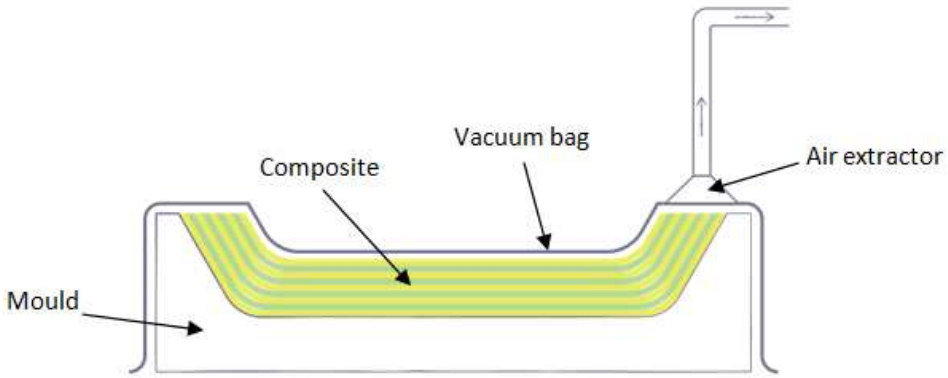

Figure 6: Sketch of composite manufacturing process performed by vacuum bag moulding (adapted from [9])

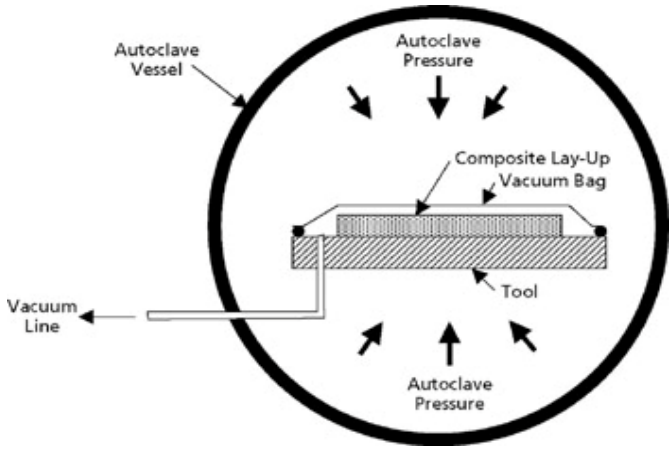

Figure 7: Sketch of a vacuum bag moulding composite being cured inside an autoclave [11]

- Injection moulding: solid resin pellets with embedded fibres are deposited into a container at high temperature where they melt (normally used in thermoplastics). The heat is generated due to viscous shearing between an inner screw and the container. The screw also pushes the melted composite material into a mould where it is left to cool down and harden, as depicted in Figure 8. Injection moulding is a cheap and fast method to produce composites.

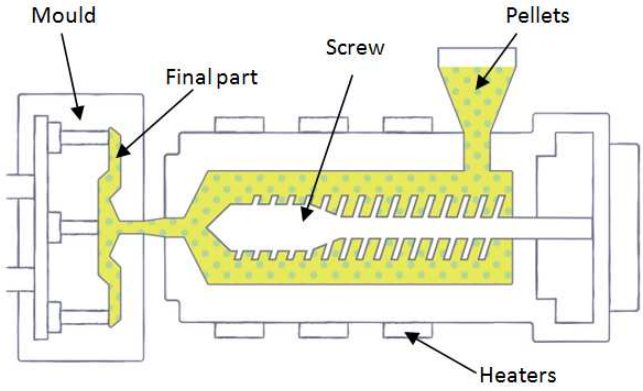

Figure 8: Sketch of composite manufacturing process performed by injection moulding (adapted from [9])

- Resin Transfer Moulding (RTM): fibres are placed with the desired orientation (even through thickness reinforcement) inside a mould. After closing the mould, a mixture of resin and catalyst is subjected to pressure so that it flows into the mould cavity through selected paths in order to impregnate the fibres, as it is shown in Figure 9. Other components may be also added to the mix, such as inhibitors and retarders to slow the reaction if needed.

  The mould includes some ventilation channels in order to evacuate any air trapped in the material. Very low viscosity resins need to be used in this process if manufacturing thick components. The structure will be cured inside the mould and the appropriate machining will be performed after tempering the structure.

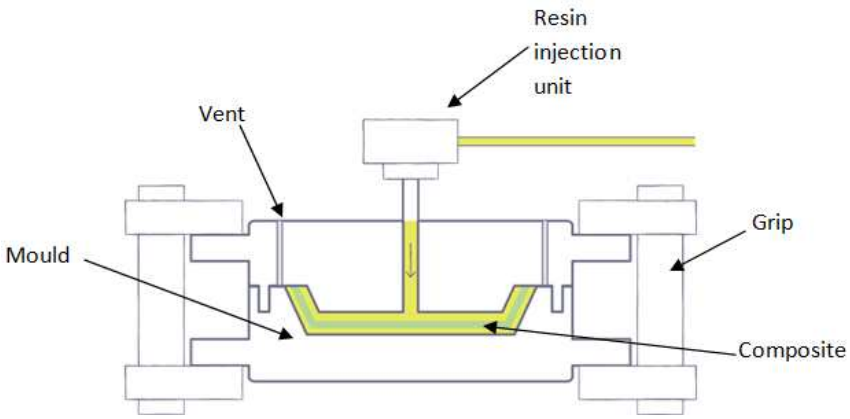

Figure 9: Sketch of composite manufacturing process perform by RTM (adapted from [9])

2.2.2. Principal composite curing techniques

The most simple way of curing composites is at ambient conditions (room temperature and pressure). However, different techniques are also used in the industry in order to accelerate the curing process and obtain final parts with better quality. In general, curing techniques can be divided into two types: thermal and radiation curing.

Thermal curing is the leading method used for both academic and industrial purposes. Due to the low thermal conductivity of most resins, this type of curing normally requires high time and energy consumption, and is driven by convection and conduction within the material. Among all the possible techniques, oven or autoclave (sketch in Figure 10) are the most popular, which involves a series of thermal and pressure programmes [12].

Autoclaves working principle is based on the difference of gas pressure. Almost any shape can be cured in an autoclave, because the application of pressure is performed isostatically. The main limitation comes with the size of the autoclave (which will limit the size of the pieces to be cured), and hence the budget that can be invested in its purchase and functioning. A conventional autoclave includes a pressure vessel.

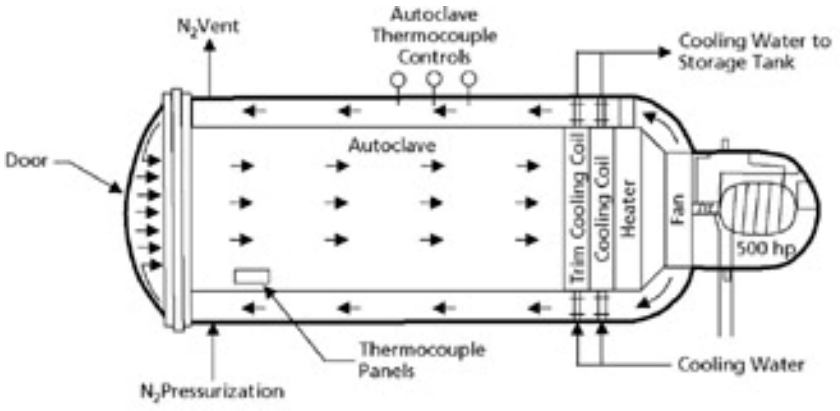

Figure 10: Sketch of a typical autoclave for manufacturing of composites [11]

Other thermally driven techniques are: microwave heating, hot shoe or induction heating. Thermal curing methods, especially when manufacturing thick components, may be challenging when requiring to achieve uniform curing [12]. Besides, the temperature gradients within the material may lead to high residual stresses, which are the cause of process induced deformations.

On the other hand, radiation curing does not rely on the increase in temperature for curing to occur. In fact, radiation sensitive polymers undergo ionization when subjected to an electromagnetic radiation. The materials that are cured using these methods exhibit faster curing speed and better resin stability, among other advantages [12]. However, the highly radioactive nature of the radiation sources (X-rays, γ-rays, UV, electron beam, etc), together with the preparation of a matrix susceptible to radiation and the disposal of the highly hazardous waste [13], make radiation curing less popular.

In this thesis, only thermally cured composites will be considered. In the following section, the (thermal) curing mechanism of thermosetting matrix composites will be explained, before introducing the cure kinetics and some available models to describe them.

3. Principles of curing simulation

This extensive chapter contains the specific theory in order to understand and perform the studies reported in this thesis. It begins by theory on curing of thermosetting resin based composites followed by the reasons and sources of manufacturing induced deformations. The material models will then be introduced: curing kinetic models and constitutive material models will be attained separately. After having introduced the necessary and the driving parameters for the simulation, a review of the required characterization techniques to find them is available.

3.1. Theory on curing of thermosetting resin based composites

Several physical and chemical reactions occur during curing of a thermosetting resin, transforming the material from liquid to a brittle solid as its viscosity increases. Curing of these materials involves an exothermic reaction that converts a low molecular weight liquid into a theoretically infinite molecular weight amorphous system. In a polymer network, the molar mass is considered at the chains between two consecutive crosslinks. Therefore, in a completely cured material, the molar mass of the network is infinite since all chains are covalently bonded forming a unique macromolecule. Normally, the resin is mixed with some hardener and catalyst in order to stimulate the curing process [2], [14].

Curing of a thermoset is an irreversible exothermic process that occurs by submitting the material to a combination of high temperature and pressure for a certain amount of time. The curing process satisfies the heat balance equation (Eq. 1), which means that the difference in heat going in and out of the system must be equal to a heat source term Q and the capacitive heat (cooling or heating of the material) [15]. This equation is the most general form of the differential thermal energy balance.

$$\frac{\partial \rho h}{\partial t} = -\nabla \bar{q} + Q \qquad \text{Eq. 1}$$

$$\bar{q} = -\lambda_{ij} \nabla T \qquad \text{Eq. 2}$$

where ρh represents the material's enthalpy, t the time, Q the heat source and $\bar{q}$ the conductive heat flux vector, which is associated to the local temperature T by Fourier's law (Eq. 2). Lastly, the conductivity coefficients are arranged in λ_{ij} matrix. Both ρh and λ_{ij} can vary spatially and can be also temperature or time dependent.

A typical temperature programme can be seen in Figure 11 for the curing of a composite in an autoclave. During curing, crosslinking occurs due to the appearance of covalent bonds among epoxy groups, which will increase the molecular weight and the viscosity of the resin (for more information on the chemical reactions, consult the PhD thesis by Karkanas [2]). Once the resin is cured, it becomes impossible to melt or fuse, but instead it degrades if elevated temperatures are applied. As explained in the following chart, the material properties of the matrix change, starting from a liquid

state (region I in Figure 11). The gel point (point A) is defined as the temperature at which covalent bonds start to appear in the material's molecular structure. As cross-linking occurs, after going through the gel point, a rubbery or visco-elastic state is attained (region II), where the stiffness of the material remains low [16]. The gel point depends on the environment and the curing system and serves as an estimation on the point at which gelation occurs [2]. Later on, vitrification (point B) takes place and the material fully solidifies (region III), indicating the end of the curing process [16].

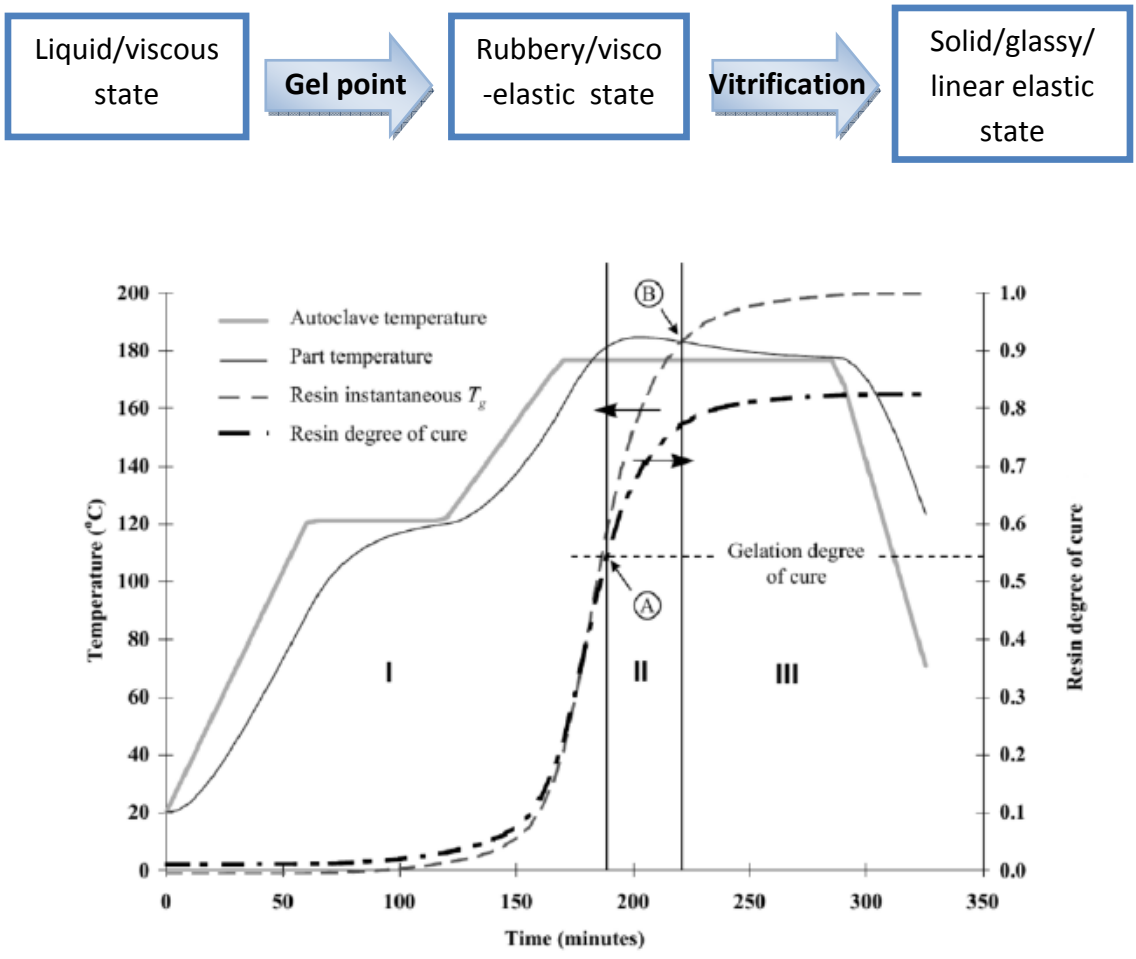

Figure 11: Typical temperature cycle for curing of a thermosetting matrix composite in an autoclave. As a result of the temperature programme, the composite's degree of cure and glass transition temperature also vary with time. Three special regions can be observed: I liquid/viscous, II rubbery/visco-elastic and III solid/glassy states [1]

Figure 11 also shows the evolution of the degree of cure X with time that is produced when subjected to the shown thermal treatment. This X parameter measures the amount of curing of the resin, and goes from zero (uncured material) to, theoretically, unity (fully cured material). It is also interesting to realize that the intervals of the three physical states of the resin depicted above can be fully determined thanks to the gel point X_{gel} (point A) and T_g as follows:

- Stage I: the matrix is in liquid state $\forall\ X \leq X_{gel}$
- Stage II: the matrix is in rubbery state $\forall\ X > X_{gel}$ and $T > T_g$
- Stage III: the matrix is in glassy state $\forall\ X > X_{gel}$ and $T \leq T_g$

On another matter, diffusion becomes important at the last stages of the curing process, after the vitrification point (point B). The reason is that, when high degrees of curing *X* are reached, the material starts to solidify, viscosity increases and the amount and mobility of reaction partners are very limited. The reactant groups are therefore required to diffuse to the reactive centres to achieve any further curing. The process then stops being controlled by the reactivity of the molecules [17] [18] and starts being controlled by their ability to diffuse. For this reason, an incomplete curing may be achieved for certain low temperature values at isothermal curing conditions (see that experimental black curve in Figure 12 does not reach a value of 1).

Diffusion may be neglected in a cure kinetic model, depending on the type of resin, if at high degrees of cure the model can resemble the experimental curves. In particular, for the resin material that is going to be used in this project, diffusion control becomes vital for low curing temperatures at high degrees of cure. In order to show an example of how diffusion control improves the analytical results, Figure 12 is shown. The black curve shows the experimental results of the curing of a thermosetting resin (see upcoming sections), the blue and red curves are analytical fits without and with diffusion respectively. It is obvious that, for the material that will be used in this project, diffusion has an important role in the modelling.

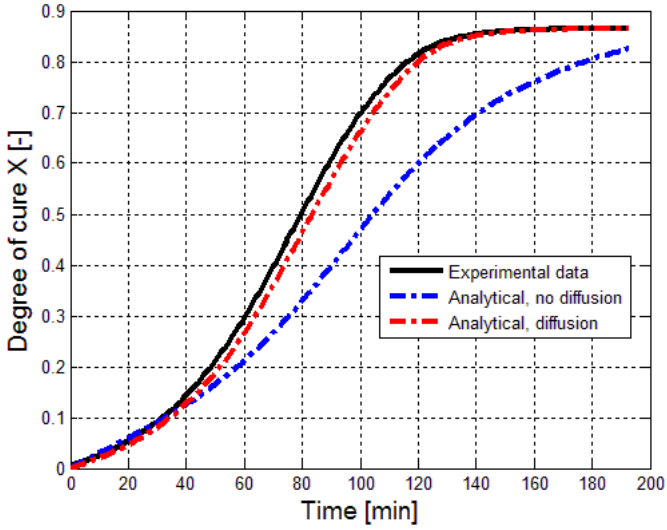

Figure 12: Curing degree of a thermosetting resin at an isothermal curing temperature of 140ºC. In black, the experimental data provided by C. Brauner [1], in blue an analytical fit with no diffusion control and in red, the same analytical fit including diffusion control (using the analytical approach developed in the current theses)

If curing happens at a constant temperature, the glass transition temperature of the material increases from an initial value (uncured resin) T_{g0} to the final value when

curing ends $T_{g\infty}$. Whereas gelation occurs at an intermediate point between these two thresholds, vitrification occurs when the glass transition temperature reaches the reaction temperature $T_{c,iso}$, which increases much slower than the T_g [19]. As can be seen in Figure 11, T_g varies as a function of time (and therefore of temperature). Furthermore, a correlation between the degree of cure X and T_g can be described by DiBenedetto's equation [20], and its equation will be given later on in this report.

An appropriate curing model should be able to represent the material behaviour at all these stages. The selected cure cycle considerably affects the properties of the final part and must therefore be selected with caution, depending on the material and desired application. The main parameters of influence that are already pointed out are: time, pressure, temperature, its gradient and the degree of cure.

3.2. Sources of manufacturing induced distortions

In certain fields (aerospace, automotive, etc.), components need to meet tough design requirements and tolerances. Dimensional changes are likely to occur when manufacturing certain materials and geometries, for example a thermally cured composite structure. The curvature of open angled components such as L, T or U beams changes as a result of the application of temperature gradients, and the variation of the angle can be to both a higher or lower angles (spring-back and spring-in respectively). Another common shape distortion induced by the manufacturing process in multi-layer laminates is warpage (see Figure 13) [17]. The mechanisms of these distortions need to be well understood and predicted so that it can help when designing a mould to compensate those deformations. The prediction of spring-in angle of an L shape composite structure is the main aim of this study.

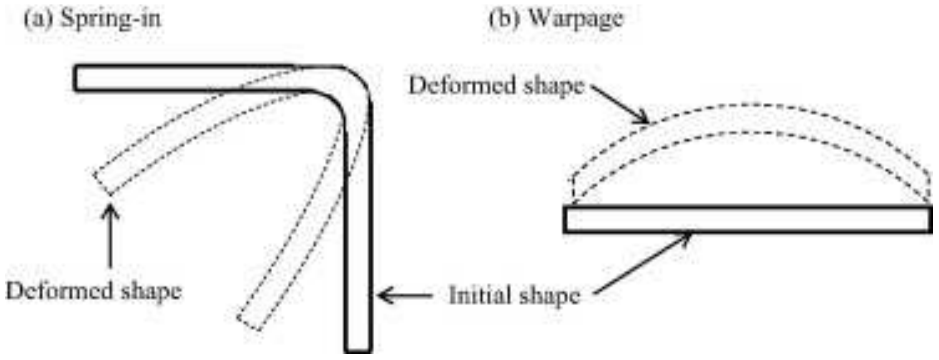

Figure 13: Spring in and warpage of composite laminates. In solid lines, the initial designed shape, and in dashed lines the deformed shape [21]

Residual stresses arise as a result of the mould or additional external loads in which the laminates are placed. If the material was isotropic, homogeneous and free to deform during those temperature gradients, little to no residual stress would exist afterwards. However, in orthotropic laminates, each ply prevents the adjacent plies with different fibre orientation to deform, hence creating residual stresses through the thickness.

The manufacturing induced shape distortions are generally due to residual stresses in the structure. They are in turn provoked by intrinsic properties such as thermal and chemical shrinkage. Some other aspects are [1], [17]:

- Material of the mould: more distortion for different coefficient of thermal expansion among tool and laminate.
- Mould surface: more distortions for rough mould surfaces.
- Fibre volume fraction: it will affect the laminate coefficients of thermal expansion.
- Void content: it will affect the fibre volume fraction.
- Stack-up sequence
- Rate of cooling from the curing to the room temperature

The volumetric change of the structure due to thermal loads or gradients is referred to as thermal strain ε^{th}, whereas the dimensional change due to the polymerization of the resin is known as chemical strain ε^{ch}. Especially when considering thermosetting resins, ε^{ch} should not be disregarded [17]. The thermal strain depends on the coefficient of thermal expansion *CTE* of the material as well as the temperature gradient (see Eq. 3). On the contrary, the chemical strain given in Eq. 4 depends on curing *X* and the coefficient of chemical shrinkage *CSh*.

$$\varepsilon^{th} = CTE\ \Delta T \qquad \text{Eq. 3}$$

$$\varepsilon^{ch} = CSh\ \Delta X \qquad \text{Eq. 4}$$

In order to have an overall view, these two types of strain contribute to the so called non-mechanical volume strain $\varepsilon^{non\text{-}mech}$ i.e. strain not produced by any external mechanical load or moment. The expression for the non-mechanical strain is given in Eq. 5 [17]. The other two components, namely the moisture absorption strain $\varepsilon^{moisture}$ and the physical aging strain ε^{aging}, will be neglected in this study.

$$\varepsilon^{non-mech} = \varepsilon^{th} + \varepsilon^{ch} + \varepsilon^{moisture} + \varepsilon^{aging} \qquad \text{Eq. 5}$$

3.3. Material models

This subsection briefly describes the cure kinetic models first, followed by the most common constitutive models for thermosetting resin composites. The material model used in this project will be an elastic one, differencing between the properties from the fibres and the matrix separately. A simple law of mixtures is applied for homogenization purposes.

3.3.1. State of the art

The material models that are applied in order to study the process induced deformations can be categorized into three different groups: elastic, incrementally elastic and viscoelastic models [1], [16].

Elastic models consider a material with constant stiffness regardless of its curing stage. This implies that process induced distortions are due to the thermal expansion of the material only, generally anisotropic (the resin has a higher thermal expansion coefficient than the fibres). Further improvements were proposed so that chemical shrinkage or the amount of moisture were included into the problem. These models are usually not accurate enough in order to capture the behaviour of certain materials or applications (normally limited to 1 or 2D geometries).

Incrementally elastic models describe the stiffness as a function of degree of cure and temperature. The most common procedure to assess the nonlinear transient computations was to assume the Young's modulus of the resin E_m to be linearly dependent on X. Further improvements are also found in the literature, where second order polynomials were used in order to describe the stiffness as a function of X for temperatures higher than the gelation temperature [1]. The Cure Hardening Instantaneously Linear Approach (CHILE) was developed by Johnston et al. [22] using an elastic material with constant E_m in each physico-chemical state, but varying with X and temperature. This approach showed accurate results when predicting induced deformations for cases in which their E_m constantly increases during cure [23]. However, due to the viscoelastic nature of resins, residual stresses suffer relaxation during the curing process as a function of time, temperature, and the position of the gel point [1], [16]. Consequently, although incrementally elastic models are faster and simpler to implement, (pseudo-) viscoelastic formulations are used instead [24].

A viscoelastic material shows both elastic and viscous properties when under deformation. Hence, energy dissipation occurs when the material is subjected to an external load and then released.

Viscoelastic models provide a more accurate prediction of process induced deformation by means of increasing the complexity of the calculation and implementation of the model, as well as the computational time. Besides, the required material characterization needs to be performed in more detail, which further increases the complexity and the time expense. One of the most common models to represent viscoelastic materials is by introducing Maxwell or Kelvin elements: a combination of springs and damping elements in series or in parallel, respectively [1], [16]. More advanced models are available, in which the viscoelastic behaviour is improved by the introduction of cure dependency, such as the ones presented by Kim and White [25] and Prasataya et al. [26].

Regarding cure kinetics, models are basically divided into two groups: phenomenological and mechanistic models. The latter ones are developed from a chemical balance of the species taking part in the reaction, whilst phenomenological models rely in the main features of the kinetics of the reaction (ignoring the in-depth information on the reaction among species). Even though mechanistic models offer a

more accurate prediction and representation of the cure kinetics, they are also very difficult to handle, complex in identifying certain required parameters, and time consuming. For that reason, phenomenological approaches are preferred from an engineering point of view. Some of these models will be explained in the following sub-section.

3.3.2. Cure kinetics models

The degree of cure *X*, introduced previously in section 3.1, can be defined as the ratio between the heat released at a time *t* over the total amount of heat released during curing. Therefore, the values of *X* range from 0 (uncured resin) to approximately 1 (fully cured resin). The volumetric heat source *Q* involved previously in Eq. 1 actually depends on the evolution of the degree of cure via Eq. 6.

$$Q = \rho H_{TOTAL} \frac{dX}{dt} \qquad \text{Eq. 6}$$

The empirical definition of *X* is given in Eq. 7, where *H(t)* is the heat distribution of the reaction, and H_{TOTAL} is the total enthalpy of the reaction of the completely cured material. Their expressions are available in Eq. 8 and Eq. 9 respectively [16], [18]:

$$X(t) = \frac{H(t)}{H_{TOTAL}} \qquad \text{Eq. 7}$$

$$H(t) = \int_0^t \left(\frac{dq}{dt}\right) dt \qquad \text{Eq. 8}$$

$$H_{TOTAL} = \int_0^{t_f} \left(\frac{dq}{dt}\right) dt \qquad \text{Eq. 9}$$

where *(dq/dt)* is the instantaneous rate of heat generated and t_f the time required for the curing reaction to be completed. These equations assume that the degree of cure is proportional to the heat flow. By differentiating Eq. 7 with respect to time, the rate of cure can be defined as per Eq. 10, which can be obtained from experimental measurements, as explained in section 4.2.

$$\frac{dX}{dt} = \frac{1}{H_{TOTAL}} \left(\frac{dq}{dt}\right) \qquad \text{Eq. 10}$$

Several phenomenological models have been developed to describe the cure rate. The simplest, known as the n^{th} order reaction model (Eq. 11), can be applied for curing reactions where no autocatalytic and no difficulty in the reaction are involved. As soon as an autocatalytic phenomenon exists, the simplest model was found to be as in Eq. 12 [27]. Nevertheless, the model by Kamal and Sourour (Eq. 13) [18], accounting for

both non-catalytic and catalytic systems, appears to be the most used, specially for epoxy resin composites.

A slightly more complex model was proposed by Karkanas et al. [27] by including an extra reaction order (*l*) as given in Eq. 14. The results show a more accurate fit between the numerical and the experimental data, although some lack of agreement was found due to the absence of modelling for diffusion control.

$$\frac{dX}{dt} = k(1-X)^n \quad \text{Eq. 11}$$

$$\frac{dX}{dt} = kX^m(1-X)^n \quad \text{Eq. 12}$$

$$\frac{dX}{dt} = (k_1 + k_2X^m)(1-X)^n \quad \text{Eq. 13}$$

$$\frac{dX}{dt} = k_1(1-X)^l + k_2X^m(1-X)^n \quad \text{Eq. 14}$$

where *l*, *m* and *n* are temperature independent reaction orders and k_i are temperature dependent rate constants that follow an Arrhenius relationship, as given per Eq. 15.

$$k_i = A_i \exp\left(-\frac{E_{ai}}{RT}\right) \quad \text{Eq. 15}$$

where *T*, *R*, A_i, E_{ai} are the absolute temperature, the universal gas constant, the pre-exponential factor of the i^{th} reaction and the activation energy of the i^{th} reaction respectively. A qualitative graph can be seen in Figure 14 comparing the four kinetic models described in Eq. 11 to Eq. 14. As it can be appreciated, the n^{th} model is the one that differs the most with respect to the three other models, which take into account the autocatalytic behaviour of resins. Among the three other models (simple autocatalytic, Kamar Sourour and Karkanas models), difference between the three methods is minimal however historically for epoxy resins, Kamal Sourour is used. This same model will be used throughout this study.

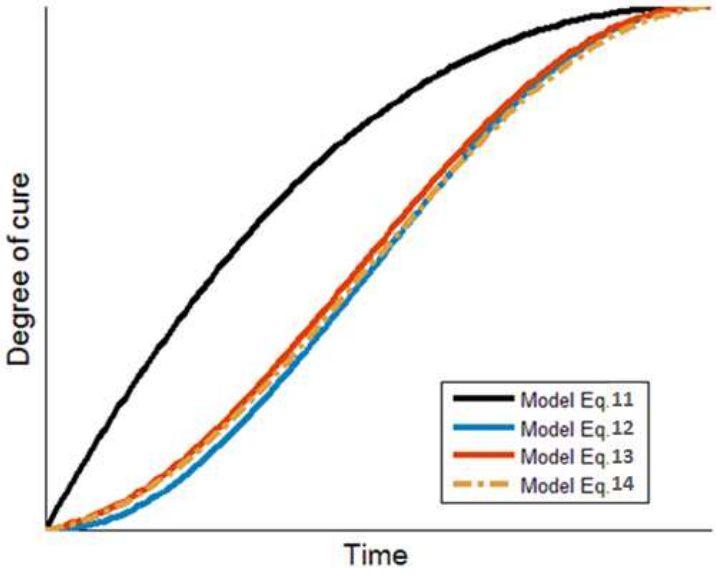

Figure 14: Kinetic models described in the equations above. Eq. 11 refers to the nth order model, Eq. 12 refers to a simple autocatalytic model, Eq. 13 is Kamal Sourour model, and Eq. 14 is Karkanas model

To overcome the drawback due to the lack of diffusion modelling (see Figure 12), different approaches can be found in the literature. The glass transition temperature can be used for such purpose [1], [27], by modifying the temperature dependent rate constant as per Eq. 16. In that equation, the total reaction rate constant k_T is given in terms of k_i (in Eq. 15) and k_D (in Eq. 17).

$$\frac{1}{k_T} = \frac{1}{k_i} + \frac{1}{k_D} \qquad \text{Eq. 16}$$

$$k_D = A_D \exp\left(-\frac{E_D}{RT}\right) \exp\left(-\frac{b_D}{0.00048(T - T_g) + 0.025}\right) \qquad \text{Eq. 17}$$

where A_D and b_D are fitting parameters and E_D is the activation energy of diffusion, and T_g the instantaneous glass transition temperature, which can be obtained thanks to DiBenedetto's equation (Eq. 18) as a function of the degree of cure of the material X. The parameter λ is a material dependent parameter that needs to be obtained when fitting the equation to the experimental measurements.

$$\frac{T_g - T_{g0}}{T_{g\infty} - T_{g0}} = \frac{\lambda X}{1 - (1 - \lambda)X} \qquad \text{Eq. 18}$$

Another method to model a diffusion controlled process, proposed by Fournier et al. as an extension of Kamal and Sourour, includes a diffusion factor f_d, Eq. 19 and Eq. 20 respectively [18], where X_f is the degree of cure obtained at the end of the curing process and b stands for an empirical diffusion parameter.

$$\frac{dX}{dt} = (k_1 + k_2 X^m)(1 - X)^n f_d(X) \quad \text{Eq. 19}$$

$$f_d(X) = \frac{2}{1 + \exp\left[\left(X - X_f\right)/b\right]} - 1 \quad \text{Eq. 20}$$

All the parameters defined in this section can either be obtained by curve fitting or deduced from different characterization techniques. This procedure will be explained in Section 3.4.

3.3.3. Mechanical material models

In this section, different models used to assess the mechanical part of the study will be introduced. They will serve to analyse and predict the process-induced deformation on the structure.

The material model that will be presented and used in the project is an elastic/visco-elastic model that will simulate the mechanical behaviour of a composite structure with a thermosetting matrix undergoing curing. It will be explained separately in three sections: the matrix, the fibres and the homogenization procedure of the properties of both.

- **The matrix:**

The thermosetting resin of a composite material can be modelled for mechanical analysis purposes in several ways. The easiest approach is to assume the material to be an isotropic elastic material and its properties to change with the degree of cure *X*.

The resin will therefore be characterized by the Young's modulus E_m and Poisson's ratio v_m, that can be both defined as a function of temperature, glass transition temperature or degree of cure. For each of these two parameters, three different values (or functions of *T*, T_g and *X*) can be recognized: one for each physical state of the matrix, i.e. liquid, rubbery and glassy states. In order to identify the physical state of the matrix material (stages I, II and III in Figure 11), the gel point X_{gel} and the evolution of T_g need to be already known, as explained previously. The definition of E_m and v_m is hence given in Eq. 21 and Eq. 22 [28], where the subscripts "*ml*", "*mr*" and "*mg*" stand for liquid, rubbery and glassy states of the matrix respectively. There is a qualitative distribution of the Young's modulus of the resin after the gelation point X_{gel}.

These matrix properties will later on be used in the homogenization for obtaining the orthotropic properties of the composite plies (together with the fibres' material properties).

$$E_m(T,T_g,X)=\begin{cases}E_{ml}(T,T_g,X) & \forall\, X\le X_{gel}\\ E_{mr}(T,T_g,X) & \forall\, X>X_{gel}, \quad T_g<T\\ E_{mg}(T,T_g,X) & \forall\, X>X_{gel}, \quad T_g\ge T\end{cases} \qquad \text{Eq. 21}$$

$$\upsilon_m(T,T_g,X)=\begin{cases}\upsilon_{ml}(T,T_g,X) & \forall\, X\le X_{gel}\\ \upsilon_{mr}(T,T_g,X) & \forall\, X>X_{gel}, \quad T_g<T\\ \upsilon_{mg}(T,T_g,X) & \forall\, X>X_{gel}, \quad T_g\ge T\end{cases} \qquad \text{Eq. 22}$$

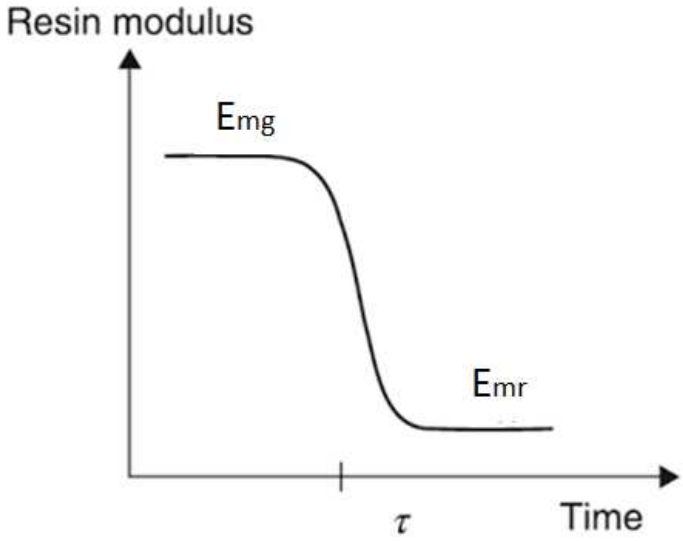

Figure 15: Relaxation behaviour of the Young's modulus of the resin after the gel point (adapted from [29])

If the elastic material model is not enough in order to represent the behaviour of the matrix, a thermovisco-elastic model can also be applied instead [30]. In order to define an expression for the Young's modulus and the stress tensor for such a matrix material (E_m), several equations need to be previously defined [24][28]: the strain ε_{ij} is given in Eq. 23, the reduced time ξ in Eq. 24, the stress tensor σ_{ij} in Eq. 25, the components of the fourth order tensor relating stress to mechanical strain C_{ijkl} in Eq. 26. The parameter a_T is the so called shift factor, which is indeed a material property that can be described using the Arrhenius expression.

$$\varepsilon_{ij}=\frac{1}{2}\left(u_{i,j}+u_{j,i}\right) \qquad \text{Eq. 23}$$

$$\xi=\int_0^t\frac{1}{a_T}d\tau \text{ and } \xi=\int_0^{t'}\frac{1}{a_T}d\tau \qquad \text{Eq. 24}$$

$$\sigma_{ij}(\xi)=\int_0^{\xi}C_{ijkl}(\xi-\xi')\frac{\partial\varepsilon_{kl}(\xi')}{\partial\xi'}d\xi' \qquad \text{Eq. 25}$$

$$C_{ijkl}(\xi)=C_{ijkl_\infty}+\sum_{n=1}^{N}C_{ijkl_n}\exp\left(-\frac{\xi}{\tau_{ijkl_n}}\right) \qquad \text{Eq. 26}$$

As it can be appreciated, Eq. 26 is represented in the form of a generalized Maxwell model (for more information about generalized Maxwell rheological model, consult

[31]), with a total number of elements *N*. With this into account, the Young's modulus of the resin can be defined by Eq. 27, where E_0 is the instantaneous Young's modulus and τ_n the characteristic time of the nth Maxwell element.

$$E_m = E_0\left[1 - \sum_{n=1}^{N} \frac{E_n}{E_0}\left(1 - \exp\left(-\frac{\xi}{\tau_n}\right)\right)\right] \quad \text{Eq. 27}$$

In this thesis, an elastic material model will be used.

- **The fibres:**

The fibres of each ply of the composite material will be assumed to be unidirectional, i.e. oriented only in one direction. Assuming that the fibres exhibit isotropic elastic properties (as done in Samcef), the parameters that ought to be defined are the fibres' Young's modulus E_f, Poisson's ratio v_f and shear modulus G_f. Also, the volume fraction of the fibres with respect to the matrix V_f and the coefficient of thermal expansion in the longitudinal and transverse direction CTE_{f1} and CTE_{f2} [28] should be defined. If the fibres are assumed not to undergo any chemical shrinkage during curing, no other material properties are needed.

- **The homogenization procedure:**

If the mechanical properties of both the fibres and the matrix are known, an homogenization procedure can be applied in order to obtain the properties of the orthotropic ply. The most common way to perform homogenization is following the law of mixtures.

The different parameters to homogenize and their expressions will be given hereinafter for the case of unidirectional plies, as described by the Samcef documentation [28]. It is assumed that the fibres and the matrix are isotropic when studied individually, but transverse isotropic when constructing a laminate.

Firstly, the hydrostatic compressive modulus for the fibres K_f and the matrix K_m should be defined, together with the transverse bulk modulus K_t of the composite material. Their expressions are given in Eq. 28 to Eq. 30, where G_m stands for the shear modulus of the matrix.

$$K_f = \frac{E_f}{2(1-2\nu_f)(1+\nu_f)} \quad \text{Eq. 28}$$

$$K_m = \frac{E_m}{2(1-2\nu_m)(1+\nu_m)} \quad \text{Eq. 29}$$

$$K_t = K_m + \frac{V_f}{\frac{1}{K_f - K_m} + \frac{1-V_f}{K_m + G_m}} \quad \text{Eq. 30}$$

Thanks to these definitions, the elastic coefficients of the homogenized composite material can be described (Eq. 31 to Eq. 36). The numerical subscript in the following formulas correspond to the principal directions of the material, i.e. 1 is the longitudinally in the direction of the fibres, 2 the transversely in plane and 3 transversely through thickness, as sketched in Figure 16.

- Longitudinal Young's modulus E_1:

$$E_1 = E_f V_f + E_m(1 - V_f) + \frac{4V_f(1 - V_f)(\upsilon_f - \upsilon_m)^2}{\frac{V_f}{K_m} + \frac{1}{G_m} + \frac{1 - V_f}{K_f}} \quad \text{Eq. 31}$$

- In-plane Poisson's ratio ν_{12}:

$$\nu_{12} = \nu_f V_f + \nu_m(1 - V_f) + \frac{V_f(1 - V_f)(\nu_f - \nu_m)\left(\frac{1}{K_m} - \frac{1}{K_f}\right)}{\frac{V_f}{K_m} + \frac{1}{G_m} + \frac{1 - V_f}{K_f}} \quad \text{Eq. 32}$$

- In-plane shear modulus G_{12}:

$$G_{12} = G_m \frac{G_f(1 + V_f) + G_m(1 - V_f)}{G_f(1 - V_f) + G_m(1 + V_f)} \quad \text{Eq. 33}$$

- Transverse shear modulus G_{23}:

$$G_{23} = G_m + \frac{G_m V_f}{\frac{G_m}{G_f - G_m} + \frac{(K_m + 2G_m)(1 - V_f)}{2K_m + 2G_m}} \quad \text{Eq. 34}$$

- In-plane transverse Young's modulus E_2:

$$E_2 = \frac{2}{\frac{1}{2K_t} + \frac{1}{2G_{23}} + \frac{2\upsilon_{12}^2}{E_1}} \quad \text{Eq. 35}$$

- Transverse Poisson's ratio ν_{23}:

$$\nu_{23} = \frac{E_2}{2G_{23}} - 1 \quad \text{Eq. 36}$$

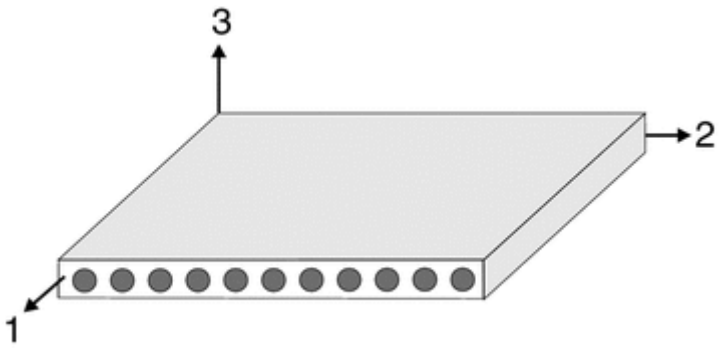

Figure 16: Sketch of the principal directions of a unidirectional composite ply. Direction 1 goes longitudinally in the direction of the fibres, 2 transversely in plane, and 3 transversely through the thickness [32]

Due to the assumption of transverse isotropy, the Young's modulus in directions 2 and 3 are equivalent ($E_2 = E_3$), and so are the out-of-plane Poisson's ratios and shear stresses ($v_{13} = v_{12}$ and $G_{13} = G_{12}$).

On top of the elastic properties, other quantities that will need homogenization are the coefficient of thermal expansion *CTE* and chemical shrinkage *CSh*. Their generic expressions for the matrix can be found in Eq. 37 and Eq. 38. When it comes to the fibres, due to transverse isotropy, CTE_{f2}=CTE_{f3}. Furthermore, the fibres are assumed not to shrink during the curing process.

$$CTE_m(T, T_g, X) = \begin{cases} CTE_{ml}(T, T_g, X) & \forall\, X \le X_{gel} \\ CTE_{mr}(T, T_g, X) & \forall\, X > X_{gel}, \quad T_g < T \\ CTE_{mg}(T, T_g, X) & \forall\, X > X_{gel}, \quad T_g \ge T \end{cases} \qquad \text{Eq. 37}$$

$$CSh_m(T, T_g, X) = \begin{cases} CSh_{ml}(T, T_g, X) & \forall\, X \le X_{gel} \\ CSh_{mr}(T, T_g, X) & \forall\, X > X_{gel}, \quad T_g < T \\ Csh_{mg}(T, T_g, X) & \forall\, X > X_{gel}, \quad T_g \ge T \end{cases} \qquad \text{Eq. 38}$$

The homogenized properties can be calculated per Eq. 39 to Eq. 42 respectively [1]. Again, the subscripts *m* and *f* refer to the matrix and the fibres correspondingly.

$$CTE_1 = \frac{CTE_m E_m (1 - V_f) + CTE_{f1} V_f E_f}{E_m (1 - V_f) + V_f E_f} \qquad \text{Eq. 39}$$

$$CTE_2 = CTE_3 = CTE_m (1 - V_f) + CTE_{f2} V_f \qquad \text{Eq. 40}$$

$$CSh_1 = \frac{CSh_m E_m (1 - V_f)}{E_m (1 - V_f) + E_{f1} V_f} \qquad \text{Eq. 41}$$

$$CSh_2 = CSh_3 = CSh_m (1 - V_f) \qquad \text{Eq. 42}$$

3.4. Review of characterization techniques

The different characterization techniques that may be used in order to determine the required parameters for modelling the curing kinetics and predicting the shape distortions will be explained in this section.

As a FEM user, there is a need to determine the values of the parameters entering the equations presented previously. In this section, the experimental analyses necessary to determine the full set of parameters for the thermal-chemical-mechanical FEM analysis will be reviewed. It will be split in two categories: experiments and identification of the thermo-chemical parameters on one side and of the mechanical analysis on the other. Lastly, a summary of all the characterization techniques will be provided for an easy overview.

The experimental characterization was not performed as part of this thesis, and it is out of the scope. Nevertheless, raw data from Differential Scanning Calorimetry (see later on) was provided by C. Brauner. These results will be used in order to identify the curing kinetic parameters, as well as the enthalpy of the reaction.

The raw data of all the other characterization techniques presented in this chapter was not accessible, but values found in the literature for similar materials are used instead. However, an explanation of these techniques is important to have an overview of the preliminary steps needed in the investigation of process induced distortions of composite structures.

3.4.1. Experiments and identification of the thermo-chemical parameters

- **Differential Scanning Calorimetry (DSC):**

Out of the results obtained from DSC, the cure kinetic parameters will be identified. Furthermore, the enthalpy of the reaction can be easily calculated. Normally, ouy of the DSC results, two other quantities can be obtained: the glass transition temperature and the heat capacity. The accesible measurements were not adequate to measure these last two parameters since more runs at lower temperatures or extra features are needed.

DSC is a technique that consists in measuring the temperature difference between two cells. One is the empty reference cell with a temperature T_R, and the other one contains the sample to study at a temperature T_S. By making a prior calibration, the equipment's thermal resistance dU_S can be determined and the temperature difference can be translated into heat flux dq/dt following Eq. 43. This method allows the quantification of chemical reactions and physical transitions.

$$\frac{dq}{dt} = \frac{T_S - T_R}{dU_S} \qquad \text{Eq. 43}$$

DSC requires the previous specification of a temperature treatment. In brief, two types of treatments can be used: isothermal or dynamic DSC. It exposes both capsules to this treatment while temperature is measured separately at each cell. The isothermal study is run at a constant temperature at each time with a fast temperature ramp until it stabilizes. It is used in order to obtain a relation between the maximum degree of cure X_{max} and temperature. On the other hand, a dynamic study is performed by continuously heating up the samples at one heating rate at a time.

When analysing the temperature at the reference capsule, it is observed to be lower than the specified temperature, since the capsule itself will absorb some heat. Temperature will be even lower for the sample capsule due to the material inside.

The measured temperature is then translated into heat flux. At the end, a graph relating heat flux versus temperature is obtained, as shown in Figure 17. Since the heating or cooling rates are imposed, the dependency on time instead of temperature can be easily obtained.

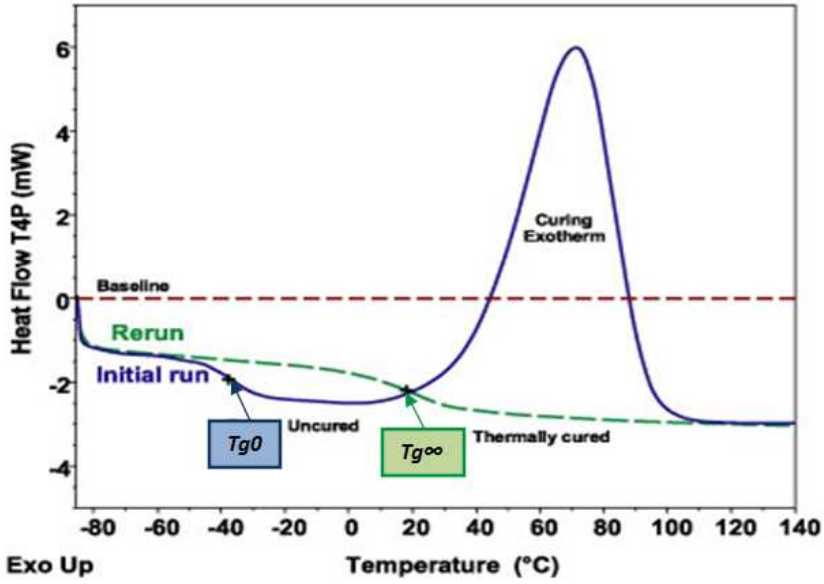

Figure 17: Characteristic DSC graph for the curing of an epoxy resin, depicting heat flow versus temperature. The characteristic transitions for this kind of materials are shown. Exothermic reactions are depicted with positive variations, whereas endothermic by negative (adapted from [33])

The blue curve in Figure 17 represents the behaviour of an initially uncured resin subjected to a dynamic temperature cycle. Then the sample is cooled down to the initial temperature of -80ºC, and the temperature is set to rise again following the same cycle as previously. The following observations can be made:

- A straight line happens if no transition has taken place. The temperature difference between both cells will be constant and equal to a value proportional to the calorific capacity of the sample material.
- The glass transition temperature T_g is a second order reversible transition that exhibits enthalpy relaxation or, in other terms, it involves just a change in calorific capacity, not in the material latent heat (energy needed for a material to change phase from solid to liquid or from liquid to gas). The calorific capacity of a material in glass state is different from the one that it will manifest above its T_g.
- Curing is represented by exothermic peak, or in other words, a transition that release heat when occurring. The area under the exothermic peak represents the total enthalpy of curing if the reaction has been completed.
- The T_g can be seen to be lower for the uncured material (T_{g0} in the blue curve) than for the cured resin ($T_{g\infty}$ in the green curve). For the latter one, since fully curing is achieved, no residual exothermic peak can be visible.

The temperature difference between the sample and the reference capsule at the beginning of the experiment is proportional to the calorific capacity C_p of the sample. The calculation can be performed following Eq. 44. This is a very simplified approach if the composite is assumed to be isotropic (or for the neat resin). Otherwise, the C_p may to be obtained at the direction of each material axis, i.e. direction of the fibres, orthogonal to the fibres and through thickness.

$$C_p = \frac{\Delta T}{q} = \frac{{}^{q}/_{t}}{{}^{\Delta T}/_{t}} \equiv \frac{Heat\ flow}{Heating\ rate} \qquad \text{Eq. 44}$$

Other more accurate ways of determining C_p are the sapphire method, or the use of ADSC (temperature-modulated DSC that allows the separation of overlapping effects in DSC curves, such as the enthalpy relaxation happening at T_g) among others.

- Sapphire method [34]: DSC signals of the sample and the calibration are compared with each other after correcting for the capsule and three measurements are performed. The first one of the empty crucible (curve a in Figure 18), the second (curve b) of the sample, and the third one of the calibration set (three small sapphire disks). The computation of the heat capacity of the sample will be performed following Eq. 45, where m_s and m_r are the masses of the sample and the reference respectively, and C_{pr} is the heat capacity of the reference capsule (curve c).

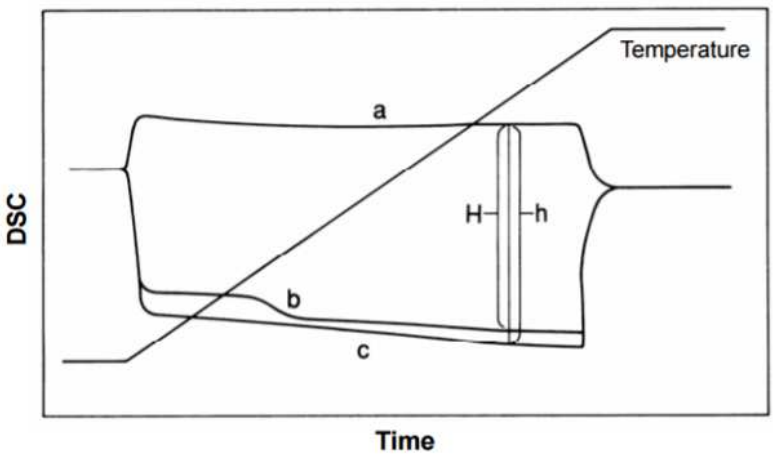

Figure 18: DSC measurements for the calculation of specific heat capacity of a sample [34]

$$C_p(t) = \frac{a(t) - b(t)}{a(t) - c(t)} \left(\frac{m_s}{m_r}\right) C_{pr}(t) \qquad \text{Eq. 45}$$

- Alternating-DSC method: ADSC is a temperature modulated DSC where the measurements are carried on with (normally) sinusoidal heating and cooling treatments and added to the average heating rate in order to create fluctuations. Three measurements are needed: the empty crucible, the sample and the reference material (aluminium in most of the cases). Using ADSC it is possible to separate the effects of different reactions that coincide in a certain time or temperature region. The heat flow resulting from the sinusoidal heat treatment is periodic as well. The heat flow is a known to be a superposition of an in-phase (reversing phenomena) and an out-of-phase (non-reversing phenomena) components. The specific heat capacity is then determined using the reversing part of the heat flow [1], [35].

- **Thermal Mechanical Analysis (TMA):**

A TMA is used in order to measure some dimensional properties of the material, such as the coefficient of thermal expansion *CTE* (due to thermal contraction) or the coefficient of chemical shrinkage *CSh* (due to molecule cross-linkage). However, these two properties will be included in the mechanical analysis of the structure since they are the main reason for the existence of process induced deformations of composite structures. In other words, they do not contribute to the curing kinetics.

However, TMA is considerably more sensitive than other characterization techniques (such as DSC) for the estimation of T_g [36]. The result out of a TMA is a plot showing the probe position versus temperature. An example corresponding to an epoxy resin can be seen in Figure 19.

The TMA probes are in contact with the sample exerting a negligible load. When the sample expands, the probe is pushed due to the expansion of the material and the probe displacement is measured. Different probe shapes are available so that the test conditions can be ideal: compression, flexure, dilatometry, extension, etc.

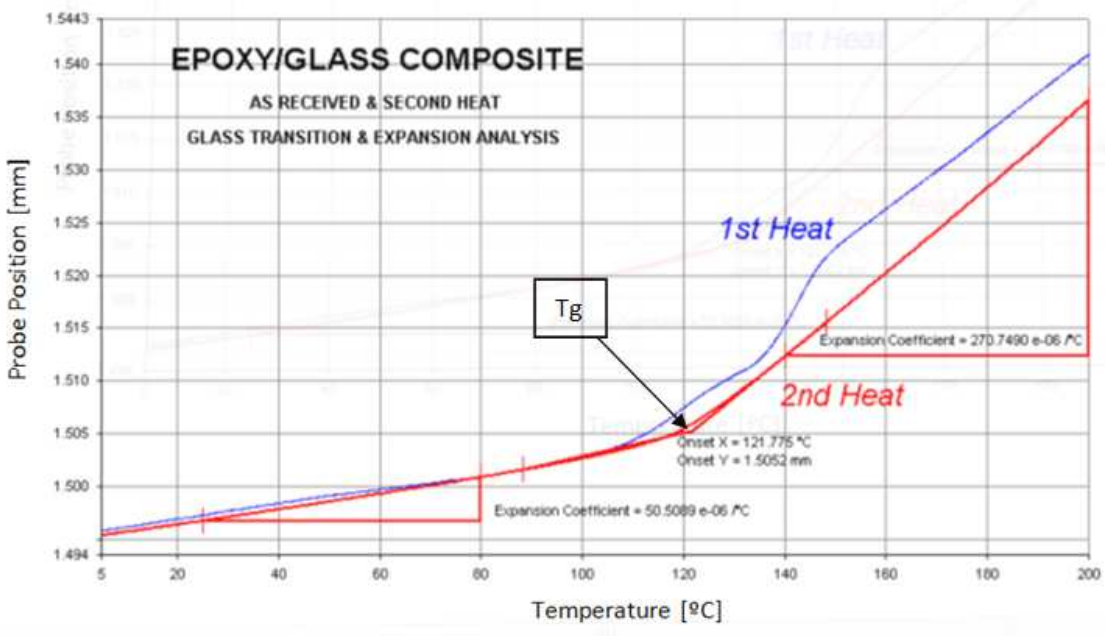

Figure 19: TMA results for an epoxy resin, showing the determination of thermal expansion coefficients and T_g [36]

- **Thermo-Gravimetric Analysis (TGA):**

TGA is a technique where the mass of a material is recorded as a function of the temperature, or as a function of time (for isothermal conditions), while it is subjected to a specified thermal treatment. Samples are placed inside a sample pan that is hanging from a balance. The pan is situated inside a furnace, which is in charge of heating or cooling the sample during the experiment. The balance measures very precisely the change in mass of the sample while the experiment is being carried out.

In order to properly design the temperature profile, the maximum temperature should be high enough so that the material has completed all chemical reactions and the weight becomes stable [37]. The temperature limit where the resin degrades gives an estimation of its thermal stability. An example of the results obtained from TGA can be seen in Figure 20, where the plot shows the relation between the mass of the epoxy sample and the time in isothermal conditions.

TGA can be used to study the change in mass during curing of the resin, and use this result to correct the DSC curves for the mass lost during the curing procedure. Depending on the material, the correction can amount to more than 30 W/g [38].

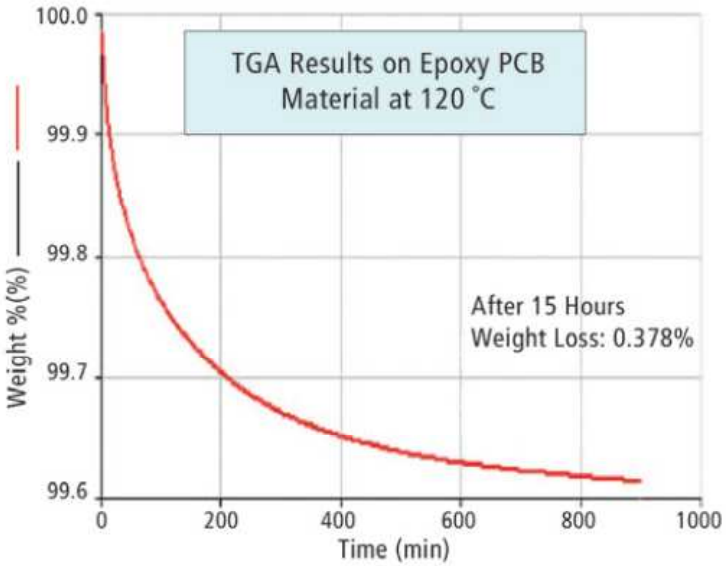

Figure 20: TGA results on mass loss of a sample of epoxy resin with encapsulated printed circuit boards (PBC) during an isothermal heat treatment at 120°C [39]

- **Laser Flash Analysis (LFA):**

LFA is used in order to acquire an estimate of the thermal conductivity (λ) or diffusivity (a) of a material. It is a technique that offers quick measurements over a wide interval of temperature and diffusivity values. The measurements are made by subjecting one face of sample to an impulse of energy, up to one millisecond of duration, emitted by a laser. The device quantifies the increase of temperature at the back face of the sample, and hence the thermal diffusivity is computed. The typical result by TFA can be seen in Figure 21 for a carbon fibre woven epoxy composite [40], where the temperature rise in percentage is represented as a function of a non-dimensional time (normalized by the time to achieve 50% of the temperature at the imposed temperature). The time required for the back face of the sample to reach a certain amount of temperature rise (in percentage) is used to calculate the diffusivity a, according to Eq. 46.

$$a = \frac{K_y \tau}{t_y} \qquad \text{Eq. 46}$$

where K_y is a constant related to a change in temperature of y %, t_y the time to achieve it and τ is once again the thickness of the sample.

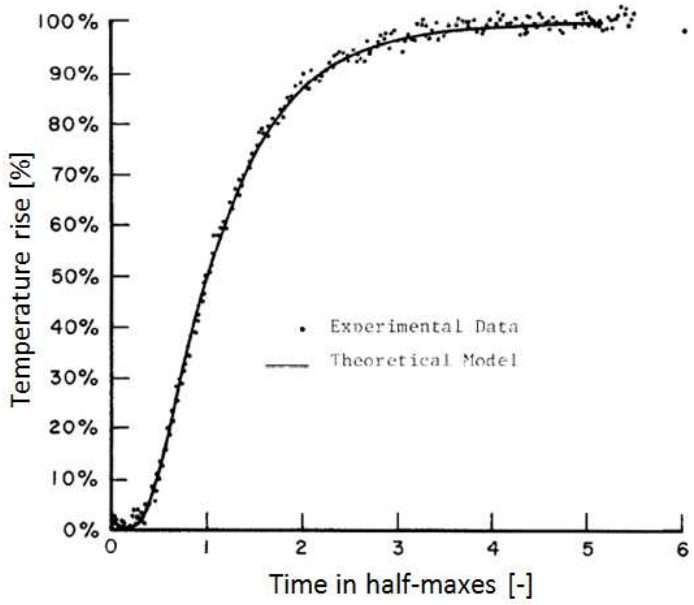

Figure 21: Temperature increase at the back face of the sample in percentage versus a non-dimensional time for a carbon fibre epoxy composite [40]

From the thermal diffusivity a and the specific heat capacity C_p (obtained using DSC, as explained before), one can compute the thermal conductivity λ of the sample [41], provided the density ρ of the material is known. The expression used to calculate the thermal conductivity is shown in Eq. 47.

$$\lambda = a(T)C_p(T)\rho(T) \qquad \text{Eq. 47}$$

3.4.2. Experiments and identification of the mechanical parameters

- **Dynamic Mechanical Analysis (DMA):**

Dynamic Mechanical Analysis is a procedure used when trying to evaluate the damping, viscosity or complex modulus of a material by applying either a controlled stress or strain on the sample. The properties are evaluated as a function of time, temperature, frequency or applied stress. The technique is found to accurately capture the motion of polymer chains in order to assess polymer transitions, being therefore able to determine the T_g. The usual way to characterize resins using DMA is by setting a temperature programme that reaches high temperatures, simulating a curing profile, and hence extracting important information on the procedure [42]. An example of a DMA analysis on a carbon fibre prepreg can be seen in Figure 22.

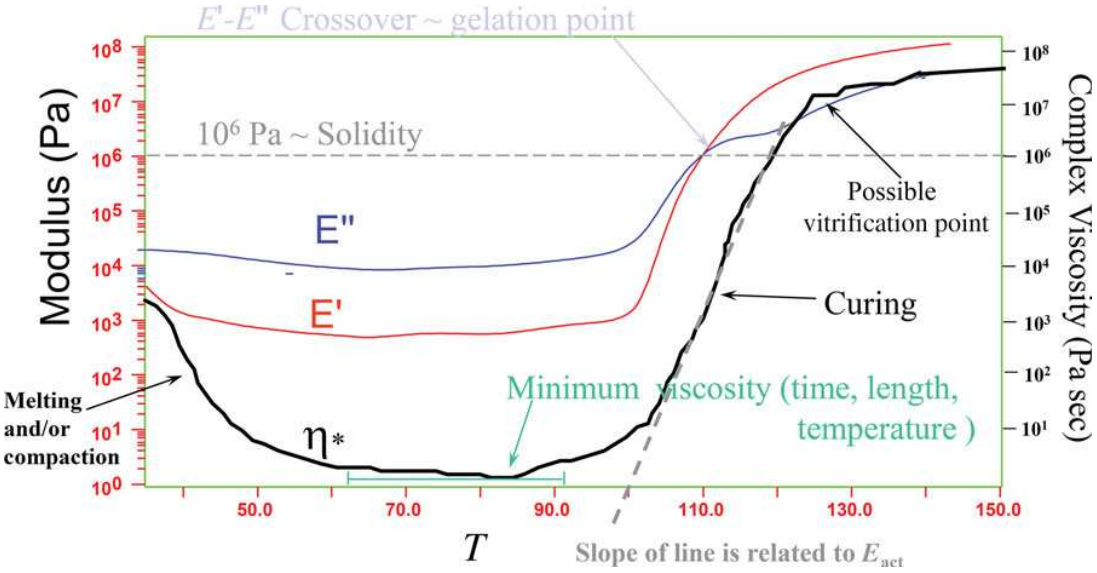

Figure 22: DMA analysis of the curing process for a beta staged carbon fibre prepreg [42]

Some parameters of importance can be obtained using DMA testing due to its capacity of evaluating modulus and viscosity at any time during a temperature scan. This way, an estimation on the best time to apply pressure during a curing process of a thermosetting resin can be assessed.

The minimum viscosity η can be determined from the graph (minimum of complex viscosity η^*), and consequently the time that the sample remains with that value η_{min}. The gelation point (where both the storage modulus E' and the loss modulus E'' curves cross) and the vitrification point can also be estimated. E' represents the elastic part or the energy stored, whereas E'' represents the viscous part or the dissipated energy to heat.

When the curing phenomenon starts, the viscosity suddenly increases. The point where E' overcomes E'' gives an approximate of the gel point of the material. However, Winter et al. [43] discovered that the gelation point is not exactly located at the cross point of E' and E'' but at the point where the damping ($tan\ \delta$ defined as the coefficient of E'' over E') becomes momentarily independent of the frequency of excitation.

Furthermore, the slope corresponding to the curing phenomenon can be used to estimate the activation energy E_a [42]. When the curve starts to get horizontal again, it indicates the vitrification point of the material.

- **Thermal Mechanical Analysis (TMA)**

A TMA, apart from being used to determine T_g as attained before, is used to measure some dimensional properties of the material, such as the coefficient of thermal expansion *CTE* (due to thermal contraction) or the coefficient of chemical shrinkage *CSh* (due to molecule cross-linkage) in conditions of constant or varying

temperature. In composites, matrix expansion or shrinkage, either from thermal or chemical nature, is a vital parameter so that process induced distortions are calculated. Both chemical and thermal expansions are a result of heat transfer within the material and, therefore, are coupled. *CSh* becomes difficult to calculate due to a few reasons: the strong coupling between chemical and thermal shrinkage, exothermic curing that affects the reaction, the volume changes when the resin is cured and the fact that the apparent shrinkage is much lower than the real chemical shrinkage [44].

Determination of *CSh* with TMA technique is performed using the dilatometry probe. Although possible, this method may not be the easiest or the fastest. Extra information needs to be retrieved from DSC (degree of cure) or from testing of partially cured samples. Hong Yu et al. [45] measured *CSh* using the correlation between DSC and TMA, as can be seen in Figure 23 for an epoxy resin. Stage III in the DSC thermogram in the inset of Figure 23 corresponds to the cross-linking zone, or in other words, where curing of the resin occurs. They found that the time required for curing (using DSC data) was the same amount than for the dimension change according to TMA, and it was affected by changes in curing rates or curing temperature. Hence, the chemical shrinkage can be determined using the dimensional change in that stage III, using Eq. 48. Furthermore, *CSh* is calculated as the slope of the curve of cure shrinkage versus degree of cure, as displayed in Figure 23.

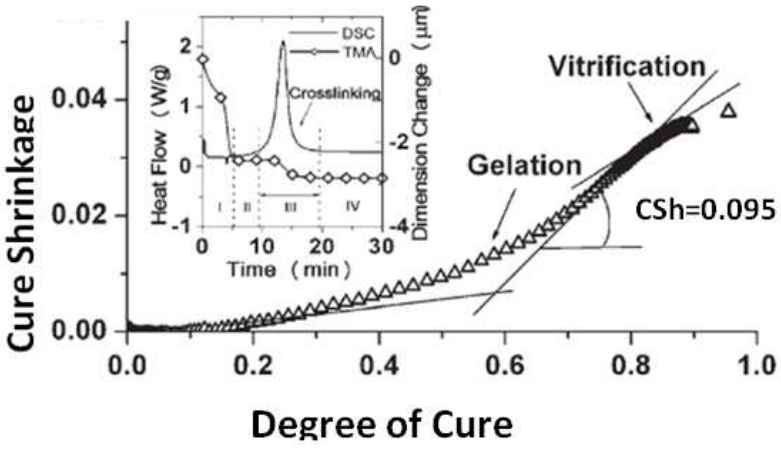

Figure 23: Correlation between cure shrinkage and degree of cure at 110°C performed by combining the change in dimension measured by TMA and the heat flow obtained using DSC, depicted in the inset, for an epoxy resin (adapted from [45])

$$Chemical\ shrinkage = \frac{\Delta\tau(t)}{\tau_0 - d} \qquad \text{Eq. 48}$$

where τ_0 is the initial thickness of the part, d is the dimensional shrinkage happening in stage I (due to the decrease of viscosity when heating and probe loads) and $\Delta\tau(t)$ is the change in dimension at a time t during the third stage.

The thermal expansion coefficient (CTE) can be calculated below the T_g as per Eq. 49 [39], where $\Delta L/\Delta T$ is the change in elongation during the temperature interval ΔT and L_0 is the initial elongation of the sample. Past the T_g, due to the partially cured state of the material, the CTE measurement becomes inaccurate. In order to properly determine it, a fully cured sample of the material has to be submitted to a temperature past the $T_{g\infty}$ and, because the material does not chemically shrink anymore, the CTE can be estimated.

$$CTE = \frac{\Delta \mathrm{L}}{\Delta \mathrm{T}\ \mathrm{L}_0} \qquad \text{Eq. 49}$$

- **Rheometer:**

A rheometer is used to study the deformation and fluidity of materials under prescribed forces and nowadays is normally equipped with DMA capability. Thermosetting resins and based composites show complex rheological properties since the viscoelasticity varies as a function of external conditions such as temperature or time of exposure. To properly study the curing process of thermosets, rheological analysis are a fundamental tool to complement DSC studies.

Rheometer testing is normally performed with an external oscillatory force that will impose a stress (or strain) of sinusoidal shape and measuring the produced strain (or stress) and phase angle between the signals. For a viscoelastic material, as it is the case of interest in this project, should lie between 0 (perfectly elastic) and 90 degrees (perfectly viscous) [46]. To identify the gel point, a shear rheological test may be performed. The test is normally carried out in three different ways:

- A oscillatory torsional force is applied on a small sample of resin at a constant frequency and amplitude of about 1Hz and 0.1% strain respectively, as sketched in Figure 24. The temperature is set to vary at a certain rate while the resistance to the rotation is measured, as well as the viscous resistance. The gel point will be encountered when these two parameters are equal.
- Isothermal conditions, fixing strain and frequency of excitation while measuring the viscoelastic properties with time. This way, a plot similar to that of Figure 22 showing the crossing point (approximately the gel point) between the storage and the loss modulus can be plotted [46]. This technique could also be performed using DMA.

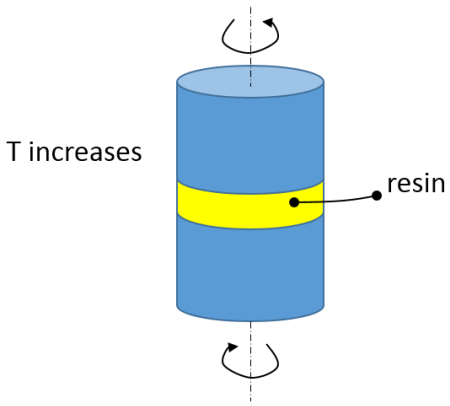

Figure 24: Sketch of a shear rheological test performed in a resin with the aim of finding its gel point

- Performing a time sweep upon a test where two or more independent mechanical waves (with different frequencies) are applied simultaneously. The total strain should be the addition of the strains created by each individual excitation. The gel point is then defined using Winters et al. [43] definition, as the point where *tan δ* remains constant regardless of the frequency of excitation, as can be seen in Figure 25. Multiple wave analyses are not always offered by DMA.

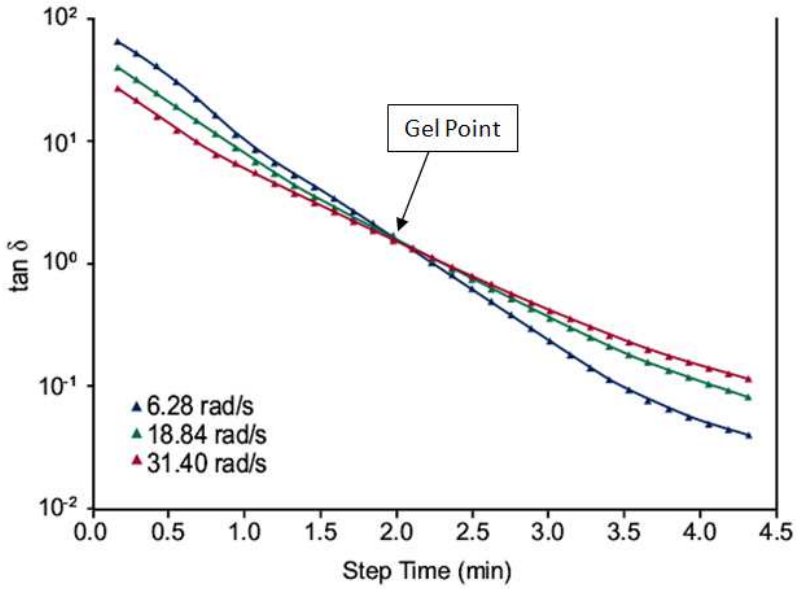

Figure 25: Time sweep multi-wave rheological test performed for the identification of the gel point during the cure of an epoxy resin [46]

3.4.3. Summary of characterization techniques

A summary of all the necessary parameters to perform the thermo-chemical and mechanical simulations to predict the deformation due to the curing of a thermosetting based composite will be given in Table 1. The tabulated information also includes the required characterization technique to be used to identify them. Note that the elastic properties of the fibres themselves are not tabulated since regular characterization techniques will be used for that purpose e.g. standard tensile test.

	DSC	TGA	DMA	TMA	Shear rheological measurement	Laser flash
X_{gel}			X		X	
λ						X
CTE				X		
CSh				X		
Cure kinetic model	X					
Cp	X (ADSC)					
E_m			X	X		
G_m			X	X		
ν_m				X		
T_g	X		X	X		
Vitrification point	X		X			

Table 1: Summary of characterization techniques used in order to find the necessary parameters to perform the thermo-chemical and mechanical simulation of a curing thermosetting based composite to predict manufacturing induced deformations

4. Cure kinetic parameters identification and validation

This chapter focuses on the thermal part of the curing simulation, including the optimization procedure followed for the identification of the curing kinetic parameters for a certain resin. The results will be validated for isothermal and dynamic DSC runs against the ones reported by C. Brauner [1].

The main focus of this chapter, and one of the big challenges of this thesis, is the procedure followed to identify the cure kinetics parameters from the DSC results provided by C. Brauner. Firstly, the experimental degree of cure and curing rate was calculated from the raw DSC data. Secondly, the dynamic DSC runs were utilized in order to calculate the total enthalpy of the curing reaction, and the average value was used. With this into account, a non-linear optimization algorithm following Levenberg-Marquadt was developed using Matlab. As a result, the different kinetic parameters (m, n, k_1, k_2 and b for diffusion control) were obtained using the isothermal DSC curves for two different cases: Kamal Sourour model (Eq. 13) and Kamal Sourour extended for diffusion control (Eq. 19 and Eq. 20). These two different approaches will be compared, and a conclusion can be withdrawn for the necessity of including diffusion control on the resin modelled in this project, RTM6.

From the values of k_1 and k_2 obtained at isothermal curing conditions, the activation energies E_{a1} and E_{a2} and the Arrhenius pre-exponential factors A_1 and A_2 (remember Eq. 15) can be calculated using the so-called Kissinger plot. Then, using these parameters and the same Matlab code mentioned before, the curing kinetics at dynamic curing conditions can be modelled.

The analytical curves of degree of cure and curing rate will be superposed to the experimental curves to check for the validity and the accuracy of the fit. In general, it can be seen that at higher isothermal curing temperatures and at faster heating rates in dynamic curing, the fit better resembles the experimental measurement. Furthermore, the analytical results obtained in this thesis will be compared to the results reported by C. Brauner [1], who also used Kamal Sourour with diffusion control. The main difference between these two sets of results are at high degrees of cure for lower isothermal curing temperatures. The results obtained in this thesis resemble slightly better the experimental ones.

4.1. Glass transition temperature T_g

The first thing to point out is that the T_g is actually a temperature range in which the motion of the resin's molecular chains is increased, rather than a precise temperature value. DSC can be used to identify T_g, which will appear as a drop in heat flux. The value of T_g that is used and reported is the midpoint of that temperature drop, although other methodologies can be used. The glass transition temperature for the uncured (T_{g0}) and for the cured resin ($T_{g\infty}$) can be both estimated (remember Figure 17). When considering thermosetting resins, the uncured material glass

transition temperature is observed to be below zero Celsius degrees, whereas $T_{g\infty}$ can be up to around 140°C [16].

For that reason, in order to get T_{g0} and $T_{g\infty}$, the temperature programme needs to be designed with an initial cool down (~-100°C) followed by heating up the sample until the resin is fully cured. The sample is then cooled down to room temperature, and re-heated to determine $T_{g\infty}$.

These two parameters can be inserted in DiBenedetto's equation (Eq. 18) so that the dependence of the instantaneous T_g can be found as a function of the degree of cure X. Having such a relation can become handy if a diffusion model is desired to be included in the curing kinetics, as explained by Karkanas et al., [27] and given per Eq. 16 and Eq. 17. Since the appropriate DSC curves were not available for this study, diffusion will be included following Fournier's approach (see section 3.3.2).

4.2. Identification of parameters of the kinetic reaction

All parameters that are needed for the cure kinetics model can be found using the results from DSC and accepting the assumption that the heat flow is proportional to the degree of cure X. By studying the exothermic peak corresponding to the curing process of the resin, X can be calculated from experimental data via Eq. 7, and by performing a numerical differentiation, the curing rate can be found. In order to do so, the total enthalpy of the reaction needs to be calculated by integrating the exothermic peak. This calculation becomes more accurate if performed in dynamic DSC runs. The reason is that in isothermal DSC runs, the beginning of the exothermal peak is hidden by the start of the thermal treatment, i.e. the quick temperature rise in order to reach the design curing temperature. Furthermore, by performing isothermal runs, the resin may not undergo the complete curing reaction.

To build the theoretical model, both isothermal and dynamic DSC should be performed. The DSC data used for fitting and developing the cure kinetics model was provided by C. Brauner, who used it as well in his PhD Thesis [1].

This chapter will study two different methods. The first one will ignore diffusion control, whereas the second one will include it. A comparison can be made between these two cases, and a conclusion on the necessity of including diffusion control can be made.

In this work, the following procedure was followed using the Matlab software:

1) Select the baseline of the exothermic curing peak at each temperature (see above in Figure 26).
2) Calculate experimental degree of cure X (Eq. 7) and curing rate $\frac{dX}{dt}$ by performing a numerical differentiation.

3) Apply Kamal Sourour model (Eq. 13 if no diffusion is considered and Eq. 19 if it is) with a set of guessed initial parameters k_{10}, k_{20}, m_0 and n_0.
4) Define an error function for $\frac{dX}{dt}$ as the difference between the results using Kamal Sourour model and the experimental data.
5) Run an optimization code that minimizes that error using a non-linear robust least square method using Levenberg-Marquadt algorithm. The optimization procedure will give as a result the final fitting parameters k_1, k_2, m and n.
6) Add diffusion control if needed (Eq. 20), and repeat steps 3 to 5, to find the extra diffusion parameter b.
7) Repeat steps 1 to 6 for all isothermal curing temperatures available.
8) With the data from all the available isothermal DSC runs, estimate the activation energies E_{a1} and E_{a2}, and the Arrhenius pre-exponential constant A_1 and A_2 from the Kissinger plot ($\ln(k_i)$ versus $1/T$).
9) Check the model against the experimental results.

Two different approaches can be followed for the optimization of the fitting parameters. The first one assumes that the reaction rates m and n are constant with temperature, and therefore all isothermal and dynamic DSC runs will have the same values, as followed by Brauner [1], Karkanas et al. [27], etc. On the other hand, the reaction orders can be assumed to vary with temperature, as applied by Ryan and Dutta [47], Zhao and Hu [48] and others. Both methods have shown similar accuracy when fitting experimental results. For that reason, and bearing in mind simplicity and faster speed of calculation, the second method was applied.

The material is a RTM6 resin. A value of the total enthalpy of the reaction of 424 J/mol was measured. This is obtained by averaging the results calculated from integrating the exothermic DSC peak for several temperatures.

4.2.1. Isothermal DSC

An example for a DSC run, showing heat flow versus time, can be seen in Figure 26 for an isothermal curing temperature of 160 and 180^{o}C (baseline visible in red). Similarly, the same curves for the rest of the tested DSC runs are available in Appendix I.

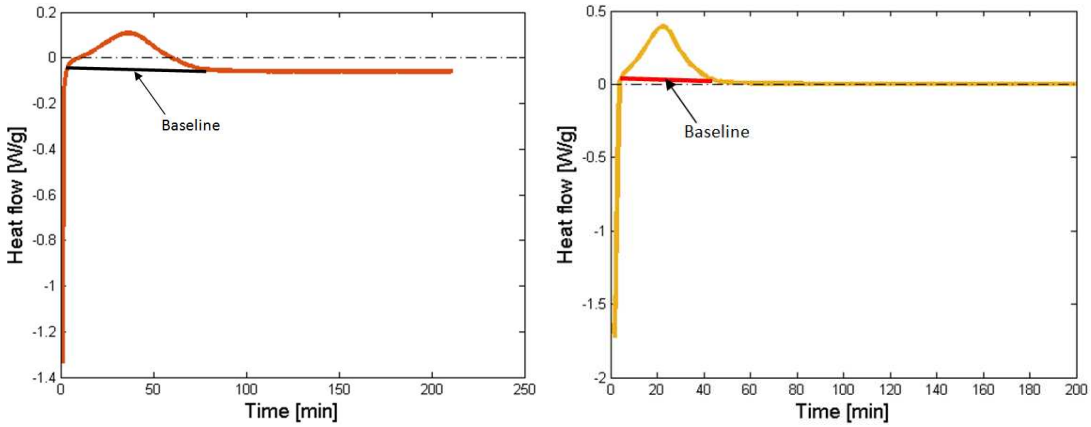

Figure 26: Example of an isothermal DSC measurement of the resin RTM6 at an isothermal temperature of 160 (left) and 180°C (right) (provided by C. Brauner [1]). The selected baseline can be seen in red

Once the experimental degrees of cure are obtained directly from the experimental DSC results, the code developed in Matlab, and presented at the beginning of section 4, was used. As a result, the analytical degrees of cure and curing rates can be accessed, together with the appropriate fitting parameters to adapt Kamal Sourour to the experimental curves.

The experimental degree of cure and curing rate are represented by coloured solid lines in Figure 27 and Figure 28 respectively for three different isothermal temperatures provided (140, 160 and 180°C). The black dashed lines correspond to the analytical model developed using the procedure above described.

For isothermal DSC runs, the final degree of cure can be seen to vary with isothermal curing temperature. The higher the isothermal curing temperature, the higher the maximum degree of cure, and the faster it gets to that amount of cure. For the lowest temperature treated, the amount of curing achieved is relatively far from the theoretical maximum of 1, i.e. $X_\infty \approx 0.87$, 13% lower. On the contrary, for high temperatures, as can happen at 180°C, the maximum degree of cure might exceed that maximum possible value of 1, which is not physically realistic. The reason might be an improper selection of the baseline of the exothermic peak, although no clear explanation has been found in the literature, where similar cases were reported. Nevertheless, if a careful selection of the baseline is performed (by trial and error) a very accurate fit can be obtained for high temperatures, as shown above in Figure 27.

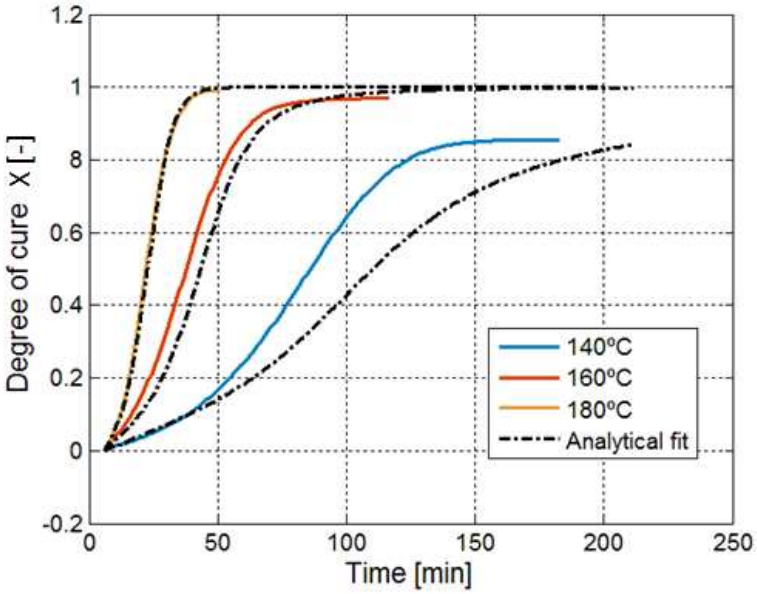

Figure 27: Isothermal DSC results for degree of cure at different temperatures (140, 160 and 180°C) in solid lines. Analytical fitting model in dashed lines

If a less appropriate baseline selection is used and degrees of cure higher than unity are obtained, the inaccuracy will induce more errors in the fit of all studied temperatures. In order to minimize this effect, while still being consistent, the code can be changed so that the values of *X* higher than one are disregarded from the fitting optimization.

Similarly, the analytical fit adequately represents the curing kinetics at temperatures higher than 160°C for this resin, once it is taking into consideration the impossibility of reaching an *X* higher than one. For lower temperatures (140 and 160°C), the theoretical degree of cure does not seem to reach a plateau as in the experimental data, but it continues increasing instead. Specially for the lowest temperature of 140°C the fit does not resemble at all the experimental degree of cure. Obviously, the analytical fit needs to be improved for lower temperatures. This improvement can be achieved, as briefly mentioned in the literature review, by including a diffusion control parameter in the curing kinetics model.

Regarding the curing rate, it can also be seen to be dependent on the isothermal curing temperature. The higher the temperature, the faster the curing reaction occurs. It can also be observed how, in general, the analytical model slightly overpredicts the curing rate at the start of the reaction. Furthermore, the fit at 180°C resembles almost perfectly the experimental data. However, for the other two curves, it can be appreciated that the fit at 160°C is somehow better than at 140°C, although both of them shifted in time.

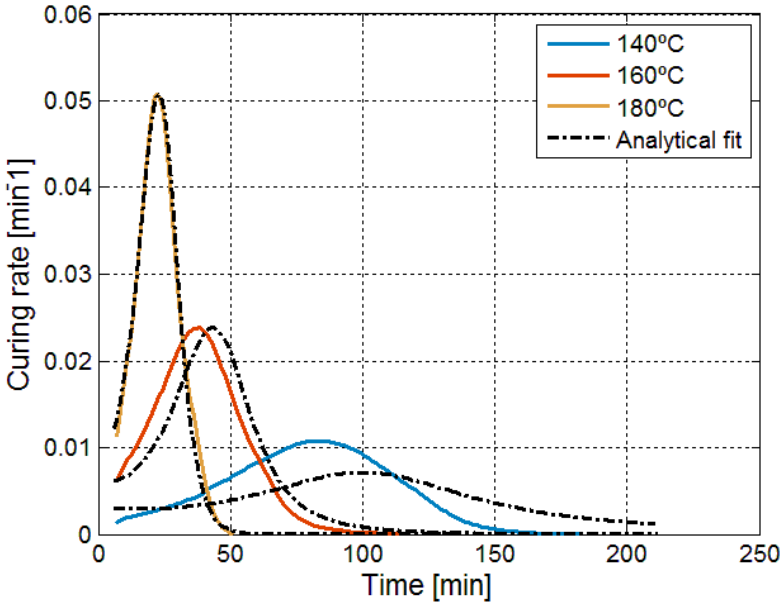

Figure 28: Isothermal DSC results for curing rate at different temperatures (140, 160 and 180°C) in solid lines. Analytical fitting model in dashed lines

As explained before, the model without accounting for diffusion may deviate from the experimental data. If that happens, it could mean that the curing phenomenon is mainly driven by diffusion at those stages. For this reason, the second method of simulating the curing kinetics correspond to the extension of Kamal Sourour for diffusion control, as proposed by Fournier (Eq. 19 and Eq. 20). This method is implemented to compare it with the previous one and show how it can overcome the limitation of the previous model for low curing temperatures at high degrees of cure. By introducing the diffusion control and re-running the optimization programme with the extra fitting parameter *b*, a better accuracy may be attained. Following this procedure, the parameters k_1, k_2, *m* and *n* still enter in the optimization procedure. The results including diffusion can be seen in Figure 29 for the degree of cure, and in Figure 30 for the curing rate and the fitting parameters obtained are reported in Table 2.

As it can be appreciated in Figure 29, the behaviour of the model at higher degrees of cure is clearly enhanced by including diffusion control for low temperatures (140°C in the graph). The final degrees of cure are appropriately predicted and coincident with the experimental data. There also exist a slight improvement in the curve at 160°C since, contrary to what happened previously, the analytic fit reaches a plateau at the same degree of cure as the experimental curve.

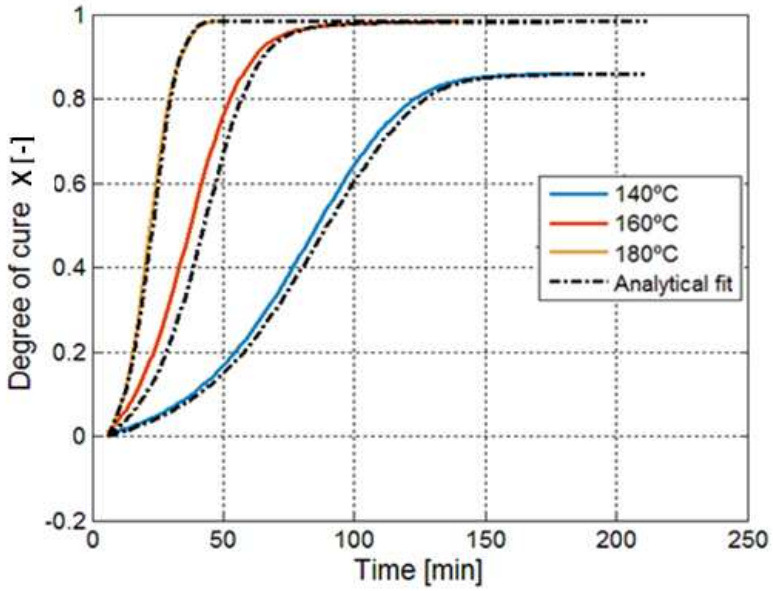

Figure 29: Isothermal DSC results for degree of cure at different temperatures (140, 160 and 180°C) in solid lines. Analytical fitting model including diffusion in dashed lines

Similarly, the improvement in the quality of the fit in Figure 30 compared to Figure 28 is also visible when including diffusion control. Hence, it is possible to state that diffusion control needs to be implemented for this resin RTM6 since it helps the model to fit the curves at low curing temperatures, although no real effect can be seen for high temperatures.

Temperature	k_1	k_2	m	n	b
140 °C	0.0019	0.0553	1.2150	1.3110	0.0263
160 °C	0.0050	0.1112	1.2168	1.0932	0.0155
180 °C	0.0125	0.2100	1.2000	1.0915	0.0036

Table 2: Fitting parameters obtained for the three studied DSC runs at isothermal conditions, including diffusion control.

Note that the fitting parameters obtained using optimization cannot be used to explain the chemistry or the physics behind the curing phenomenon. They are just some parameters that aid to apply a phenomenological model. In other words, the calculated reaction orders m and n are different from the true chemical reaction orders. On the other hand, the parameters k_1 and k_2 should verify the Arrhenius relation of Eq. 15. With the data of all available runs, the activation energies (E_{a1} and E_{a2}) and the pre-exponential factors (A_1 and A_2) can be obtained from the Kissinger plots (Figure 31). In order to do that, the natural logarithm of the values of k_1 and k_2 reported in Table 2 are represented versus the inverse of the corresponding temperature . A linear fit needs to be superposed. The pre-exponential factors A_1 and A_2 are found as the exponential of the value at which the linear fit cuts the y axis. The activation energies are defined as the absolute value of slope of the linear fit times the constant R (8.31447 J/g mol K). The values obtained using this procedure are reported in Table 3.

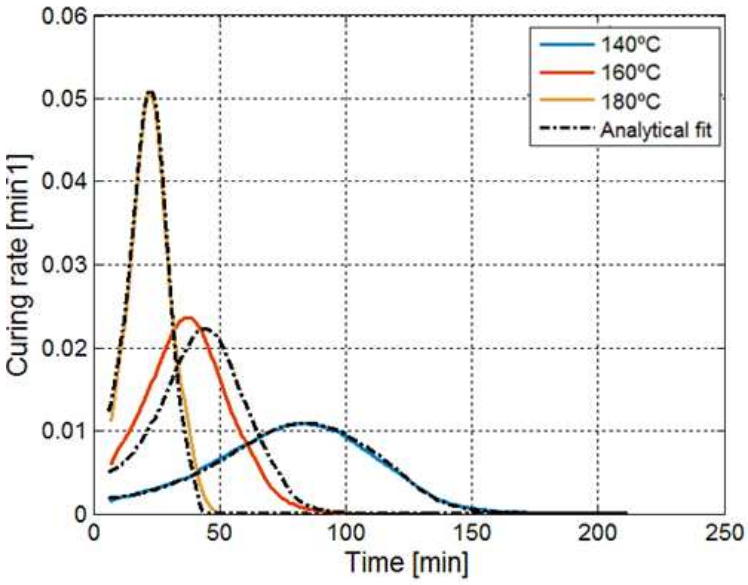

Figure 30: Isothermal DSC results for curing rate at different temperatures (140, 160 and 180°C) in solid lines. Analytical fitting model including diffusion in dashed lines

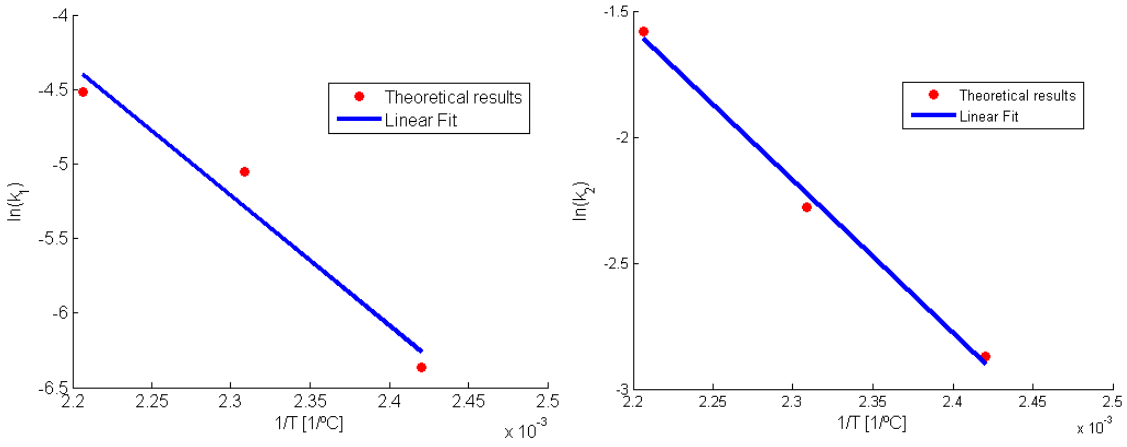

Figure 31: Kissinger plot relating the natural logarithm of k_1 (left) and k_2 (right) with the inverse of the temperature

A_1 [1/s]	A_2 [1/s]	E_{a1} [J/mol]	E_{a2} [J/mol]
3.883e6	2.017e5	73661	51883

Table 3: Values of Arrhenius pre-exponential factor and reaction activation energies obtained from the Kissinger plots

4.2.2. Dynamic DSC

The DSC results for the dynamic runs used in this thesis were also provided by C. Brauner. The DSC result of the slowest and highest heating rate available (2 and 20°C/min) is provided in Figure 32 with the selected baseline depicted in red. The rest of the heating rates will be given in Appendix I.

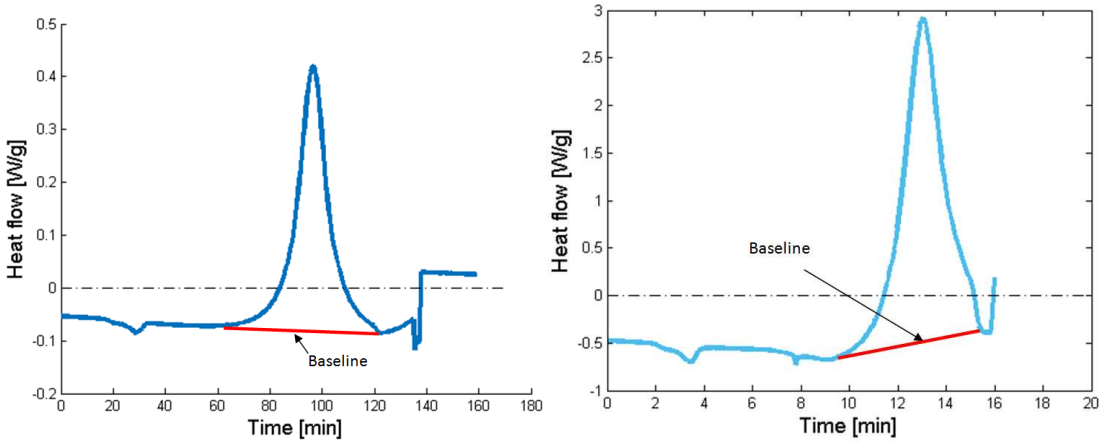

Figure 32: Example of a dynamic DSC measurement of the resin RTM6 at heating rate of 2 (left) and 20ºC/min (right) (provided by C. Brauner [1]). The selected baseline can be seen in red

With the calculated activation energies and Arrhenius' pre-exponential factors, the temperature dependent rate constants k_i can be calculated as a function of the instantaneous temperature (following Eq. 15) that is prescribed for the dynamic DSC runs. Kamal and Sourour model was then applied for each DSC curve at different heating rates, and an optimization was performed in order to obtain the reaction orders *m* and *n* using the same methodology as for the isothermal DSC runs.

The same type of results can be obtained for dynamic DSC runs and are shown in Figure 33 and Figure 34. Since it has been already shown that diffusion control is necessary for an adequate fit, only the results with diffusion control will be reported in this thesis. Besides, diffusion control was also found to help when modelling the dynamic cure kinetics of RTM6.

The prediction of the degree of cure for all heating rates is very accurate. For lower temperatures small deviations can be seen for low and high curing degrees, overpredicting the experimental curves. When studying the curing rate (Figure 34), it can be seen that the model underestimates the maximum value, although in this case, better agreement is found for the lower heating rates. Nevertheless, the overall shape of the model agrees with the experimental values.

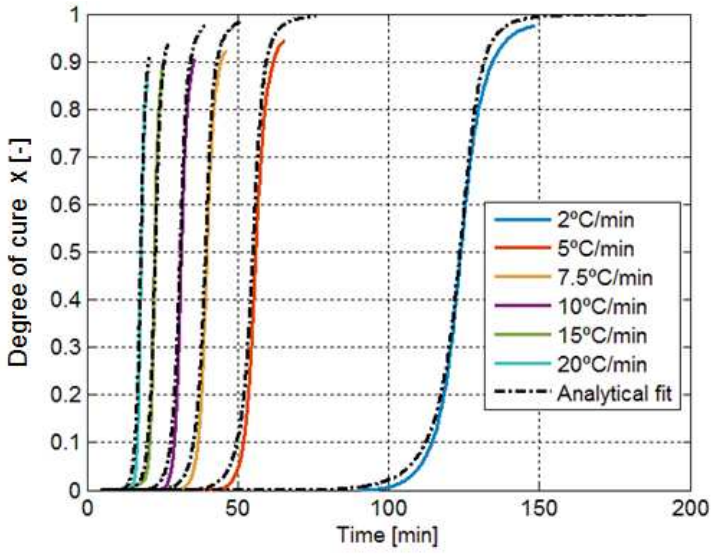

Figure 33: Dynamic DSC results for degree of cure at different heating rates (2, 5, 7.5, 10, 15 and 20°C/min) in solid lines. Analytical fitting model including diffusion in dashed lines

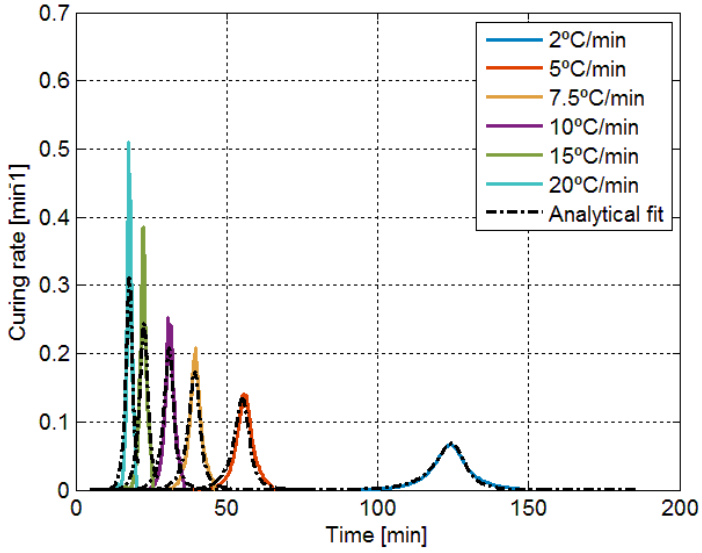

Figure 34: Dynamic DSC results for curing rate at different heating rates (2, 5, 7.5, 10, 15 and 20°C/min) in solid lines. Analytical fitting model including diffusion in dashed lines

4.2.3. Comparison with results by C. Brauner

The curing kinetic model used by C. Brauner follows Kamal Sourour including diffusion control (Eq. 19 and Eq. 20), as used in this thesis. When comparing the model developed in this thesis with the one used by C. Brauner in his, Figure 35 and Figure 36 show that there is a better fit using the curing kinetic as developed in this project for low isothermal curing temperatures (140°C).Only the isothermal curing results are shown, even though the same conclusion can be withdrawn when analysing the dynamic DSC runs. The colours stand for the three experimental isothermal curing conditions studied, black solid line for the analytical model developed in this thesis, and grey dashed line for the results reported by C. Brauner.

The improvement in the results obtained in this thesis comes from the identification of the final degree of cure X_f that enters Eq. 20. The identification was directly made at each one of the experimental degrees of cure as the final value. However, C. Brauner used the theoretical value of 1 as X_f. In Figure 35 one can see that at a curing temperature of 180°C where the final degree of cure reaches unity, no difference can be observed among the experimental, analytical and C. Brauner's results. However, at lower values (e.g. 140°C), the curve reported by C. Brauner does not reach a plateau but continues increasing past the experimental X_f.

It can be seen in Figure 35 an improvement at 140°C of the black with respect to the gray line at high degrees of cure, which is indeed the region where the implementation of diffusion control becomes important. For the other two curves at 160 and 180°C little or no improvement can be observed even though the fit is quite accurate.

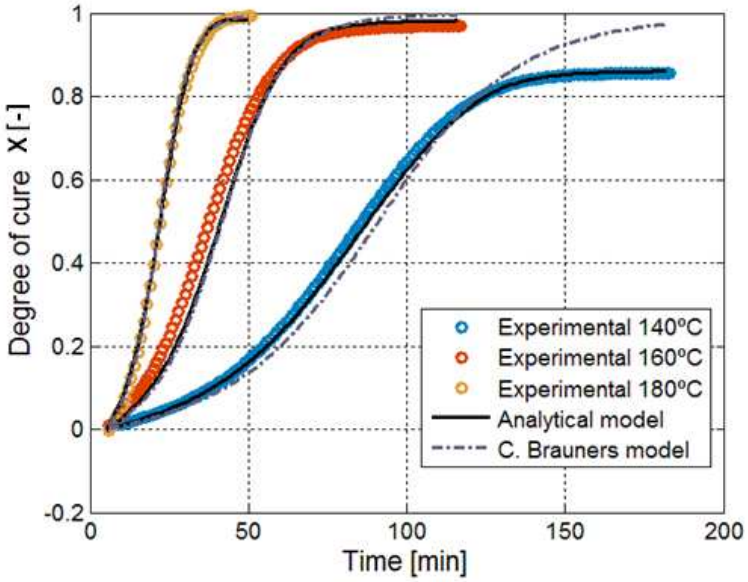

Figure 35: Degree of cure comparison between the analytical model proposed in this thesis and the one developed by C. Brauner [1] with respect to the experimental values for the RTM6 resin at three different isothermal curing temperatures of 140, 160 and 180°C

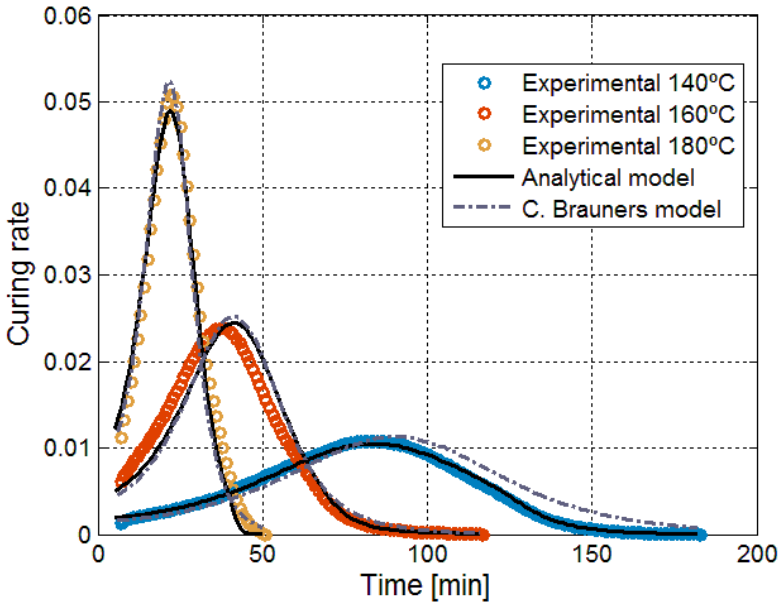

Figure 36: Curing rate comparison between the analytical model proposed in this thesis and the one developed by C. Brauner [1] with respect to the experimental values for the RTM6 resin at three different isothermal curing temperatures of 140, 160 and 180ºC

In order to assess the quality of the fits, the area underneath the curve was calculated for the isothermal DSC runs (as an example, but the same can be done for the dynamic runs) and each result: experimental, analytical model by C. Brauner and analytical model developed in this project. These last two results will be normalized dividing them by the integral of the experimental values. This data is represented in bar plots in Figure 37 and Figure 38 for the degree of cure and the curing rate respectively. The closer the bars get to unity, the more similar they are (overall) to the experimental values. Again, it can be seen how the analytical model used in this thesis better resembles the experimental values than the model developed by C. Brauner for lower isothermal curing temperatures. In general, the overall fit quality is either equal or slightly better for the analytical model developed in this thesis.

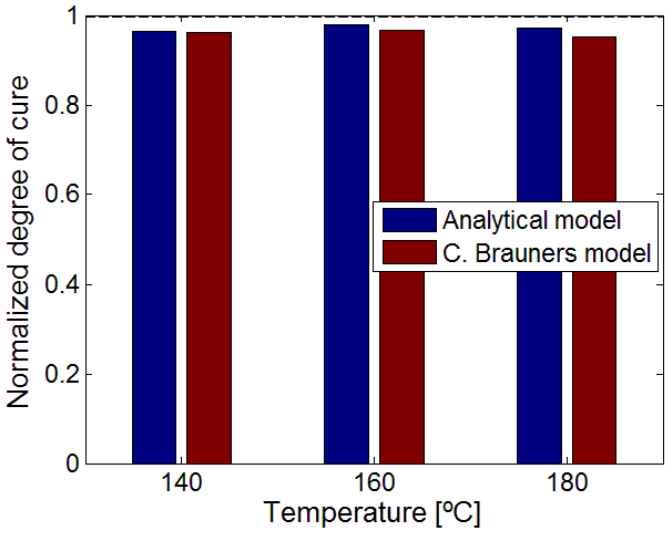

Figure 37: Degree of cure fitting quality comparison between the analytical model proposed in this thesis and the one developed by C. Brauner [1] with respect to the experimental values for the RTM6 resin at three different isothermal curing temperatures of 140, 160 and 180ºC

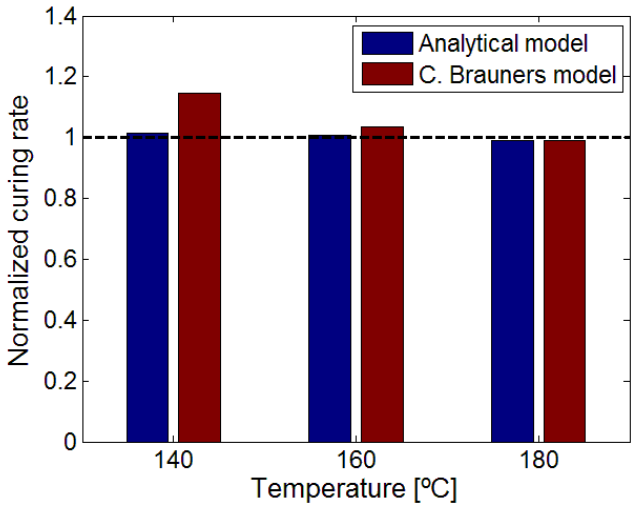

Figure 38: Curing rate fitting quality comparison between the analytical model proposed in this thesis and the one developed by C. Brauner [1] with respect to the experimental values for the RTM6 resin at three different isothermal curing temperatures of 140, 160 and 180ºC

5. Thermo-mechanical modelling of curing

The curing process as well as the distribution of stresses and induced deformations is studied using the software package Samcef. It uses a finite element method approach and can handle both mechanical and thermal analyses, among other types. The modules that were used for this project were: Mecano-thermal for the thermal analysis and Mecano for the structural part.

The results presented in chapter 4 served as an starting point for the thermal simulations. The fitting parameters taking part in Kamal Sourour with diffusion control (m, n, k_1, k_2, b and X_f) will be an input for Mecano-thermal, together with the specification of a thermal treatment. The implementation in Samcef of the curing kinetics and the prediction of the degree of cure with time will be studied and compared to the results presented in chapter 4. It will be seen that the Samcef implementation and the analytical procedure followed with the parameter fitting in Matlab give the results for isothermal curing. Nevertheless, a slight difference will be observed when dynamic curing is considered.

Out of the thermal simulation, the development of the curing degree, of the temperature inside the structure, and of the glass transition temperature of the resin will be obtained as a function of time. This information will be an input of the mechanical simulation, together with other material parameters that, although can be obtained from characterization techniques (chapter 3.4), were taken from the literature.

The mechanical simulation calculates the deformation of an L-shaped beam made of composite material upon the specified thermal treatment. The results will show a spring-in effect. From the displacement of the flanges of the L beam, the angle of deformation are calculated using basic trigonometry. The result obtained from Samcef is compared to the ones calculated with an analytical expression for such geometry. The difference between the analytical and the calculated deformation angle lies below 1%, which suggests that Samcef, and using the curing kinetic parameters obtained in this thesis, is capable of predicting appropriately the process induced deformation of a composite structure.

Furthermore, and with the purpose of better understanding the curing phenomenon and its effect on the process induced deformations, several sensitivity analyses will be carried. It was proven that the main parameters influencing the process induced deformations is the coefficient of thermal expansion in the longitudinal and transversal directions, together with the gelation point.

The main assumptions made in order to proceed with the curing simulations are:

- Initially, the composite part is stress-free.
- The and shape distortions will appear only due to the curing process.
- Even though it has been proved how viscoelastic models improve the quality of the simulation results [26], this model will assume an elastic material model.
- The model will not simulate the mould directly but instead the mechanical boundary conditions will offer a symmetry with respect to the corner of the L shape.
- A homogeneous temperature is assumed to be applied initially in the structure.
- Known thermal boundary conditions at the material's surface, that will be unaffected by the degree of cure of the composite. This means, that the temperature will be directly imposed in the surfaces instead of calculated from heat conduction through the mould.

The last two assumptions becomes specially important because this way, the thermo-mechanical analysis of curing can be split in two steps (thermal analysis first and the mechanical) instead of doing a fully coupled analysis. The results from the thermal analyses, particularly temperature, glass transition temperature and degree of cure, will serve as input for the mechanical analyses. Furthermore, this way it becomes possible to compare a point model (chapter 4) to a 3D simulation.

This section is divided in a preliminary study on the curing of the thermosetting resin RTM6 using Samcef followed by the thermal analysis of a structure designed in composite material and the subsequent structural analysis in order to discover the induced deformations.

5.1. Description of the problem and application

The thermal module of Samcef is able to simulate the curing of thermosetting resins using several cure kinetics models (including Kamal Sourour, as used previously). It is also possible to account for the effect of diffusion control, but only in the Samcef default kinetic model, which is given below in Eq. 50 and follows the notation already presented. In order to do so, both methods explained in this thesis can be chosen, i.e. using Fournier's approach by including the function f_d (Eq. 20) in the cure kinetics expression or by using the distribution of the glass transition temperature together with Eq. 16. Note that the Samcef default curing kinetics model resembles Kamal Sourour when n_1 and n_2 are equal.

$$\frac{dX}{dt} = k_1(1-X)^{n_1} + k_2 X^m (1-X)^{n_2} \qquad \text{Eq. 50}$$

Furthermore, it is also possible to insert a user defined cure kinetic model with a different definition. This aspect becomes handy, for example, if diffusion control is wished to be applied to another model rather than the default one in Samcef. For the

sake of comparison with the previously shown results calculated in Matlab (see section 4.2), Kamal Sourour was extended for diffusion control using Fournier's method in Samcef.

In order to do that, different parameters ought to be defined as material properties, such as the density, the conductivity, the total enthalpy of the curing reaction, etc. Since no direct access to the characterization of the material was obtained, except for DSC curves, the remaining parameters were taken from either C. Brauner [1] or Balvers et al. [49] for RTM6. The expressions and values will be given in the coming paragraphs.

- Curing kinetic parameters: this data was inserted as obtained analytically using the Matlab code mentioned before (see Table 2).
- Matrix heat capacity [1]: given as a function of temperature, glass transition temperature in Eq. 51. The constants a_1 to a_5 and b_1 to b_3 are given below in Table 4.

$$c_{p,m} = a_1 T + a_2 + a_5(T - T_g) + (a_3 - a_5 T_g)\tanh\left(m^{-} a_4 (T - T_g)\right), \quad T \le T_g$$

$$c_{p,m} = a_1 T + a_2 + a_5(T - T_g) + (a_3 - a_5 T_g)\tanh\left(m^{+} a_4 (T - T_g)\right), \quad T \ge T_g$$

$$m^{+} = \frac{a_5 + F}{F} \qquad m^{-} = \frac{-a_5 + F}{F} \qquad F = a_4(a_3 - a_0 T_g) \qquad \text{Eq. 51}$$

- Matrix conduction [1]: given as a function of temperature and degree of cure in Eq. 52. The constants a_1 to a_5 and b_1 to b_3 are given below in Table 4 and Table 5.

$$k_{c,m} = b_1 + b_2 T + b_3 X \qquad \text{Eq. 52}$$

Fit parameters [-]	
a_1	0.00264
a_2	1.1
a_3	0.172
a_4	0.0423
a_5	0.000242

Table 4: Fitting parameters for the expression of the matrix heat capacity [1]

Fit parameters	
b_1 [W/mK]	0.15
b_2 [1/K]	0.0000245
b_3 [-]	0.07

Table 5: Fitting parameters for the expression of the matrix conductivity [1]

- Total enthalpy of the reaction: its value can be calculated from the integration of the exothermic peak. However, it can only be directly done for dynamic DSC data. On the other hand, the integration of the isothermal DSC exothermic peak is not accurate and therefore the value is inserted as reported by the DSC machine. In particular, the values inserted can be seen in Table 6. The enthalpy of the curing reaction should not vary with temperature of curing or curing rate, and the mean value of the data reported in should be used.

Treatment		Enthalpy of the reaction [J/mol]
Isothermal [ºC]	140	430
	160	424
	180	440
Dynamic [ºC/min]	2	432
	5	423
	7.5	428
	10	390
	15	423
	20	451
Mean value		424

Table 6: Total enthalpy of the curing reaction obtained directly from the DSC for the isothermal DSC runs and from the integration of the exothermic peak for the dynamic DSC

- Parameters for DiBenedetto's equation [49]: the required parameters to input into the DiBenedetto's equation are the glass transition temperature for the uncured resin T_{g0} (-13.09ºC), for the cured resin $T_{g\infty}$ (217.88ºC) and a material constant λ (0.453).
- Density of the resin [1]: the density of the resin is 1110 g/cm^3.
- Reference temperature: the reference temperature was needed once the capacity was entered in order to include it in Fourier's law. Since no reference temperature was given at which the capacity was measured, a guessed room temperature of 20ºC was assumed.
- Parameters of the curing kinetic model derived in order to fit the experimental data using Matlab as explained before in section 4.2 (m, n, b,Ea_1, Ea_2, A_1, A_2, X_f).

5.1.1. Geometry and boundary conditions

The geometry used in this thesis for modelling of curing process is an L shaped beam taken from the thesis by Johnston [22]. The geometry and boundary conditions can be seen below in Figure 39. In his thesis, Johnston investigated the residual stresses and the spring back arising after the curing process on a different composite material than attained in this study. Spring back refers to the change in angle, in this case going from the designed value of 90 degrees to a slightly higher value (see sketch in Figure 40 for a better understanding).

There is an analytical formula to calculate the spring back angle of an L shape beam depending on the thermal expansion coefficients of the homogenized structure. This expression was firstly developed by Nelson and Cairns and it can be seen in Eq. 53 [22], where θ is the initial angle of the L shape beam (90 degrees), and ΔT is the difference in temperature between the isothermal curing temperature and the initial temperature. The equation is defined in such a way that a positive $\Delta\theta$ will give a decrease in the L shape angle. Note that this expression neglects the effect of chemical shrinkage, moisture or aging.

$$\Delta\theta = \theta\left[\frac{(CTE_1 - CTE_3)\Delta T}{1 + CTE_3\Delta T}\right] \qquad \text{Eq. 53}$$

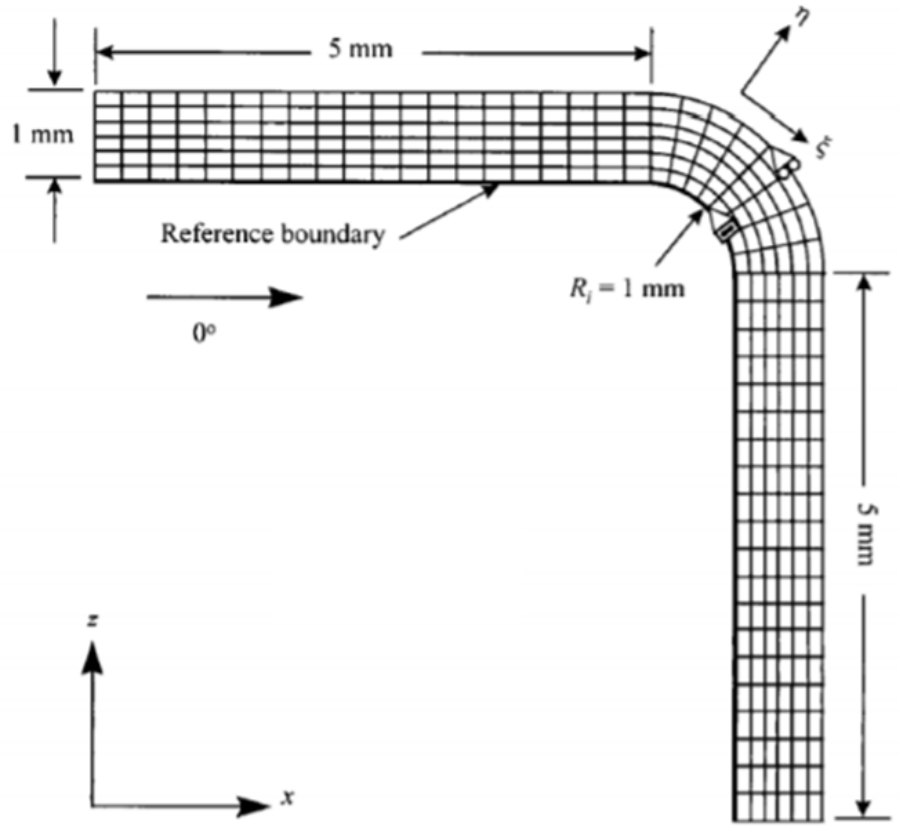

Figure 39: Geometry and boundary conditions used to model the curing manufacturing process of an L shaped beam with the aim of predicting spring back [22]

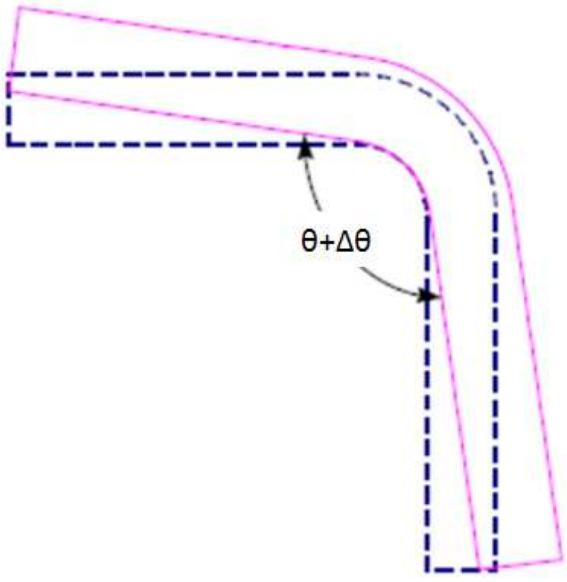

Figure 40: Sketch of spring back that arises as a result of the curing process in an L shaped beam. In dashed blue lines, the designed geometry, in solid pink lines the resulting geometry after curing (adapted from [22])

The mechanical boundary conditions depicted in Figure 39 were not implemented in the preliminary curing modelling. The reason is that the main aim of these

simulations was to validate the Samcef implementation and compare it with the experimental and analytical results using Matlab. The boundary conditions for the preliminary curing simulations were of the thermal kind. Specifically:

- Assumed initial temperature of 20^{o}C on all internal nodes that simulates the material to be at room temperature.
- A constant temperature of all external faces, simulating this way the contact of the structure with the closed mould, which is at higher temperature.

The temperature described in the external faces corresponds to either the isothermal (140, 160 and 180^{o}C) or the dynamic curing conditions (2, 5, 7.5, 10, 15 and 20^{o}C/min) used previously.

5.1.2. Results of the preliminary thermal simulation

The results of the preliminary study of the curing simulation focus only on the validation of the Samcef code with respect to the experimental and analytical results presented previously in section 4. The simulations using the Samcef package were performed using both the default model and the Samcef user defined model (extended Kamal Sourour for diffusion control). The simulations were performed for the available isothermal and dynamic DSC runs. Nevertheless, for the sake of an easier representation, and since the results of all curves show the same qualitative behaviour, the example of the isothermal run at 140^{o}C curing temperature is shown in Figure 41.

It is clearly seen that both Samcef cure kinetic implementations agree perfectly. Furthermore, in the case of isothermal DSC runs, they also agree with the analytical model developed in Matlab. For this reason, the choice of which model to use in Samcef relies only on the user. In this project, the default kinetic model will be used from this point on because it is easier and faster to implement in the Samcef code.

As far as dynamic DSC is concerned, Figure 42 shows the curing degree for all dynamic DSC curves as reported previously in Figure 33, but superposing the Default Samcef cure kinetic model in gray. Contrary to the isothermal case, the simulations for dynamic DSC runs deviate from the experimental results and the analytical fit, specially for low heating rates. Up to date, no explanation is found for this difference. Several time steps and residual thresholds were tried in the simulations in order to find if it was a numerical issue. However, no improvement was achieved.

Even though the difference is not excessively big, it is important to take into consideration their existence and adjust any potential experimental curing procedure to account for it in order to avoid undercuring. Besides, this slight difference may provoke great deviations in the successive mechanical simulation.

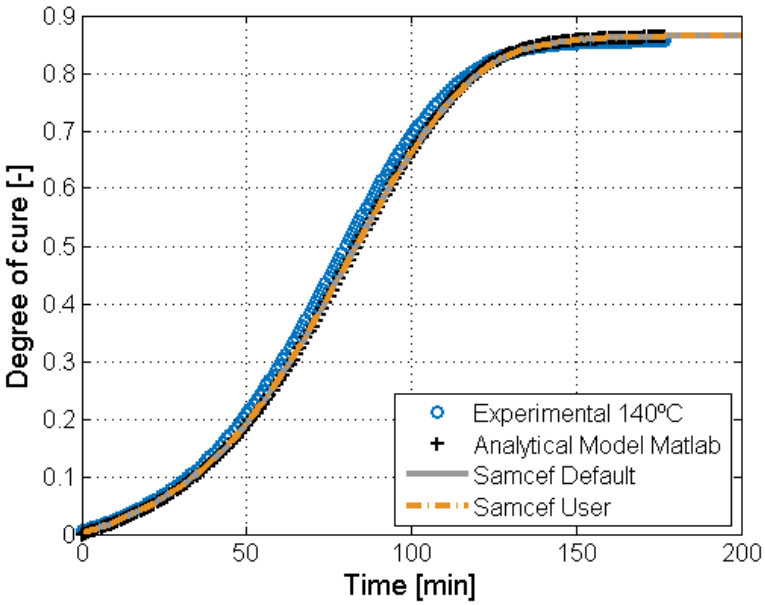

Figure 41: Comparison among the results of curing degree obtained from different sources: in blue the experimental values, black the analytical model developed in this thesis (section 4), grey solid line the Samcef default kinetic model and in dashed orange the user default kinetic model

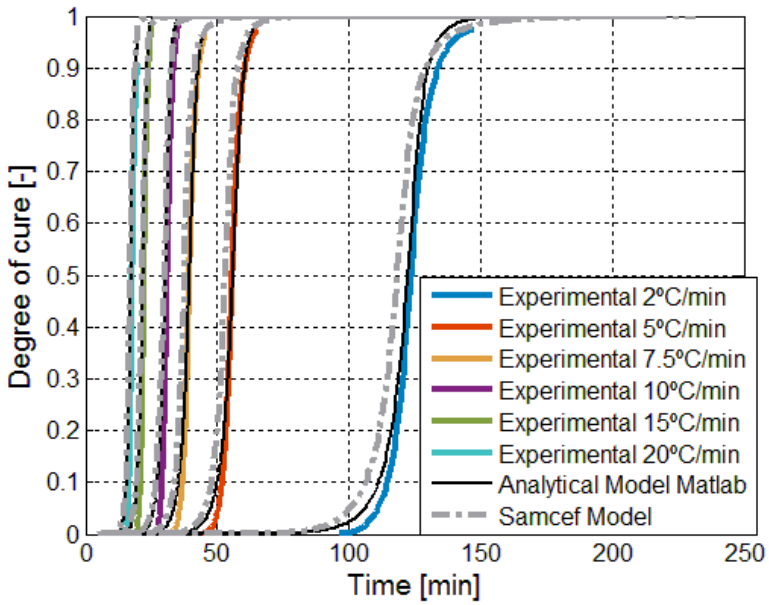

Figure 42: Dynamic DSC results for degree of cure at different heating rates (2, 5, 7.5, 10, 15 and 20ºC/min) in solid lines. Analytical fitting model including diffusion in black solid lines, Samcef default user kinetic model in dashed gray

5.2. Preliminary thermo-mechanical simulation

The goal of this thermo-mechanical simulation is to predict the spring-in angle that results from the curing cycle. The induced deformation predicted with Samcef will be compared to the analytical value computed via Eq. 53.

The mechanical part of the simulation in Samcef is able to use the information from a previous thermal simulation. This way, the evolution of degree of cure, temperature and glass transition temperature are transferred into the mechanical

simulation. In order to facilitate the transfer of values among nodes, the geometry and same mesh are used for the mechanical than for the thermal simulations.

As mentioned before, the amount of elements through the thickness should be constant along the L shape, and will be the same amount of layers in the composite laminate. The plies, their orientation, thickness and stack-up should therefore be defined in this stage. The first case to be studied is a laminate with 8 identical plies with $[0]_{4s}$ orientation and 0.125mm thickness (to amount to 1 mm for the whole structure).

For the mechanical simulation, other set of characteristic parameters need to be inserted. Some examples of the parameters that should be input will be given in Table 7. The coefficients of thermal expansions and chemical shrinkage are given as homogenized properties for the composite laminate in the three principal directions. Since it was not found a previous study where an L shaped beam was studied with the matrix material (RTM6) for which experimental curing results are available, these values will be considered as default conditions.

Parameter	Value	**Parameter**	Value
E_{ml}, E_{mr} [N/mm^2]	5000	ρ [g/mm^3]	1.35e-9
E_{mg}[N/mm^2]	5	CTE_{1l}, CTE_{1r}, CTE_{1g} [1/ºC]	0
ν_{ml}, ν_{mr}, ν_{mg} [-]	0.35	CTE_{2l}, CTE_{2r}, CTE_{2g} [1/ºC]	0
X_{gel} [-]	0.4	CTE_{3l} [1/ºC]	0
E_f [N/mm^2]	210000	CTE_{3r}, CTE_{3g} [1/ºC]	2.3804e-5
G_f [N/mm^2]	50600	CSh_l, CSh_r, CSh_g [%]	0
V_f [-]	0.47		

Table 7: Default values of required parameters to set up the mechanical part of the curing simulation (m = matrix, f = fibres, l = liquid, r = rubbery, g = glassy)

Some observations can be made regarding the selected data presented just above:

- The resin properties E_m and ν_m are specified at each stage of the resin during the curing procedure (Eq. 21 and Eq. 22).
- The homogenized values of *CTE* and *CSh* are specified for each stage of the resin during the curing procedure i.e. liquid, rubbery and glassy states.
- The values of ρ, V_f *and* X_{gel}, are taken from the thesis by C. Brauner [1].
- The elastic properties of the matrix and the fibres are of the same order as the ones reported by C. Brauner [1]. However, these parameters should not influence the prediction of the spring-in angle of the L shape beam, and therefore can be varied. A sensitivity analysis was performed to prove this fact, as will be explained in **¡Error! No se encuentra el origen de la referencia.**.
- The homogenized properties $CTE_{3r} = CTE_{3g}$ were calculated using data from C. Brauner [1] and applying the formulas given in Eq. 39 to Eq. 42.
- The values that are set to zero, in reality a value of to 1e-12 was set in order to avoid any numerical problem during the calculations.

As one of the main goals is to predict the geometric distortion of the L shape, a way of measuring the angle deflection from the numerical analysis in Samcef is required. For this purpose, simple trigonometry is used. Because the corner of the L is not straight but has a curvature instead, and because the L has a certain thickness, measuring the angle deflection between the two flanges of the L might not be a good idea. This procedure was tried, but the resulting values of the angle were not very close to the analytical solution. The reason is that, depending on what point is used for the trigonometric calculation, a different value of $\Delta\theta$ will be obtained. For that reason, the angle that the left-most side (green side in Figure 43, going from point A to point B) with the vertical direction is calculated following Eq. 54. Figure 43 offers a visual explanation of this methodology. For this particular application, this method of measuring the deflection will give very similar results to the analytical solution. However, due to the variability of the results, one needs to take into account that the experimental way of measuring the angle could be different, and that for other applications, different methods may need to be applied.

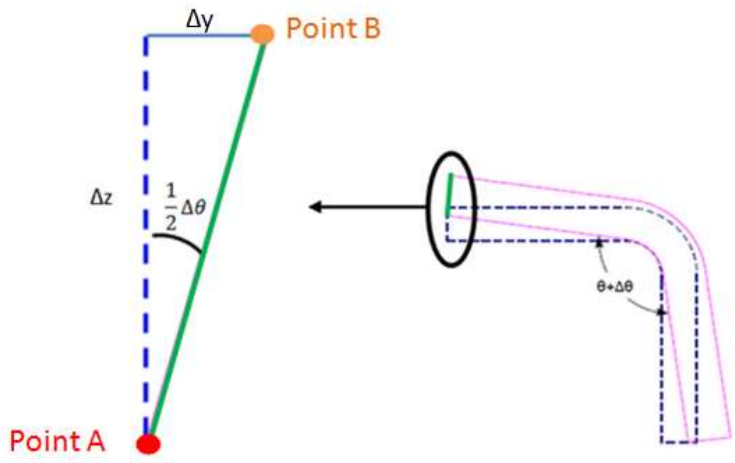

Figure 43: Visual explanation of the methodology used to calculate deflection of the angle of the L shaped beam when subjected to curing. The side going from point A (red) to point B (orange) is used to measure its angle with respect to the vertical direction

$$\frac{1}{2}\Delta\theta = \arctan\left(\frac{\Delta y}{\Delta z}\right) \qquad \text{Eq. 54}$$

5.2.1. Boundary conditions

The thermal boundary conditions used in the preliminary curing simulations are kept, excepting the thermal cycle of the external faces. All nodes are again set to 20°C initially. The curing cycle will consist of an increase in temperature up to the isothermal curing temperature (140°C), and a cool down to room temperature (20°C). Firstly, the curing cycle will resemble the one in Figure 44, with a duration of 500 min and temperature ramps of 0.6°C/min.

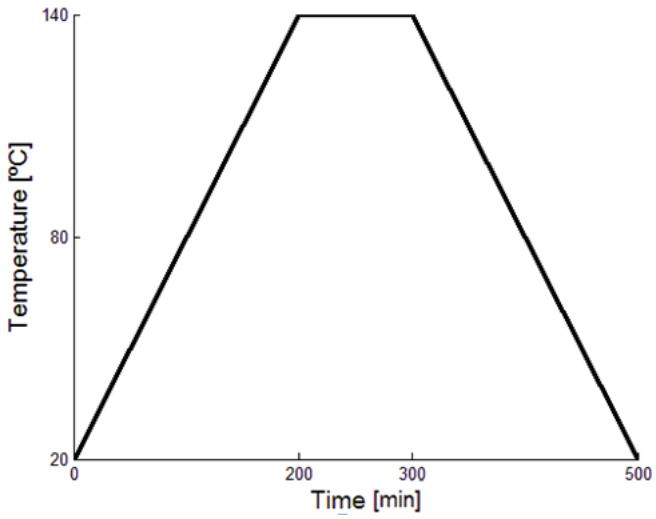

Figure 44: Curing cycle

The times and heating rate will be subjected to variations depending on the topic to study, as it will be attained later on.

With respect to the mechanical boundary conditions, similar conditions as the ones depicted in Figure 39 are used. However, a small variation was implemented to ensure symmetry conditions on the L shape beam. All nodes constructing the straight line (depicted in red in Figure 45) between the fixed and the pinned nodes will be pinned supported as well.

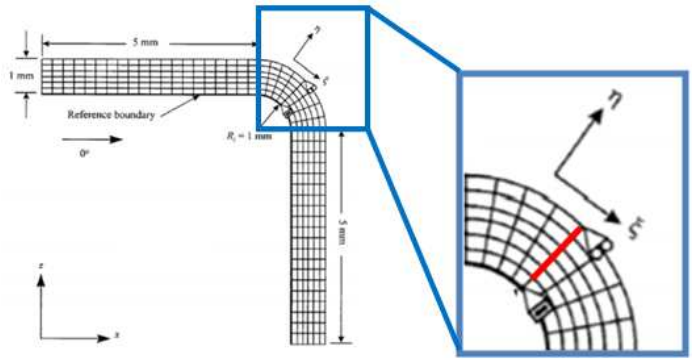

Figure 45: Mechanical boundary conditions for the thermal-mechanical curing simulations

5.2.2. Mesh

The mesh was formed by bricks of volume elements of first order (eight nodes per element). By default, Samcef allocates nine incompatible displacement modes corresponding to the exact pure bending solution (Figure 46 left-hand side) in order to improve the element behaviour. The strain calculated in these extra modes is orthogonal to the ordinary strain modes. This way, shear and volumetric locking (Figure 46 on the right) is prevented. These modes may be thought of as internal degrees of freedom in each element (not shared among the surrounding elements, but affecting locally instead).

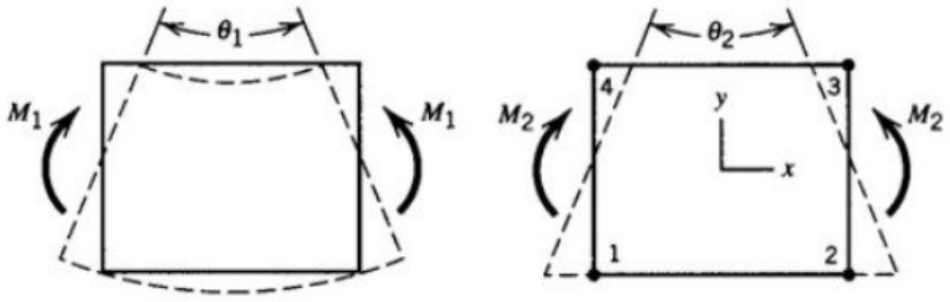

Figure 46: On the left, the exact elastic solution for a beam under bending conditions and on the right, the locking phenomenon that simple first order elements may suffer

The displacement field formulation u^h of these kind of elements is defined by Eq. 55. The first summation term refers to the contribution by the standard bilinear shape functions $N_i(\xi,\eta)$ of a first degree of freedom element. The second term refers to the nine extra shape functions.

$$u^h(\xi,\eta,\zeta) = \sum_{i=1}^{4} N_i\,(\xi,\eta,\zeta) d_i^e + \sum_{i=5}^{13} N_i\,(\xi,\eta,\zeta) s_i^e \qquad \text{Eq. 55}$$

where ξ, η and ζ are the element 3D natural coordinates, d_i^e are the nodal displacements of the i^{th} node and s_i^e are the generalized displacements of the e^{th} element. The definition of the natural coordinates is provided by the aid of Figure 47 for a 2D first degree quad element, and can be extended for the third dimension to account for ζ. For more information about this type of element, the reader can refer to [50].

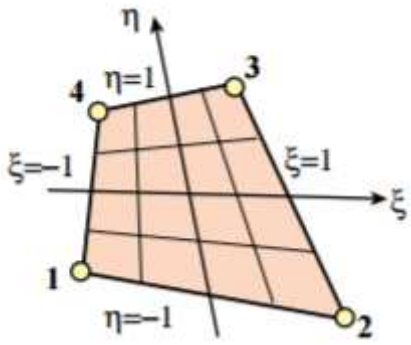

Figure 47: 4-node bilinear quadrilateral element representation in natural coordinates [51]

The utilization of shell elements was quickly disregarded since the studied part is quite thick and shell elements cannot reproduce normal stress along the thickness direction, which is important for this application.

A preliminary mesh is defined with 20 elements located at the radius section in the tangential direction. In the two flanges of the L shape 50 elements of 0.1mm side length are allocated. Since a composite laminate is being studied, the number of

elements through the thickness of the structure will be the same as the number of plies to be used. Initially, 8 elements are allocated through the thickness. Furthermore, the mesh will be extruded to have a spanwise dimension of one cell and plain strain conditions are defined. The resulting mesh can be seen in Figure 48.

The number of elements of this mesh have been varied in order to try achieve convergence in the results, although as it will be seen, this mesh will provide accurate enough results. This sensitivity analysis, together with different element formulations will be given later on in section 5.3.1.

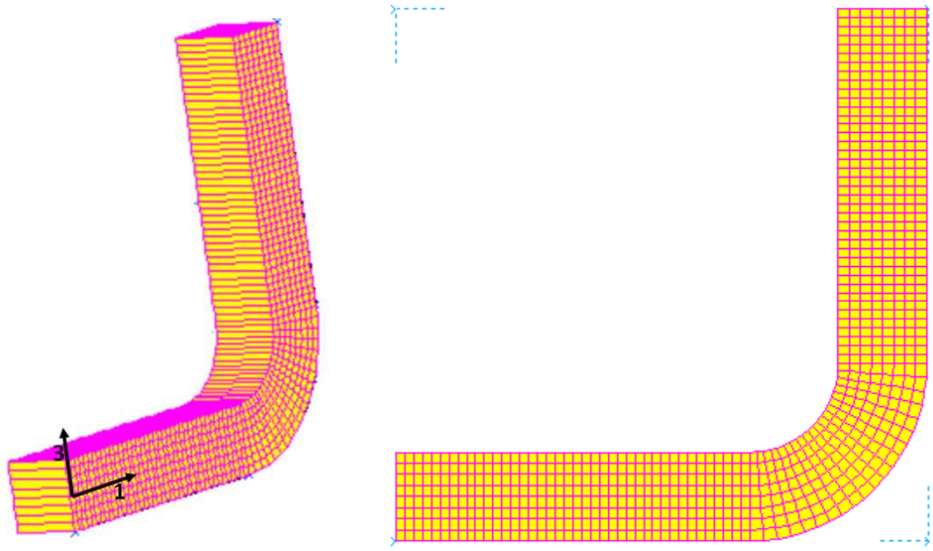

Figure 48: Initial mesh of the L shape beam, consisting of 50 elements along the horizontal and vertical flanges, 20 elements along the radius tangential direction, and 8 elements through thickness. The principal direction 1 follows the contour of the L shape longitudinally, and defines the 0 degree direction

5.2.3. Results of the preliminary thermo-mechanical curing simulation

The variation in angle of the L shape composite beam is obtained from the simulations in Samcef. The position before and after the shape deformation are recorded for points A and B (see Figure 43). The displacement is obtained for each point, and plotted in Figure 49 and Figure 50 respectively (note the different displacement axis) together with the temperature cycle. The exact values obtained at the end of the simulation are reported in Table 8, together with the analytical and numerical results for $\Delta\theta$.

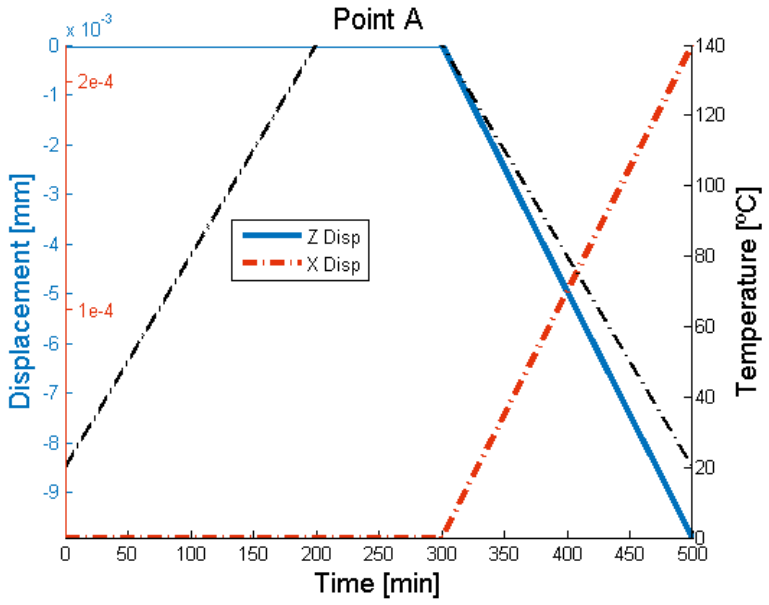

Figure 49: Displacement in x (orange) and z (blue) directions of point A versus curing time. The temperature cycle is also shown in black

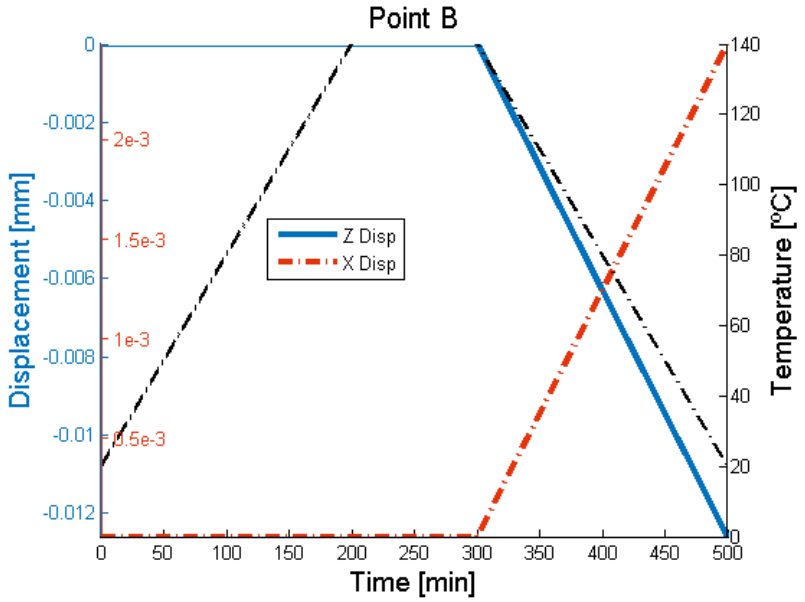

Figure 50: Displacement in x (orange) and z (blue) directions of point B versus curing time. The temperature cycle is also shown in black

	Point A	Point B
X displacement [mm]	2.16e-4	2.48e-3
Z displacement [mm]	-9.9e-3	-1.26e-2
Analytical $\Delta\theta$ [deg] (Eq. 53)	0.258	
Numerical $\Delta\theta$ [deg] (Eq. 54)	0.260	

Table 8: Numerical values for X and Z displacement for points A and B. The analytical and numerical values for $\Delta\theta$ due to curing are also reported

Notice that the obtained $\Delta\theta$ is a positive value, which, due to the convention used for its definition, corresponds to a decrease on the original angle. This behaviour can be observed in Figure 51, where the deformations are plotted multiplied by a factor of 20 for an easier visualization. The final shape is depicted by solid lines on top of the dashed lines corresponding to the initial shape.

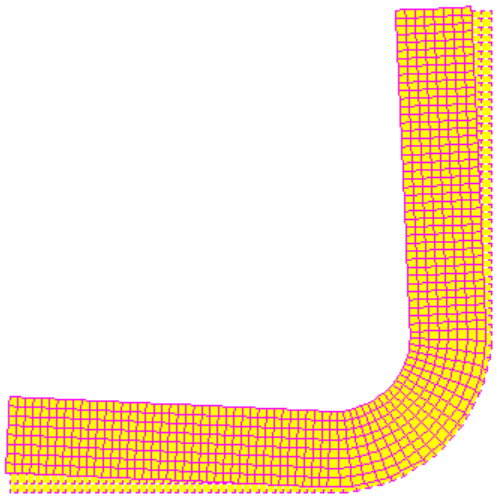

Figure 51: Process induced deformations due to the curing process of the L shape composite structure. The deformation has been exaggerated by a factor of 20

Also, comparing both the analytical and the numerical $\Delta\theta$, Samcef predicts a 0.77% higher angle reduction than the analytical formula. Bearing in mind that chemical shrinkage, aging or moisture absorption are not considered in either the analytical nor the numerical case, this difference might come from some numerical inaccuracy. Nevertheless, the accuracy of the prediction is appropriate enough.

It is interesting to realize that the change in angle $\Delta\theta$ begins at 300 minutes of curing (recall the blue and red curves in Figure 49 and Figure 50), which corresponds to the cool down from the curing temperature (140ºC) to the room temperature (20ºC). No deformation is seen in previous stages (up to 300 minutes). This behaviour is due to the specification of the gel point of the resin. For this particular case, the gel point X_{gel} was set to 0.4 (remember Table 7), which indeed occurs at a temperature of 140ºC (see Figure 52, where the orange dashed lines specify the temperature at which $X = X_{gel} = 0.4$), or in other words, at the maximum temperature of this particular curing cycle. In the next section, the gel point will be varied in order to show that, if gelation occurs while the temperature is being increased, a first deformation will appear during heat up.

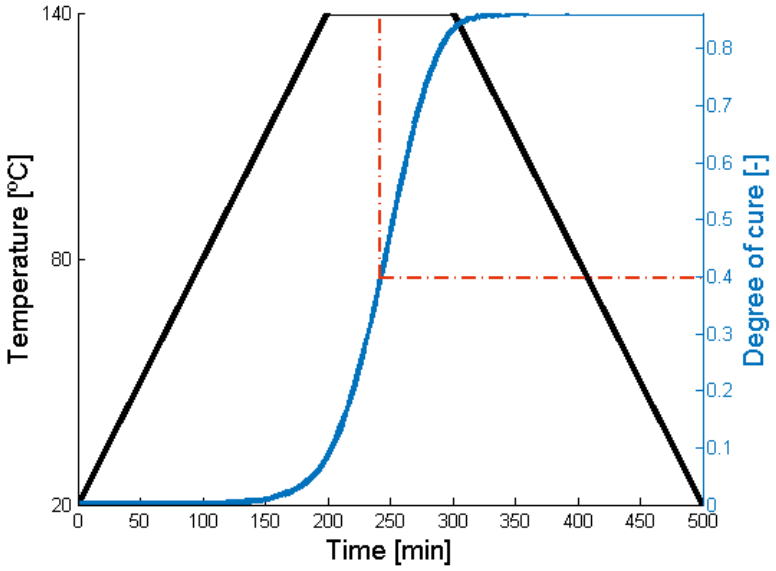

Figure 52: Temperature cycle (black) and degree of cure (blue) versus time. The gel degree of curing of 0.4 is marked by the orange dashed line

5.3. Sensitivity analyses

In this section, a series of sensitivity analyses will be presented in order to understand how the process induced deformations will be affected upon various parameters. The reference case will be the previous preliminary thermo-mechanical curing simulation presented in section 5.2. Hence, unless otherwise specified, the simulations will be performed for a curing temperature of 140ºC (with the respective curing kinetic parameters in Table 2) and with the mesh described in 5.2.2.

Firstly, a mesh sensitivity study will be performed, varying the amount of elements in the different regions of the L shape, as well as the element formulation. The second case, and probably the most important conceptually, will attain the curing of the composite material with different gelation points. It will explain why the shape distortion only occurs when there is a temperature gradient after the gelation point. Later on, the cure kinetic parameters will be varied, together with the thermal properties of the matrix that are required in the thermal part of the simulation. This study will simulate how the results will be affected by small variations or inaccuracies in the thermal characterization of the resin.

5.3.1. Mesh sensitivity analysis

The original mesh explained in 5.2.2 will be subjected to some variations to see whether or not its solution can be improved by refining the mesh or by changing the element formulation. To start with, the number of elements in the radial and circumferential directions at the corner will be attained. The different mesh configurations can be seen in Table 9.

Mesh	# circumferential elements	# Radial elements	Predicted spring-in [deg]	Error [%]	Max. stress [Pa]
Reference	20	8	0.2600	0.77	38.09e3
M1.2	10	8	0.2565	-0.60	156.70e3
M1.3	6	8	0.2561	-0.72	474.00e3
M1.4	30	8	0.2601	0.83	28.90e.3
M2.2	20	4	0.2567	-0.51	34.40e3
M2.3	20	3	0.2572	-0.33	32.60e3
M2.4	20	10	0.2572	-0.33	39.00e3

Table 9: Number of elements in the tangential and radial directions at the corner of the L shape for the mesh sensitivity analysis with the computed predicted spring in angle, its error with respect to the analytical solution, and the maximum stress at the end of the simulation

As it is reported in Table 9, no direct relation can be seen between refining the mesh and getting a more converged or accurate result for the spring-in angle. Nevertheless, the error in the prediction when compared to the analytical result for all the tested cases is quite low (less than 1%) and therefore any of these cases could be used, as far as the prediction of $\Delta\theta$ is concerned. Nevertheless, by reducing the amount of elements in the circumferential direction, the values of the maximum stress at the end of the process are one order of magnitude bigger. Therefore, this might suggest that, if any other elastic quantity is desired to be inspected, less converged results may arise.

Besides, the number of elements in the radial direction seem to not have an influence in the final results. One has also to have in mind that this number is directly related to the number of plies to be used in the laminate.

The reference mesh was decided to be used due to four main reasons:

- Good distribution of elements, with an adequate aspect ratio as it could be seen in Figure 48.
- Conservative result, overpredicting the analytical spring-in angle by 0.77%.
- More computationally efficient that the mesh M1.4, which has 30 elements at the corner in the tangential direction.
- Initial case of study designed to have 8 plies at 0 degrees orientation.

On top of varying the number of elements, the sensitivity analysis was also performed upon different element formulations. As explained previously in section 5.2.2, the reference case formulation consists of first order hexahedral elements with extra incompatible modes located within each element. This section will also study the case where no incompatible modes are considered, and an Enhanced-Assumed Strain (EAS) formulation.

By removing the extra incompatible modes, first order solid elements may exhibit shear and volumetric locking, that may corrupt the calculations. Another way of

avoiding this situation, besides the addition of incompatible modes, is the use of the EAS formulation.

Samcef has the EAS implementation used by Simo and Armero, which consists of the utilization of 3D constitutive laws with the enhancement of the material displacement gradient (instead of the Green-Lagrangian strain tensor) in order to extend the method to non-linear theory. This method is more numerically expensive due to the large amount of extra modes included in the computations (15 elements for composite volume elements) [28]. The predicted spring-in deflection when using these two other formulations are compared to the reference case in Table 10.

Mesh	Formulation	Predicted spring-in [deg]	Error [%]
Reference	Incompatible modes	0.260	0.77
M3.2	No additional modes	0.261	1.09
M3.3	EAS	0.257	-0.33

Table 10: Element formulation for the mesh sensitivity analysis with the obtained predicted spring-in angle and the error when compared to the analytical solution

The absence of incompatible modes provides a less accurate solution for the spring-in angle when compared to the reference case. It is then obvious that incompatible modes are necessary for this type of simulations. Regarding EAS, it offers a further improvement, resulting in an error of only -0.33% with respect to the analytical case. Nevertheless, due to the increased computational time (almost doubled) with respect to the reference case, and due to the over-estimation of the latter which will lead to a more conservative result, the reference case was decided to be implemented.

5.3.2. Sensitivity on gelation point X_{gel}

The gelation point becomes important because the matrix properties change depending on the stage of curing. In the reference case, even though the chemical shrinkage is set to zero, the coefficient of thermal expansion becomes different from zero after the gel point, as depicted in Figure 53. For this reason, the composite will only undergo distortion due to temperature gradients only for $X > X_{gel}$.

If X_{gel} lies within the temperature ramp from the room to the curing temperature, some process induced distortion will appear. In this case, the ΔT will be defined as the final curing temperature (T_{cure} = 140°C) minus the temperature at which the gel point is located (T_{Xgel}), instead of the room temperature.

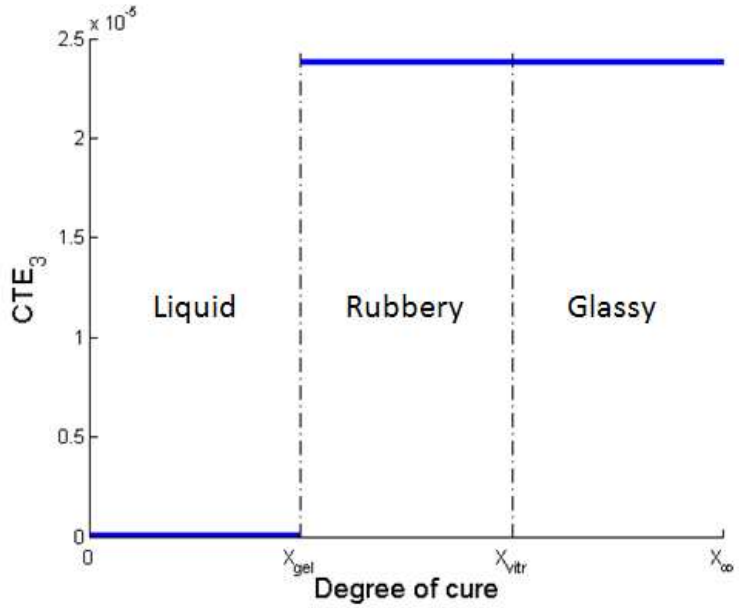

Figure 53: Coefficient of thermal expansion along the third principal direction (matrix *CTE*) as a function of the three different curing stages

For a better visualization of this phenomenon, the X_{gel} is lowered exaggeratedly so that T_{Xgel} differs considerably from T_{cure}. The information for these first sensitivity runs (S1.1 and S1.2) is tabulated in Table 11 together with the reference case. The displacement in the X and Z directions for points A and B are displayed, as well as the analytical and theoretical $\Delta\theta$. This data is recorded for the increase (↑T) and decrease (↓T) in temperature separately.

For S1.1 a good agreement is obtained during the cool down of the laminate since the difference between analytical and numerical $\Delta\theta$ is low. However, the percentage difference for happening after the heat up gets up to 2.04%.

The case for S1.2 aimed to prove that if X_{gel} is very low, or if CTE is constant for any degree of cure (meaning no jump from zero to a non-zero value when crossing X_{gel}), the deflection happening during the cool down of the process compensates the deflection during heat up. This phenomenon happens for both the analytical and the numerical analysis, and was also shown by Johnston [22].

Hence, this sensitivity study may show that the analytical expression can be applied for cases where T_{Xgel} lies on a temperature ramp. Nevertheless, the difference in temperature needs to be set up accordingly.

		Reference case	S1.1	S1.2
X_{gel}		0.4	0.02	0.000001
T_{Xgel} [ºC]		140	118	20
Point A	Disp x ↑T [mm]	0	-4.20E-5	-2.16e-4
	Disp x ↓T [mm]	2.16E-4	1.75E-4	0
	Disp z ↑T [mm]	0	1.90E-3	9.99e-3
	Disp z ↓T [mm]	-9.90E-3	-8.00E-3	0
Point B	Disp x ↑T [mm]	0	-4.80E-4	-2.48e-3
	Disp x ↓T [mm]	2.47E-3	2.00E-3	0
	Disp z ↑T [mm]	0	2.50E-3	0.0126
	Disp z ↓T [mm]	-1.26E-2	-1.05E-2	0
Analytical $\Delta\theta$	↑T	0.000	-0.049	-0.256
	↓T	0.258	0.208	0.000
Numerical $\Delta\theta$	↑T	0.000	-0.050	-0.260
	↓T	0.260	0.210	0.000
% Difference	↑T	0.00	2.04	1.56
	↓T	0.77	0.96	0.00

Table 11: Sensitivity on the gelation point. The temperature at which X_{gel} happens, and the displacements for points A and B are used to calculate the numerical $\Delta\theta$. The difference between the numerical and the analytical $\Delta\theta$ is also reported

Similarly, Figure 54 and Figure 55 show the X and Z displacements during the curing cycle for points A and B respectively. The horizontal gray dashed lines depict T_{Xgel}. At the time where that temperature is achieved, the matrix changes from liquid to rubbery, which means that CTE_3 becomes non-zero and the laminate will undergo a deformation when subjected to a temperature gradient. That is the reason why the vertical gray dashed line is placed.

Note that the temperature gradient for the temperature rise (140-118 = 22ºC) is much lower compared to the cool down (20-140 = -120ºC). For that reason, the deformation due to cool down counteracts the one happening during the temperature rise, and exceeds it on the opposite direction.

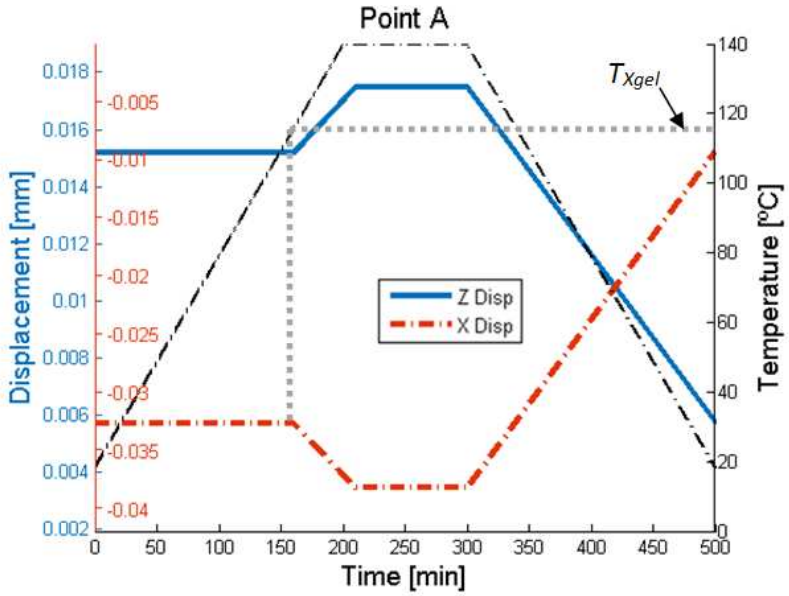

Figure 54: Displacement in x (orange) and z (blue) directions of point A versus curing time. The temperature cycle is also shown in black. The gelation temperature is depicted with a horizontal gray dashed line

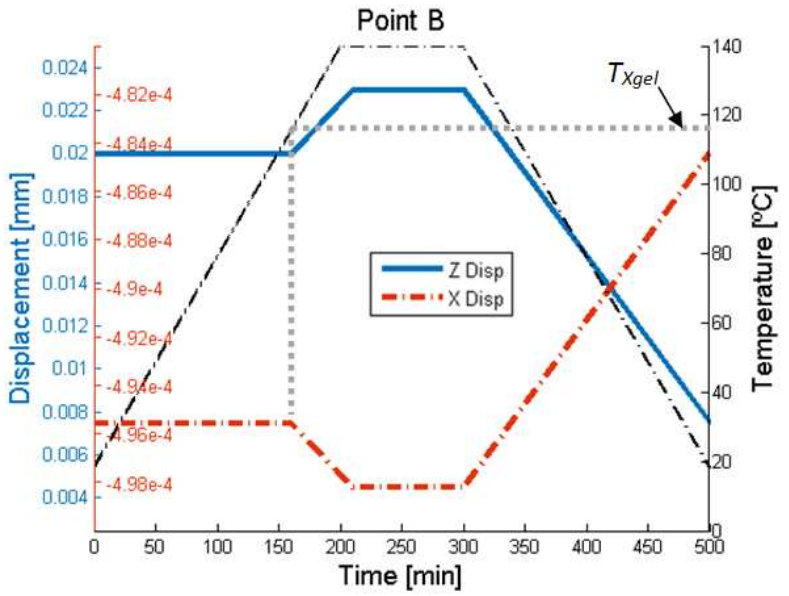

Figure 55: Displacement in x (orange) and z (blue) directions of point B versus curing time. The temperature cycle is also shown in black. The gelation temperature is depicted with a horizontal gray dashed line

5.3.3. Sensitivity on cure kinetic parameters

In this section, the parameters identified during the optimization presented in section 4.2 will be varied. These parameters correspond to the curing kinetics fit to resemble Kamal Sourour model with diffusion control (see Eq. 15, Eq. 19 and Eq. 20). This way, the importance of an accurate fit will be assessed. All these numerical computations in Samcef will be performed with a curing cycle similar to the one in Figure 44, but with temperature ramps of 1.2°C when heating up and -1.2°C when cooling down.

The values of the parameters that were used in this sensitivity analysis are tabulated in Table 12 together with a reference case. The cells highlighted in orange serve as a quick view of which parameters are changed with respect to the reference case. The parameters that are not tabulated but needed for the simulations (such as the coefficient of thermal expansion, the Young's modulus, etc.) are left as specified in the preliminary thermo-mechanical simulation (section 5.2).

Name	A_1[1/s]	A_2[1/s]	E_{a1}[J/mol]	E_{a2}[J/mol]	m	n	b	X_f
Reference	3.883e6	2.017e5	73661	51883	1.311	1.215	0.0263	0.864
S2.1	7.767e6	2.017e5	73661	51883	1.311	1.215	0.0263	0.864
S2.2	1.942e6	4.034e5	73661	51883	1.311	1.215	0.0263	0.864
S2.3	3.883e6	1.008e5	73661	51883	1.311	1.215	0.0263	0.864
S2.4	3.883e6	2.017e5	73661	51883	1.311	1.215	0.0263	0.864
S3.1	3.883e6	2.017e5	88393	51883	1.311	1.215	0.0263	0.864
S3.2	3.883e6	2.017e5	58929	51883	1.311	1.215	0.0263	0.864
S3.3	3.883e6	2.017e5	73661	62259	1.311	1.215	0.0263	0.864
S3.4	3.883e6	2.017e5	73661	41506	1.311	1.215	0.0263	0.864
S4.1	3.883e6	2.017e5	73661	51883	1.967	1.215	0.0263	0.864
S4.2	3.883e6	2.017e5	73661	51883	0.874	1.215	0.0263	0.864
S4.3	3.883e6	2.017e5	73661	51883	1.311	1.823	0.0263	0.864
S4.4	3.883e6	2.017e5	73661	51883	1.311	0.810	0.0263	0.864
S5.1	3.883e6	2.017e5	73661	51883	1.311	1.215	0.0526	0.864
S5.2	3.883e6	2.017e5	73661	51883	1.311	1.215	0.0132	0.864
S6.1	3.883e6	2.017e5	73661	51883	1.311	1.215	0.0263	0.980
S6.2	3.883e6	2.017e5	73661	51883	1.311	1.215	0.0263	0.650

Table 12: Data used for the sensitivity analysis of the curing kinetic parameters. Data in orange highlights the parameters that are changed with respect to the reference case

The following graphs will represent the calculated degree of cure versus time for each of the cases above tabulated:

- Group S2 (Figure 56): it corresponds to the variation in Arrhenius pre-exponential factors A_1 and A_2. By doubling and halving the reference values for each pre-exponential factor, it is possible to appreciate that $X(t)$ has higher sensitivity towards the variation of A_2 (yellow and purple dashed lines).

  The higher the values of A_1 and A_2, the faster the curing. Nevertheless, there is an upper limit of the degree of cure, which is set by the parameter X_f. For that reason, even though the curing is faster, the final degree of cure remains the one for the reference case (0.864).

  When calculating the $\Delta\theta$ for all this cases, no difference with respect the reference case can be observed. Taking into consideration that, according to the analytical expression $\Delta\theta$ only depends on the CTE, the reasons are:

- A_1 and A_2 enter the system by modifying X and its derivative with respect to time. For the range tested, the degree of cure gets above the specified X_{gel} of 0.4. For this reason and because *CTE* will be non-zero after the gelation point, thermal strain will occur.
- A difference in X will influence the evolution of T_g through DiBenedetto's equation (Eq. 18). However, this evolution will be mainly taken into consideration for the vitrification point. Since the CTE at the rubbery and glassy states is the same (remember Figure 53), no variation in $\Delta\theta$ with respect to the reference case will be obtained.

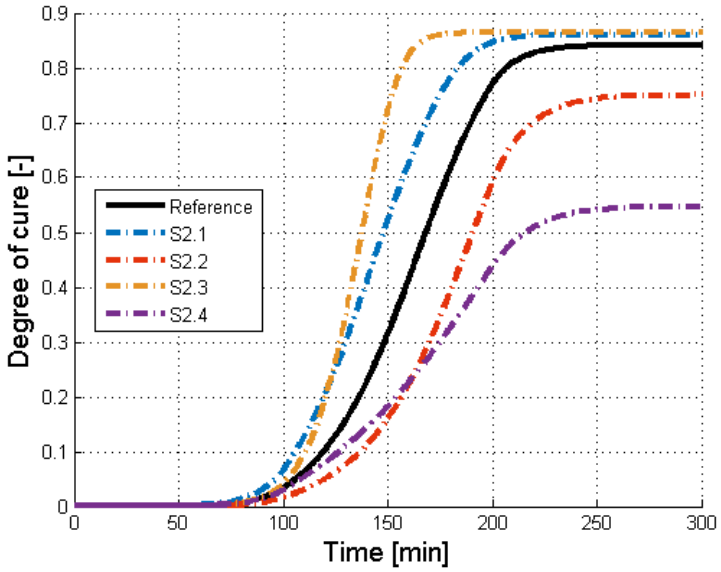

Figure 56: Sensitivity of degree of cure to the variation of Arrhenius pre-exponential factors A_1 and A_2

- Group S3 (Figure 57): this group pretends to show the variation of degree of cure and process induced deformations with the activation energies E_{a1} and E_{a2}. Each parameter have been individually increased and decreased by 20% from the reference value. As it is clear, the lower the activation energy, the earlier and faster curing happens.

  What differs from group S2 is that, when the higher activation energies are used (blue and yellow lines), X never reaches the gel point of 0.4. In these two cases, the CTE never goes beyond the non-zero value, and therefore no process induced deformation occurs, i.e. $\Delta\theta = 0$.

  For the smaller activation energies, the degree of cure reaches X_{gel} during the heat up ramp, and not during the constant curing temperature. Similarly to what observed in section 5.3.1, the variation in the angle θ will be different from the reference case. The displacements of these two cases and the reference cases can be found in Table 13, together with the final $\Delta\theta$.

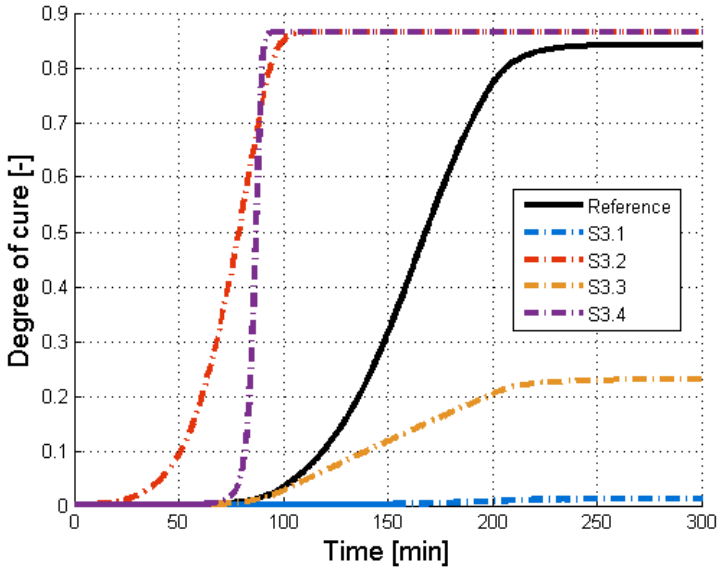

Figure 57: Sensitivity of degree of cure to the variation of the activation energies E_{a1} and E_{a2}

As happened previously, the lower the T_{Xgel}, the earliest gelation occurs. If the gel temperature lies during the increase in temperature, there will be a first deformation that will be later counteracted at cool down. Hence, the final induced deformation $\Delta\theta$ will be lower than for the reference case (for which no deformation exists during heat up). Compared to the percentage of difference between this sensitivity and section 5.3.1, the numerical analysis deviates more: up to 4.44% compared to 2.04%. Nevertheless, these results can still be valid, considering the order of magnitude of $\Delta\theta$.

		Reference case	S3.2	S3.4
X_{gel}		0.4	0.4	0.4
T_{Xgel} [ºC]		140	104	116
Point A	Disp x ↓T [mm]	2.16E-4	1.60e-4	1.80e-4
	Disp z ↓T [mm]	-9.90E-3	-7.20e-3	-8.20e-3
Point B	Disp x ↓T [mm]	2.47E-3	1.80e-3	2.05e-3
	Disp z ↓T [mm]	-1.26E-2	-9.20e-3	-0.0105
Analytical $\Delta\theta$	↓T	0.258	0.180	0.205
Numerical $\Delta\theta$	↓T	0.260	0.188	0.214
% Difference		0.77	4.44	4.39

Table 13: Sensitivity on the activation energies (group S3). The temperature at which X_{gel} happens, and the displacements for points A and B are used to calculate the numerical $\Delta\theta$. The difference between the numerical and the analytical $\Delta\theta$ is also reported

- Groups S4 to S6: these groups study the variation of the curing thermo-mechanical simulation upon the variation of the reaction orders (m and n), the geometric parameter b and the final degree of cure X_f, in that order. The evolution of curing degree versus time can be seen in Figure 58, Figure 59 and Figure 60 for groups S4, S5 and S6 respectively.

As happened previously in group S2, none of these tests exhibit any difference in the final $\Delta\theta$ compared to the reference case. The same reasons as described previously for S2 can apply here.

From each figure, some observations can be pointed out. In Figure 58, one can see how the higher the reaction orders m and n (blue and yellow curves), the slower the conversion and the lower its final degree X_f. For S4.2 and S4.4, the final degree of cure is determined by the specified value of 0.864. This suggests that without the identification of such value, the final degrees of cure would be very overestimated.

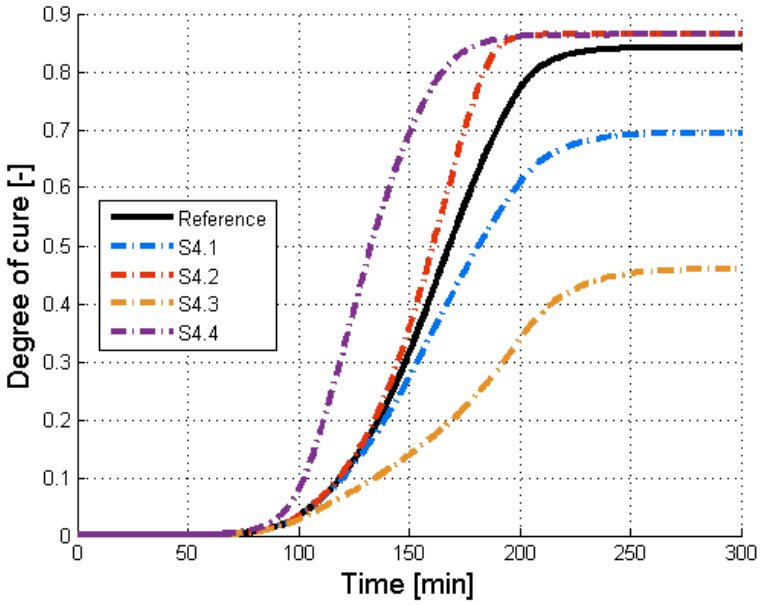

Figure 58: Sensitivity of degree of cure to the variation of the reaction orders *m* and *n*

The sensitivity towards the geometrical parameter *b*, which affects the diffusion control mechanism of the cure kinetics model, can be seen in Figure 59. As diffusion control is only implemented to help the kinetic model in the vitreous stage, varying *b* will only affect during the last stage of curing. By halving and doubling the reference value, little effect can be observed in the evolution of *X*.

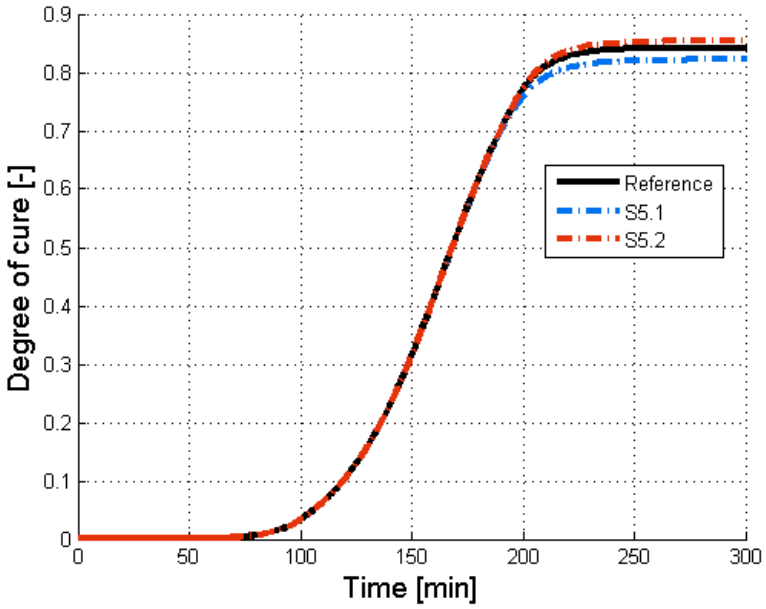

Figure 59: Sensitivity of degree of cure to the variation of the geometric parameter *b* affecting the diffusion control

Lastly, group S6 (shown in Figure 60) describes the sensitivity of the degree of cure when varying the final degree of cure X_f. Although a value close to X_f = 0.95 was set for S6.1 (blue curve), it can be seen that the curing conditions would not allow the material to cure over a degree of approximately 0.88. For a lower value, such as in S6.2 (red curve), the limit of the final degree of cure is reached. This results suggests that, as long as the predicted final degree of cure is sufficiently higher than X_{gel}, no real effect will be seen in the prediction of process induced distortions.

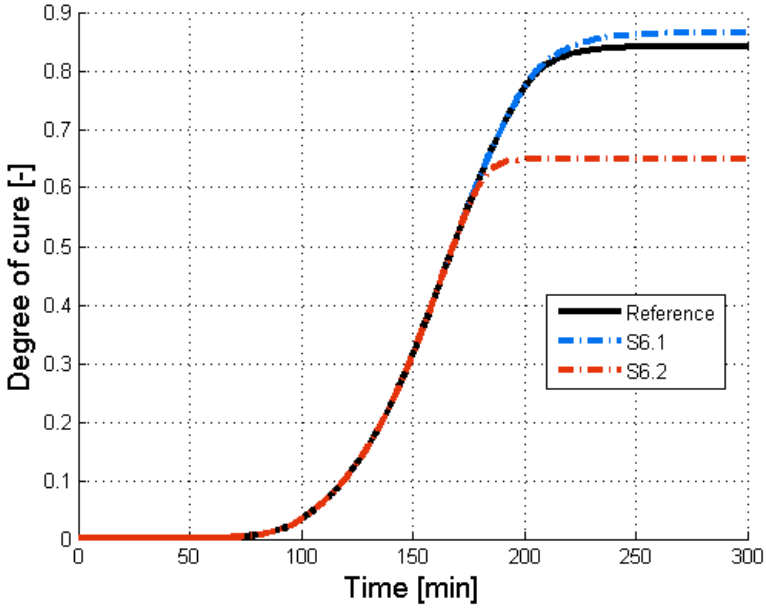

Figure 60: Sensitivity of degree of cure to the variation of the final degree of cure X_f

6. Conclusion and future work

In this thesis, the curing process of a composite laminate with a thermosetting resin has been studied. A brief review of the different curing and material characterization techniques was provided in order to have an overview of the curing process of such a material. Later on, the theory on curing kinetics of a thermosetting resin was introduced. With that in mind, and thanks to the Differential Scanning Calorimetry results provided by C. Brauner, a Matlab programme was created to model the curing kinetics of the resin RTM6 using a non-linear least-square method to fit the experimental data.

A further step was taken when using the Samcef package with the aim of predicting the process-induced deformation of a composite L-shape beam due to the thermal treatment suffered when curing. These simulations are thermo-mechanical analysis with an elastic material model that required the definition of several material parameters, some of which were previously predicted with the aforementioned Matlab programme. For the material properties and geometry implemented, a spring-in angle of around 0.260 degrees was obtained from the numerical simulations. This value is a 0.77% bigger than the estimated analytical deflection of 0.258 degrees. It is interesting to observe that these deflections can be accurately predicted using a numerical software.

It was shown that the coefficient of thermal expansion in the tangential and radial direction is the main parameter that influences the calculation of the spring-in angle, assuming a near-zero value for the chemical shrinkage. It is therefore vital to perform an accurate material characterization of these parameters, which may be sometimes difficult, especially for highly anisotropic stack-up configurations.

Further sensitivity analyses were performed to show that mesh convergence in the results is not a trivial issue. Also, the variation upon the position of the gel point was assessed. These results showed the importance of an accurate prediction of the gel point, as well as the conceptual temperature difference implemented in the analytical prediction of the spring-in angle. It could be seen how an adequate temperature cycle can be implemented in order to minimize the process induced distortions.

The curing kinetic parameters predicted using the Matlab code developed were also varied to observe how a wrong optimization of the experimental data could affect the final shape distortion. The results suggest that, even though the curing cycle is altered and therefore gelation may occur earlier/later, a relatively accurate result is obtained. The parameters that exhibit the biggest influence in the results are the curing activation energies.

As future work, several aspects could be studied:

- It will be interesting to observe if the Matlab code and the thermo-mechanical models implemented in this project are also applicable to other materials with other resins. For the particular material used in this project, the variation in angle was very low and it will most likely be within the manufacturing tolerance. This means that no mould compensation will be required. Nevertheless, other authors have reported wider changes in the angle for different materials (with different homogenized coefficient of thermal expansion).
- Studying the influence of different lay-up on the results, and observing if the analytical formula can predict the process induced deformations arising for a highly anisotropic laminate.
- The implementation of a (quasi-)visco-elastic model, rather than elastic, may induce some changes in the predicted distortion, leading to more realistic results.
- Comparison of the analytical and numerical results with experiments, although there is an added difficulty of experimentally determining the variation in angle after the curing process.
- Studying the behaviour of the final composite structure (including deformation) upon different conditions such as pre-stress, inherent material defects (voids, undercuring, decohesion, etc.), and the consequent failure that may occur.

References

[1] C. Brauner, “Analysis of process-induced distortions and residual stresses of composite structures,” University of Bremen, 2012.

[2] P. I. Karkanas, “Cure modeling and monitoring of epoxy/amine resin systems,” Cranfield University, 1998.

[3] Y. Nawab, P. Casari, N. Boyard, and F. Jacquemin, “Characterization of the cure shrinkage, reaction kinetics, bulk modulus and thermal conductivity of thermoset resin from a single experiment,” *J. Mater. Sci.*, vol. 48, pp. 2394–2403, 2013.

[4] A. T. Nettles, “Basic Mechanics of Laminated Composite Plates,” *NASA Ref. pulication*, no. October, p. 103, 1994.

[5] P. K. Sinha, “Macromechanical Behavior,” in *Composite Materials and Structures*, Kharagpur: Composite Centre of Excellence, AR & DB, 2006.

[6] M. Bruyneel, “Schémas d’approximation pour la conception optimale de structures en matériaux composites,” Université de Liège, 2002.

[7] Federal Aviation Administration, “Advanced composite materials.,” in *Aviation Maintenance Technician Handbook - Airframe*, vol. 1, US Department of Transportation, 2012, pp. 7-1-58.

[8] M. Henne, “Modelling of Thermal Aspects in Liquid Composite Moulding for Industrial Application,” Eidgenössischen Teschnischen Hochschule, 2003.

[9] American Composites Manufacturers Association ACMA, “Compositeslab,” *Processes*. [Online]. Available: http://compositeslab.com/composites-manufacturing-processes/. [Accessed: 10-Mar-2017].

[10] Gardner Business Media Inc., “Composites World,” *Fabrication methods*, 2014. [Online]. Available: http://www.compositesworld.com/blog/post/fabrication-methods. [Accessed: 09-Mar-2017].

[11] F. C. Campbell, “Curing,” in *Manufacturing Technology for Aerospace Structural Materials*, Amsterdam: Elsevier B.V.

[12] D. Abliz, Y. Duan, L. Steuernagel, L. Xie, D. Li, and G. Ziegmann, “Curing Methods for Advanced Polymer Composites - A Review,” *Polym. Polym. Compos.*, vol. 21, no. 6, pp. 341–348, 2013.

[13] F. Wolff-Fabris, V. Alstadt, U. Arnold, and M. Doring, *Electron Beam Curing of Composites*. Münich: Hanser Publications, 2011.

[14] R. Hardis, “Cure kinetics characterization and monitoring of an epoxy resin for thick composite structures,” Iowa State University, 2012.

[15] E. Gutierrez-Miravete, “The Heat Equation,” in *Conduction Heat Transfer Lecture Notes*, 2006, pp. 1–9.

[16] R. Hein, T. Wille, K. Gabtni, and J. P. Dias, “Prediction of Process-Induce Distortions and Residual Stresses of Ancomposite Suspension Blade,” *Defect Diffus. Forum*, vol. 362, pp. 224–243, 2015.

[17] M. Zarrelli, “Cure Induced Property Changes and Warpage in Thermoset Resins

and Composites," Cranfield University, 2003.

[18] N. Rabearison, C. Jochum, and J. C. Grandidier, "A cure kinetics, diffusion controlled and temperature dependent, identification of the Araldite LY556 epoxy," *J. Mater. Sci.*, vol. 46, pp. 787–796, 2011.

[19] G. Wisanrakkit, J. K. Gillham, and J. B. Enns, "The glass transition temperature (Tg) as a parameter for monitoring the cure of an amine/epoxy system at constant heating rates," *J. Appl. Polym. Sci.*, vol. 41, pp. 1895–1912, 1990.

[20] S. Saseendran, "Effect of Degree of Cure on Viscoelastic Behavior of Polymers," Lulea University of Technology, 2016.

[21] L. M. M. Florina, A. Seman, B. Castanie, K. M. Ali, C. Schwob, "Spring-in Prediction for Carbon/Epoxy Aerospace Composite Structure," *Compos. Struct.*, vol. 168, pp. 739–745, 2017.

[22] J. A., "An integrated model of the development of process-induced deformation in autoclave processing of composite structures," The University of British Columbia, 1996.

[23] N. Zobeiry, A. Forghani, C. Li, R. Thorpe, R. Vaziri, G. Fernlund, and A. Poursartip, "Multiscale characterization and representation of composite materials during processing," *Phil. Trans. R. Soc. A*, 2016.

[24] N. Zobeiry, R. Vaziri, and A. Poursartip, "Computationally efficient pseudo-viscoelastic models for evaluation of residual stresses in thermoset polymer composites during cure," *Compos. Part A Appl. Sci. Manuf.*, vol. 41, no. 2, pp. 247–256, 2010.

[25] S. R. White and Y. K. Kim, "Process-induced residual stress analysis of AS4/3501-6 composite material," *Mech. Compos. Mater. Struct.*, vol. 5(2), pp. 153–186, 1996.

[26] P. Prasataya, "A Viscoelastic Model for Predicting Isotropic Residual Stresses in Thermosetting Materials," University of Pittsburgh, 2001.

[27] P. I. Karkanas, I. K. Partridge, and D. Attwood, "Modelling the Cure of a Commercial Epoxy Resin for Applications in Resin Transfer Moulding," *Polym. Int.*, vol. 41, pp. 183–191, 1996.

[28] Siemens, "SAMCEF User Manual 17.1," *Curing thermoset composite behavior*, 2016. .

[29] M. M. Shokrieh, *Residual Stresses in Composite Materials*. Cambridge: Woodhead publishing, 2014.

[30] M. a. Zocher, S. E. Groves, and D. H. Allen, "A Three-Dimensional Finite Element Formulation for Thermoviscoelastic Orthotropic Media," *Int. J. Numer. Methods Eng.*, vol. 2288, no. December 1995, pp. 2267–2288, 1997.

[31] S. P. C. Marques and G. J. Creus, "Rheological Models: Integral and Differential Representations," in *Computational Viscoelasticity*, Springer, 2012, pp. 11–20.

[32] J. Harrington, C. Hoffarth, S. D. Rajan, R. K. Goldberg, K. S. Carney, P. DuBois, and G. Blankenhorn, "Using Virtual Tests to Complete the Description of a Three-Dimensional Orthotropic Material," *J. Aerosp. Eng.*, vol. 30, no. 5, 2016.

[33] ASI, “ASI Adhesives & Sealants Industry,” *Enhanced DSC Instrumentation Design and Characterization of adhesives*, 2002. [Online]. Available: http://www.adhesivesmag.com/articles/83126-enhanced-dsc-instrumentation-design-and-characterization-of-adhesives. [Accessed: 02-Mar-2017].

[34] Hitachi High-Tech Science Corporation, “Specific Heat Capacity Measurements using DSC I,” *Application brief*, Tokyo, pp. 1–4, 1981.

[35] Mettler Toledo, “Measuring specific heat capacity,” *Mettler Toledo Therm. Anal. UserCom 7*, vol. UC 71, no. June, pp. 1–5, 1998.

[36] W. J. Sichina, “Characterization of polymers by TMA,” Norwalk (CT), 1999.

[37] E. Öner, “Uzaktan Egitim Platformu,” *Thermogravimetric Analysis (TGA)*, 2007. [Online]. Available: http://www.uzaktanegitimplatformu.com/UEP/uep_ylisans/ey2/ey2_download/Practice Guide_Section 2_TGA.pdf. [Accessed: 02-Dec-2014].

[38] Mettler Toledo, “Thermal Analysis of Polymers,” *Selected Applications. Thermal Analysis*, pp. 8–38.

[39] Perkin Elmer, “Characterization of Electronic Materials Using Thermal Analysis,” *Therm. Anal.*, 2014.

[40] R. E. Taylor, J. Jortner, and H. Groot, “Thermal diffusivity of fiber-reinforced composites using the laser flash technique,” *Carbon N. Y.*, vol. 23, pp. 215–222, 1985.

[41] NETZSCH Pumps and Systems, “Thermal Diffusivity – Thermal Conductivity. Method, Technique, Applications,” *LFA 447 NanoFlash*.

[42] K. P. Menard and N. R. Menard, “Dynamic Mechanical Analysis of Polymers and Rubbers,” in *Encyclopedia of Polymer Science and Technology*, John Wiley & Sons, Inc., 2002.

[43] H. H. Winter, E. E. Holly, S. K. Benkataraman, and F. Chambon, “Fourier transform mechanical spectroscopy of viscoelastic materials with transient structure,” *J. Non-Neutonian Fluid Mech.*, vol. 27, pp. 17–26, 1988.

[44] Y. Nawab, S. Shahid, N. Boyard, and F. Jacquemin, “Chemical shrinkage characterization techniques for thermoset resins and associated composites,” *J. Mater. Sci.*, vol. 48, pp. 5387–5409, 2013.

[45] H. Yu, S. G. Mhaisalkar, and E. H. Wong, “Observations of gelation and vitrification of a thermosetting resin during the evolution of polymerization shrinkage,” *Macromol. Rapid Commun.*, vol. 26, pp. 1483–1487, 2005.

[46] TA-Instruments, “ARES-G2 Rheometer,” 2014.

[47] M. E. Ryan and A. Dutta, “Kinetics of epoxy cure: a rapid technique for kinetic parameter estimation,” *Polymer (Guildf).*, vol. 20, p. 203, 1979.

[48] L. Zhao and X. Hu, “A variable reaction order model for prediction of curing kinetics of thermosetting polymers,” *Polymer (Guildf).*, vol. 48, no. September 2007, pp. 6125–6133, 2007.

[49] J. M. Balvers, H. E. N. Bersee, A. Beukers, and K. M. B. Jansen, “Determination of Cure Dependent Properties for Curing Dimulation of Thick Walled Composites,”

in *49th AIAA/ASME/ASCE/AHS/ASC Structures, Structural Dynamics, and Materials Conference, 16th AIAA/ASME/AHS Adaptive Structures Conference,10th AIAA Non-Deterministic Approaches Conference, 9th AIAA Gossamer Spacecraft Forum, 4th AIAA Multidisciplinary Desi*, 2008.

[50] T. J. R. Hughes, “Nonconforming Elements,” in *The Finite Element Method: Linear Static and Dynamic Finite Element Analysis*, 1987, pp. 242–250.

[51] K. H. Huebner, “Natural Coordinates,” in *The Finite Element Method for Engineers*, John Wiley & Sons, 2001, pp. 151–160.

Appendix I: Figures of DSC results of RTM6 resin

- Isothermal DSC at 140ºC

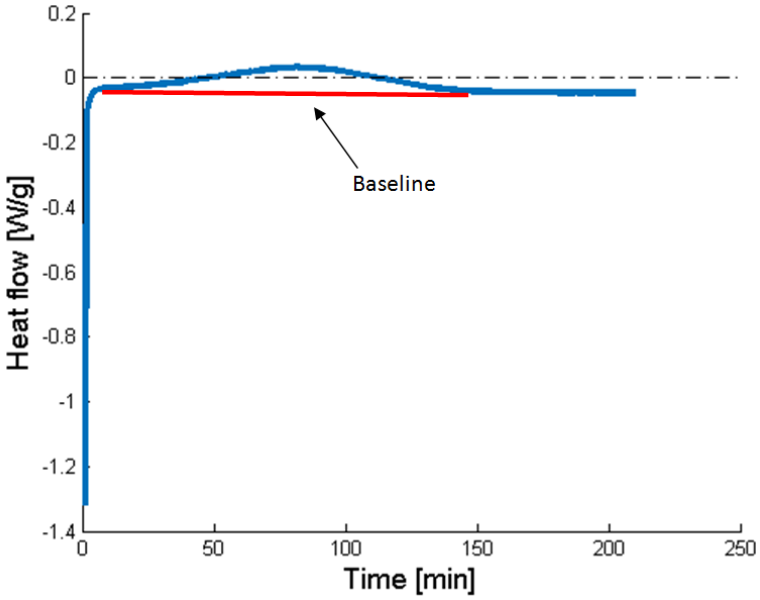

- Dynamic DSC at 5ºC/min

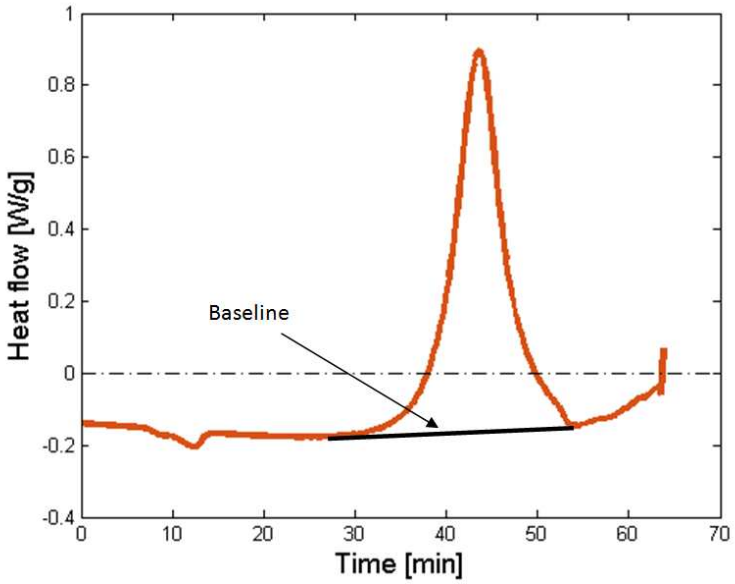

- Dynamic DSC at 7.5ºC/min

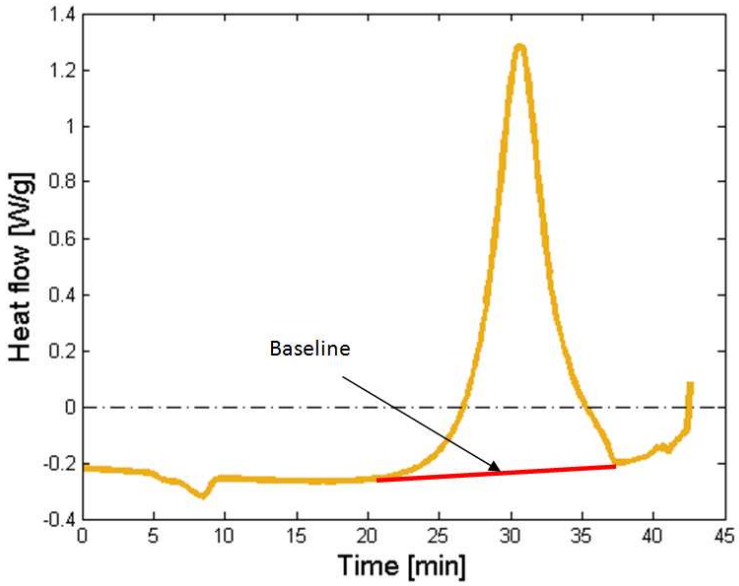

- Dynamic DSC at 10ºC/min

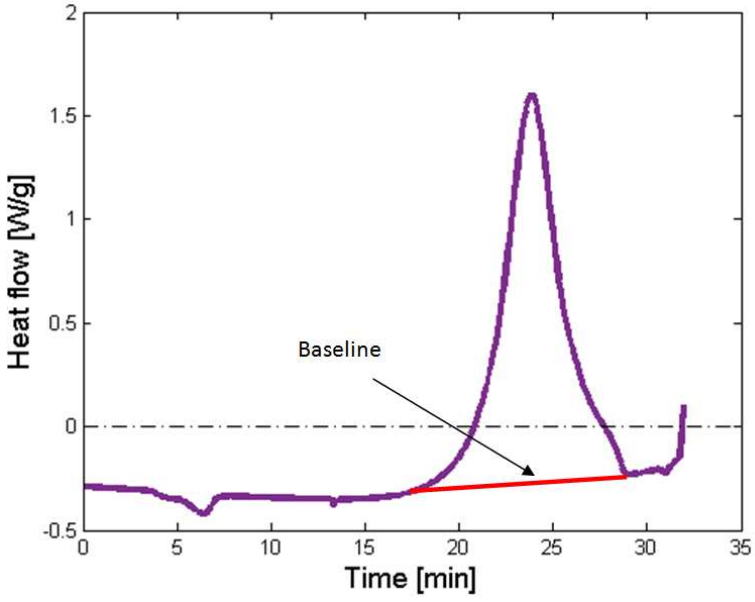

- Dynamic DSC at 15ºC/min